MECHANICAL CHARACTERIZATION OF SHAPE MEMORY POLYMERS TO ASSESS CANDIDACY AS MORPHING AIRCRAFT SKIN

by

Korey Edward Gross

B.S. in Mechanical Engineering, University of Pittsburgh, 2006

Submitted to the Graduate Faculty of

Swanson School of Engineering in partial fulfillment

of the requirements for the degree of

Master of Science in Mechanical Engineering

University of Pittsburgh

2008

UNIVERSITY OF PITTSBURGH

SWANSON SCHOOL OF ENGINEERING

This thesis was presented

by

Korey E. Gross

It was defended on

July 31, 2008

and approved by

Dr. William W. Clark, Professor, Department of Mechanical Engineering and Materials Science

Dr. Jeffrey S. Vipperman, Associate Professor, Department of Mechanical Engineering and Materials Science

Thesis Advisor: Dr. Lisa Weiland, Assistant Professor, Department of Mechanical Engineering and Materials Science

MECHANICAL CHARACTERIZATION OF SHAPE MEMORY POLYMERS TO ASSESS CANDIDACY AS MORPHING AIRCRAFT SKIN

Korey Edward Gross, M.S.

University of Pittsburgh, 2008

This thesis presents the results of research with the purpose of determining the mechanical properties of shape memory polymers and evaluating the material's potential use as a morphing aircraft skin. Morphing aircraft undergo large scale deformations to their wing planforms in order to perform better in different types of missions. The skin on the wing must be ductile enough to stretch but remain strong enough to withstand out of plane aerodynamic loads. Shape memory polymers exhibit large decreases in their elastic modulii when heated above a glass transition temperature which allows them to withstand large strains. This ability has lead to the belief that shape memory polymers could perform well as morphing aircraft skins. Several tests that reveal mechanical properties important to a morphing wing skin are performed on a commercially available shape memory polymer and the results are presented and discussed in this study.

TABLE OF CONTENTS

LIST OF TABLES

LIST OF FIGURES

ACKNOWLEDGEMENTS

I would like to begin by thanking the three most influential people in my life: my mother Shelleen Gross, my father Edward Gross Jr., and my sister Kristin Gross. Thanks to my parents for supporting all of my endeavors in and out of the classroom and telling me anything is possible. Thank you, Kristin, for always providing a "moving target" for me to aim for in the scholastic world. Following the model you set has kept me on task throughout my high school and university years.

I must next thank Dr. Lisa Weiland at the University of Pittsburgh. I don't know where I would have been if you hadn't picked out my graduate school application because of our shared aerospace interests. You have pushed me hard enough to achieve great things but gently enough so I have a good amount of hair left on my head.

Thanks also go out to everyone at NextGen Aeronautics who has supported my research and given me great experience during my summer internships. I would not trade those two summers in Los Angeles for anything. Finally I would like to thank my fellow researcher Rich Beblo who helped introduce me to SMPs and was readily available to answer any questions I came up with. Good luck with the P.H.D.

1.0 INTRODUCTION

Currently, there is considerable interest in creating effective morphing aircraft. This interest has been inspired by watching predatory birds change how they hold their wings while in different flight situations. For example, a raptor will have its wings stretched wide while hovering in search of prey, but will tuck its wings in close to its body when swooping down on prey. Morphing aircraft development seeks to mimic this kind of change by radically changing an aircraft's wing area and orientation while in flight. During different segments of a mission, a morphing aircraft will use different wing configurations that include: takeoff, loiter, cruise, and dash [9]. The difficulty in creating wings that can accomplish these changes is in finding skins that are ductile enough to withstand the large in-plane deformation while being stiff enough to support out-of-plane aerodynamic loading.

Shape memory polymers (SMPs) were first introduced by the Nippon Zeon Company of Japan in 1984 [1]. Since this introduction, SMPs have been used in a broad variety of applications. SMPs are typically employed in one of two temperature dependent phases, a fixed phase and a thermally reversible phase [2]. While a SMP is below its glass transition temperature, T_g, it is in the fixed phase and is capable of carrying large loads. When heated above its T_g, the same SMP will be soft and demonstrate very high ductility. Above T_g, the SMP is in its thermally reversible phase where even large deformations are reversible upon removing external forces. In most cases, all of the residual deformation is recovered. This shape memory

effect is the result of the SMPs molecular structure and can be tailored by using different processing techniques [3]. Also tailorable is a SMPs glass transition temperature. By altering the material's chemical make up, its T_g can be varied over a range of hundreds of degrees [4]. This versatility as well as low production costs and excellent chemical resistance have sparked interest for using SMPs in morphing aircraft, medical devices, and compliant structures [1, 5].

As the potential applications for SMPs grow, so does the need for mechanical properties characterization such as elastic moduli and yield strengths for various SMPs [1, 6]. Veriflex® (CRG Industries), a relatively new SMP formulation, is the SMP characterized in this study, with an emphasis on establishing whether this material is suitable for morphing aircraft applications. In August of 2006, Torrance, CA based NextGen Aeronautics became the first company to fly a UAV that morphed while in flight. Their aircraft, dubbed MFX-1, flew while demonstrating changes in wing area, cord, and sweep [7]. Along with the results of this study, data from this flight will be used to assess the potential effectiveness of Veriflex® as a morphing aircraft skin.

.

2.0 BACKGROUND

This section is dedicated to introducing and giving background on materials. Included in this section is a brief introduction to material requirements for morphing aircraft wings followed by a brief overview of the shape memory polymer Veriflex®. After the first two overview sections, a literature review is presented and then the section is summarized.

2.1 GOALS OF MORPHING AIRCRAFT RESEARCH

Today's military airplanes are designed to be used in a specific mission role. For example, the Global Hawk is used solely for reconnaissance because of its long endurance while an F-14 is used in short bombing runs and aerial combat because of its high speed. In order to eliminate the need for a separate aircraft for each mission type, research is being conducted into creating an aircraft that can perform effectively in different missions by actively changing the shape of its wings.

A morphing aircraft will change its wing planform in order to drastically change in flight performance during different mission roles. In a loiter mode, the plane will have a large span and high surface area in order to minimize fuel consumption while a fighter in attack or dash mode would have a small span and low surface area to increase speed and handling [8]. Figure 2.1-1 depicts the different wing shapes of a morphing aircraft concept.

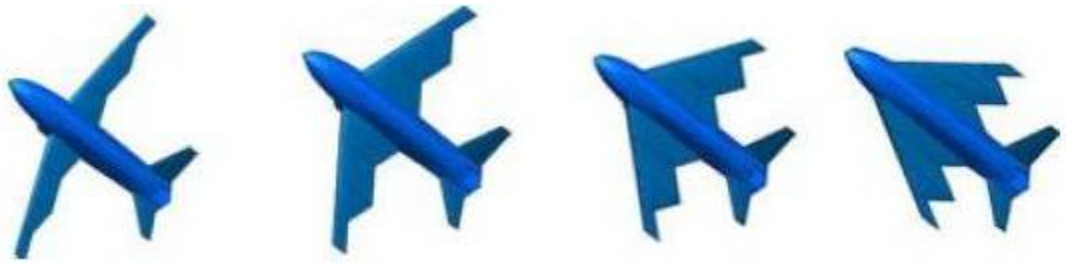

(a) Cruise **(b) Loiter** **(c) Take-off** **(d) Dash**

Figure 2.1-1 Different Wing Configurations of a Morphing Aircraft. [9]

2.2 MORPHING AIRCRAFT BACKGROUND

This section briefly reviews the past efforts in the development of morphing aircraft. Included are variable sweep aircraft, the Active Aeroelastic Wing (AAW) and the Morphing Aircraft Structures (MAS) Program. Each of these programs has created aircraft that have been at least through early phases of flight testing.

2.2.1 Variable Sweep Aircraft

The original morphing wing came in the form of variable sweep wings, sometimes called swing wings. Aircraft with variable sweep wings employ kinematic strategies to change the wing's sweep angle. Examples of variable sweep wings are the F-111, B-1 and F-14.

The variable sweep wing allows an aircraft to operate in a small range of different flight situations. Swinging the wing out such that the leading edge approaches a perpendicular position with respect to the fuselage allows for greater lift and less fuel consumption while tucking the wings closer to the fuselage allows for much higher speeds. This change in performance is

mostly based on the reduction of drag across the decreased wetted area of the wing surface. Sweeping the wing backward lowers overall drag and thus makes it easier to attain higher speeds. However, this configuration comes at the cost of less control and higher fuel consumption.

2.2.2 Active Aeroelastic Wing (AAW)

The AAW program was a joint venture between the United States Air Force Research Laboratory, Boeing's Phantom Works, and NASA Dryden. The program aimed to create an aircraft with increased roll control via purposely inducing a degree of wing twist [10]. This technique was actually seen in the very beginnings of aviation. The Wright brothers' Wright Flyer allowed for wing warping to increase the roll control. However, as aircraft speed and performance have increased, application of wing warping has become a considerably tougher puzzle to solve.

Figure 2.2-1 F/A-18A in Flight [10]

An F/A-18A hornet fighter jet was chosen as the test platform for the AAW program. This plane, originally developed by McDonnell Douglas (now Boeing), was designed for both air to air and air to ground combat and has the capability to take off from an aircraft carrier. The hornet was modified to allow the outer wing to twist upward 5 degrees by using modestly softer skins. The aircraft was demonstrated in its first successful flight test at Edward's Air Force base on November 15, 2002.

2.2.3 Morphing Aircraft Structures (MAS) Program

For Projects in the MAS program, there are specific requirements that had to be met by each aircraft. The wings had to be able to meet the following performance criterion [8] :

- 200 % change in Aspect Ratio
- 50 % change in Surface Area
- 5º change in Wing Twist
- 20º change in Wing Sweep

The aspect ratio of a wing gives a measure of slenderness from tip to tip. Aspect ratio can be determined using Equation 2.2-1 where s is the wing's span and A is the wing's surface area. Figure 2.2-2 shows a diagram of key wing dimensions including how the wing's span is measured. A high aspect ratio means a long slender wing while a low aspect ratio signifies a shorter span with a larger chord. Higher aspect ratio wings exhibit less drag because passing air flows a shorter distance across the wing surface [11].

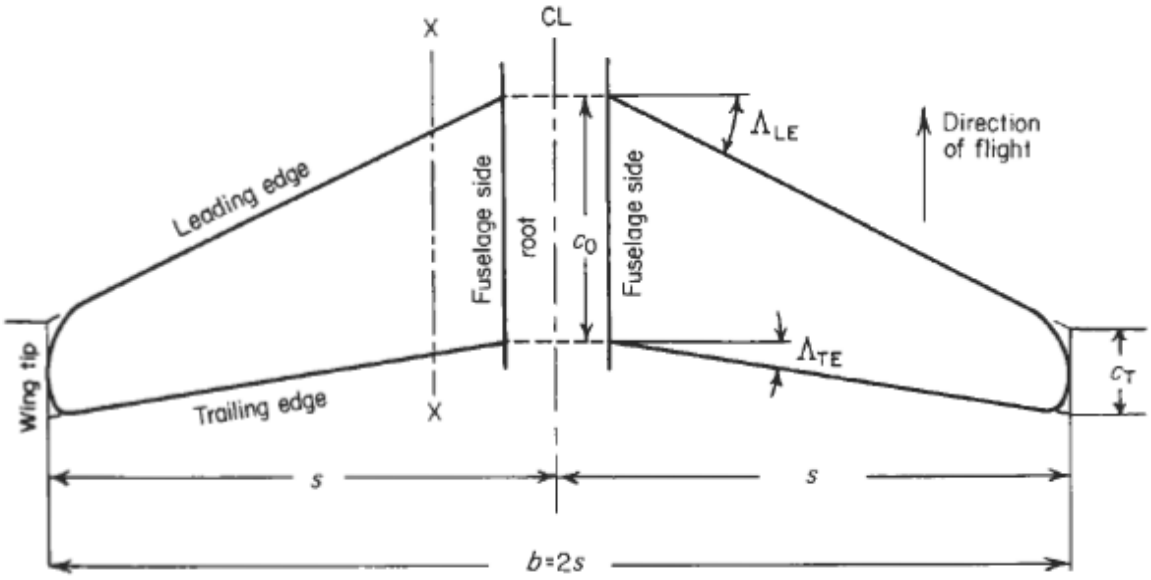

Figure 2.2-2 Diagram of Wing Dimensions [11]

$$\frac{s^2}{A} \qquad \textbf{(2.2-1)}$$

The MAS program produced two prototype morphing aircraft. Lockheed Martin created a morphing UAV that used a folding mechanism. During cruise mode, the wing would be completely flat like a typical airplane. However, to shift into different modes, the wing could fold out of its horizontal plane and move toward the fuselage. This UAV was dubbed the "Z-Wing" because the wing resembled the shape of a 'Z' when folded against the fuselage (Figure 2.2-3). The wing was rumored to have shape memory polymers in its joints as a locking mechanism but this was never confirmed by the company. The Z-Wing program has been stopped after the company experienced several problems during the initial flight testing.

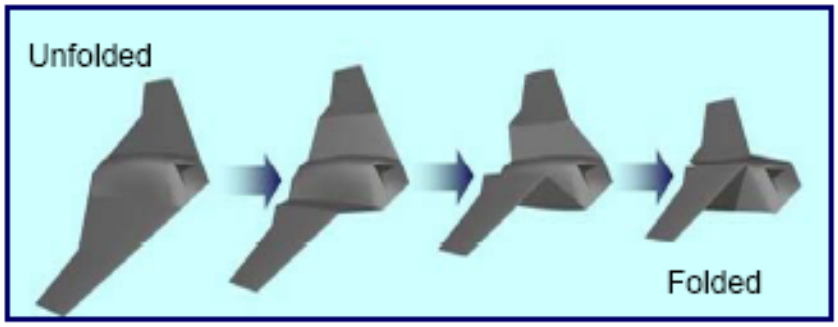

Figure 2.2-3 Lockheed Martin Z-Wing Morphing UAV [9]

Alternatively, NextGen Aeronautics created a morphing UAV that utilized a wing that folded in the horizontal plane (Figure 2.2-4). This UAV was originally referred to as a "BatWing" but has since been named MFX-1 by NextGen. MFX-1 is a 100 pound remote controlled UAV powered by a single jet engine. In order to accommodate the necessary deformations, MFX-1 was outfitted with a flexible silicone skin. Metal ribbons were used as a support structure under the silicone so the wing could properly support aerodynamic loads.

Figure 2.2-4 NextGen Aeronautics' MFX-1 [7]

In August of 2006, NextGen successfully flight tested MFX-1 in Camp Roberts, California. The UAV sustained an area change of 40 percent, span change of 30 percent and

sweep varying from 15 to 35 degrees while in flight. It also attained airspeeds of about 100 knots during the test cycle. This was the first recorded successful test of an aircraft that morphed during flight.

After the success of MFX-1, NextGen developed a larger 300 pound morphing UAV named MFX-2. MFX-2 used twin jet engines for propulsion and also encompassed a flight control system that allowed autonomous flight. A September 2007 flight test of the aircraft once again garnered success while demonstrating a 40 percent change in wing area, 73 percent change in span and 177 percent change in aspect ratio.

In both cases, application of silicone as a flexible skin enabled demonstration of the morphing concept. However, silicone is not an adequate long term solution. The following details the requisite properties of an appropriate skin solution.

2.3 INTRODUCTION TO MORPHING SKIN MATERIAL REQUIREMENTS

In order to accommodate the drastic changes in wing geometry required for morphing aircraft, the skins on the wings must have certain characteristics:

(1) The material needs to be able to sustain large in-plane normal and shear strains. This allows it to be stretched during morphing.

(2) After the material is stretched, it must also be able to recover its original shape. This property will keep the wing skin from sagging after the wing returns to its original (not stretched) position. A dip in the wing skin would otherwise increase the drag across the wing surface thus decreasing the wing's efficiency.

(3) The skin must withstand large out-of-plane aerodynamic loads during flight. This requirement tends to compete with requirement (1). To compensate, most flexible skins are expected to be employed with a support structure. However, optimization of the material's ability to support out-of-plane loads remains a significant constraint.

(4) Because a support structure is needed, the skin must be able to resist abrasion due to its contact with metal supports and other wing structures. A tear in the skin during flight could be catastrophic.

(5) The skin must also be weather and oil resistant. The skin will be exposed to different atmospheric conditions during flight and also could come into contact with an assortment of different oils and lubricants that are used in the mechanical structure of the wing [12].

(6) Finally, the skin must transition in a reasonable amount of time. A morphing aircraft will not have twenty minutes to spare so that its skin can fully transition. This transition must also be accomplished using a reasonable amount of energy. Size restraints on aircraft mean that there is a limit to the size of power supplies that could be used to transition the material.

2.4 OVERVIEW OF VERIFLEX®

Most of the SMPs that have been under previous study have been polyurethane based. More specifically, segmented polyurethane thermoplastic polymers have garnered a large amount of attention. Polyurethane SMPs consist of alternating hard and soft segments. Cross-links are created and destroyed through polar forces, hydrogen bonding and crystallizations [5].

Cross-links are the covalent or ionic bonds that link polymer chains together. The more polymer chains that are cross linked together, the stiffer the polymer will be. In SMPs, these cross links can be weakened or destroyed to allow the polymer chains to move more freely thus increasing ductility [4, 13, 14].

A SMP can possess both chemical and physical cross-links. Through synthesis, the material may have a certain degree of chemical cross-links as well as solid regions that embody physical cross links. When the material is transitioned, these cross-links are weakened allowing the bonds to be stretched much further than the untransitioned material [14]. When the material is deformed after transitioning, the stretched bonds store internal energy which tend to restore the bonds to their unstretched position. This is the mechanism for the memory effect in SMPs.

Veriflex® is a styrene based SMP. Compared to their polyurethane brethren, very little research has been directed at polystyrene SMPs [6,7]. Further research into styrene SMPs such as Veriflex® will provide a critical base of knowledge that can help determine if polystyrenes are practical for a plethora of potential applications.

Veriflex® has a glass transition temperature of 62º C. Above this temperature, cross-links are broken down and weakened. Because stiffness is approximately proportional to cross-link density, this coincides with a significant decrease in Young's modulus. Below this temperature, CRG Industries reports that Veriflex® has an elastic tensile modulus of 1241 MPa

(180 ksi) [8] below T_g and an independent study has reported a modulus of 0.2 MPa [6] above T_g. This significant range in stiffness variation over a relatively short temperature range makes Veriflex® attractive for consideration as morphing aircraft skins.

2.5 LITERATURE REVIEW

Due to the unique functionality of shape memory polymers, a large amount of attention is being paid to them in both academic and commercial settings [1, 3, 4, 9, 12, 13, 15]. Research is being conducted into using SMPs as key material components in applications such as morphing aircraft, smart structures, biomedical devices, deployable structures and sensors, and actuators [1, 9, 12, 13, 16-22]. The large range of potential uses is derived largely from SMPs shape memory effect.

SMPs can be programmed to memorize an original stress free shape through varying production methods. The SMP can then be stimulated by any of multiple activation methods, deformed and then fixed into a temporary position by removing the stimulus. A thermal stimulus example can be seen in Figure 2.5-1.

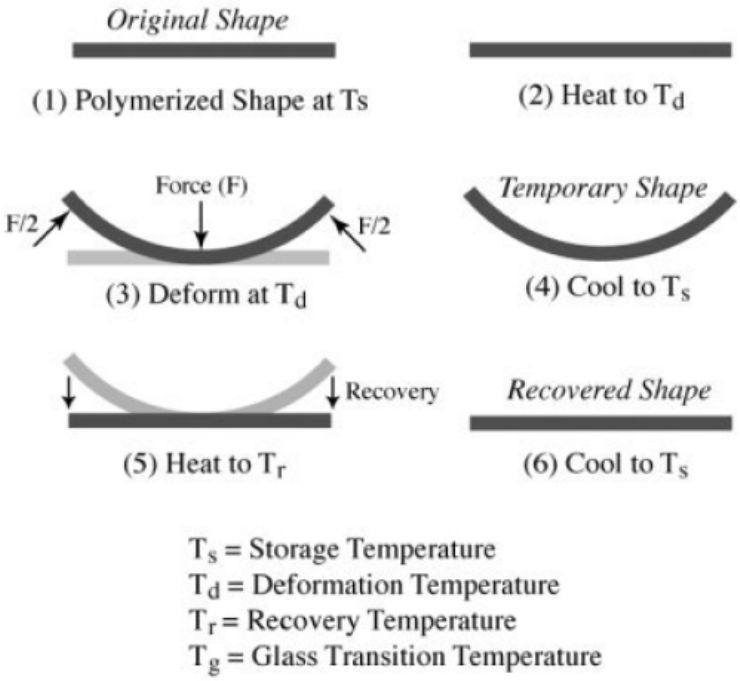

Figure 2.5-1. Thermally Driven Shape Memory Cycle [4]

As illustrated, the SMP's Young's modulus will decrease significantly when the activation stimulus is applied. While in this ductile state, the SMP can be stretched and deformed with relatively small force and sustain strains as high as 200%. Once it is stretched into a desired shape or form, it can be frozen in that state by removing the stimulus which returns the Young's modulus to its original higher value [1, 3, 4, 9, 13-17, 21-28]. After restimulating the SMP and removing forces, it will return to its original shape (usually with 100 % strain recovery) [14, 28].

In order to elicit the shape memory effect, the material must first be activated by a stimulus. The most researched activation methods are thermal and light stimuli. In the case of a thermal stimulus, heating is most easily accomplished by simply placing the SMP in an elevated ambient temperature, but it has also been accomplished by doping SMPs with electrically conductive materials and running a current through the material [29]. There are also research projects being conducted that use infrared lasers to heat SMPs [3, 13]. On the other hand, light

activated SMPs are stimulated by shining different wavelengths of ultra violet light onto the SMP. Thermally stimulated SMPs have been the most researched to date [1, 3, 13, 14, 17] while light activated SMPs are not yet mature enough to be applied in adaptive structures [23].

An important property of a thermally activated SMP is its glass transition temperature T_g. At temperatures below T_g the SMP is in a fixed hard state. In this state, the material can support loads without much deformation. When heated above T_g, the SMP is in a soft rubbery state with a Young's modulus orders of magnitudes lower than that of the hard state. Through different modes of chemical synthesis and production, the T_g of an SMP can be tailored to specific applications within a range of hundreds of degrees Celsius [4]. So, specific SMPs can be created to suit the needs of different development programs.

The relationship between Young's modulus and temperature in thermally activated SMPs has been heavily explored [1, 3, 4, 13, 14, 17, 21, 30]. Figure 2.5-2 shows the typical relationship between Young's modulus and temperature in an SMP. A Dynamic Mechanical Thermal Analyzer (DMTA) is used to plot the SMP's Young's modulus versus temperature. SMP response to uniaxial loading represents another common characterization approach [4, 6, 12, 14, 24, 30]. Most of these tests are aimed at finding the material's Young's modulus, and strain recovery attributes above and below T_g [3, 5, 6, 12-14, 21].

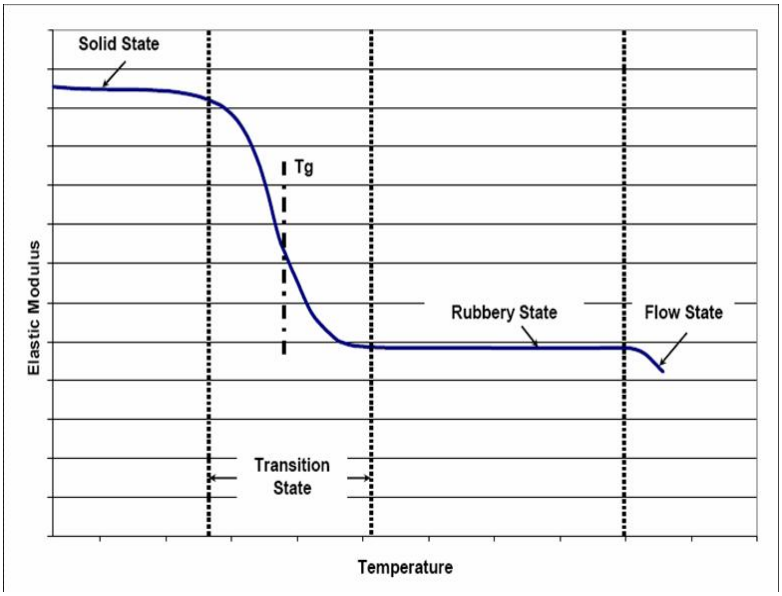

Figure 2.5-2 Typical Modulus vs. Temperature Curve for SMPs [12]

Figure 2.5-3 (a) and Figure 2.5-3 (b) show two examples of typical results of uniaxial tension and compression tests of an SMP at two different temperatures. The key attribute shown in these particular studies is that each material's modulus changes significantly. In the first study the modulus is 750 MPa at 273K (below T_g) but drops to 8.8 MPa at 358K (above T_g). The second study shows a similar decrease in modulus from 620 MPa to 1 MPa. These tests show two different SMPs both exhibiting the typical thermal transition characteristics in all SMPs.

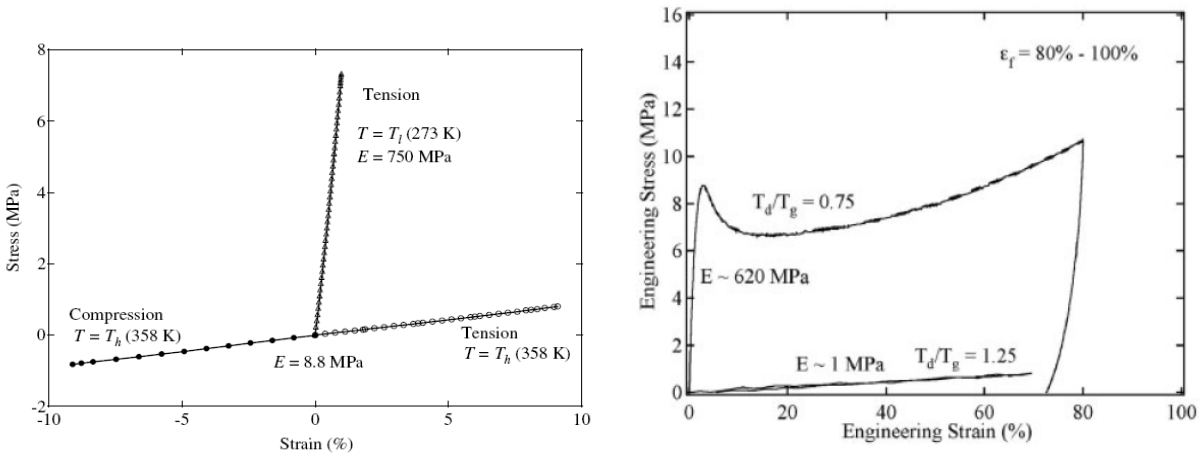

(a) (b)

Figure 2.5-3 Results from Uniaxial Tension and Compression Tests for Young's Modulus [14]

Shape recovery is important to SMPs because it is the material's ability to completely return to its original shape after stretching. Shape recovery is most often studied by loading and unloading an SMP at various temperatures [4, 13, 21]. The SMP's recovery characteristics are then best illustrated by producing a shape-memory plot of Strain vs. Temperature. This plot also shows the material's shape fixity which is its ability to hold a shape after it has been deformed. Figure 2.5-4 gives a break down of the shape-memory plot and what each section represents. The material is first loaded at a constant temperature above T_g (process 1). The loading is then held constant over a time period to determine if there is any creep present (process 2). The material is then cooled below T_g under the still constant stress (process 3). After cooling the load is released and shrinkage is measured (process 4). Finally the material is reheated to the original temperature above T_g and a recovery profile is seen in the final section of the graph (process 5).

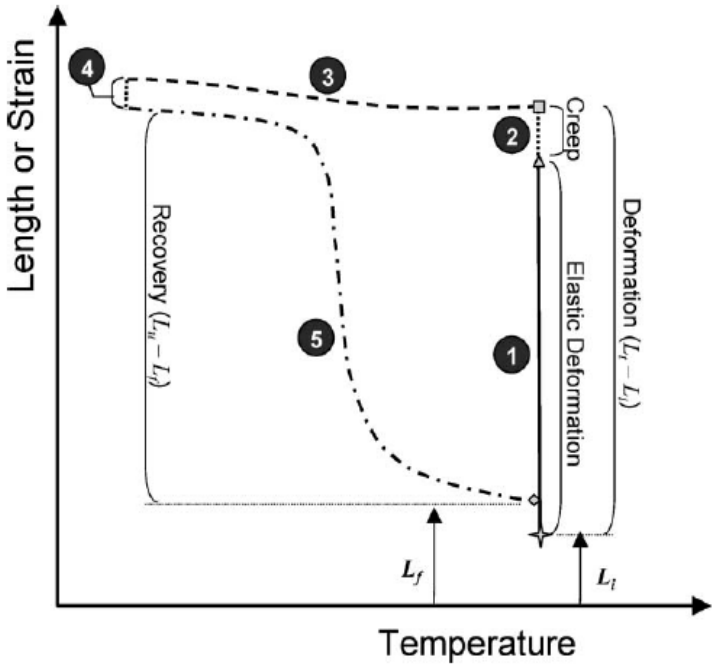

Figure 2.5-4 Shape-Memory Profile of SMP[13]

The shape memory profile may also offer a more quantitative way to classify SMPs based on their recovery ability. This is accomplished by introducing a "shape-memory fill-factor" [13]. The fill factor is the ratio of the area in a material's shape-memory profile compared to an ideal shape-memory profile. Figure 2.5-5 shows an example of the different classifications of an SMP based on the fill factor.

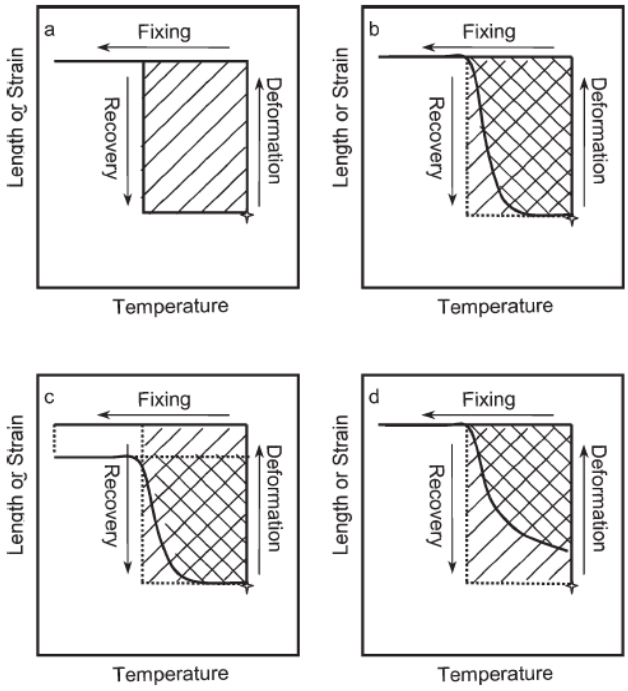

Figure 2.5-5. Fill Factor Classification of SMPs. (a) ideal (b) excellent recovery and fixity (c) excellent recovery poor fixity (d) attractive fixity but poor recovery [13]

There have also been several efforts to model the behavior of SMPs [4, 25, 30]. An early study applied the standard linear viscoelastic (SLV) model to express mechanical properties [30]. The SLV model relates stress and strain as:

$$\dot{\varepsilon} = \frac{\dot{\sigma}}{E} + \frac{\sigma}{\mu} - \frac{\varepsilon}{\lambda} \qquad \textbf{(2.5-1)}$$

$$\varepsilon_s = C\left(\varepsilon_c - \varepsilon_l\right) \qquad \textbf{(2.5-2)}$$

Equation 2.5-1 represents a spring in parallel with a Maxwell model [30] where σ, ε, E, μ, and λ represent stress, strain, Young's modulus, viscosity and retardation time respectively and the dot is a time derivative. In Equation 2.5-2, ε_c is the creep strain, ε_s is the recoverable strain and C is a proportionality coefficient. ε_l represents a critical creep strain, above which ratio C of the creep strain cannot be recovered.

The relationship between elastic modulus and temperature in the SLV model is represented by

$$E = E_g \exp\left[a\left(\frac{T_g}{T} - 1 \right) \right] \qquad \textbf{(2.5-3)}$$

Where E_g is the modulus at the glass transition temperature and a is the slope of the modulus vs. temperature graph in the transition phase. The other material parameters σ, μ, and C are represented in the same way by replacing E and E_g with each parameter's corresponding value at the glass transition temperature.

This linear model shows promising results when compared to experimental data for stress-strain, and stress-temperature tests of a thin film SMP [30]. However, the strain-temperature relationship is not represented well (Figure 2.5-6). The model's strain recovery calculation is significantly less than the experimental strain recovery (process 4). This is one factor that prompted the development of a non-linear model [25].

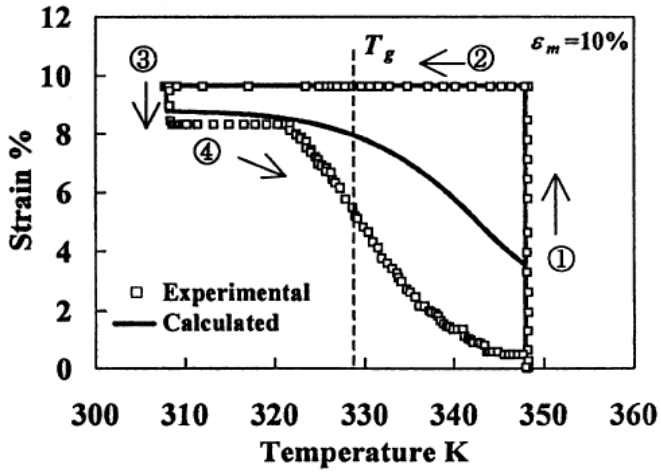

Figure 2.5-6. Strain-Temperature Relationship of SLV Model for SMP [30]

The non-linear model simply adds non-linear terms the to SLV model. Inserting, σ_y and σ_y as proportional limits of stress into the time dependent and viscous terms results in the stress strain relationship:

$$\dot{\varepsilon} = \frac{\dot{\sigma}}{E} + m\left(\frac{\sigma - \sigma_y}{k}\right)^{m-1}\frac{\dot{\sigma}}{k} + \frac{\sigma}{\mu} + \frac{1}{b}\left(\frac{\sigma}{\sigma_c} - 1\right)^{n} - \frac{\varepsilon - \varepsilon_c}{\lambda} + \alpha\dot{T} \qquad \textbf{(2.5-4)}$$

Similar to the linear model, temperature dependence of the parameters *E, σ, μ, k*, and *C* are found using the experimental methods of Equation 2.5-3.

The comparison between the actual and calculated results of the stress vs. strain and strain vs. temperature curves for the non-linear model can be seen in Figures 2.5-7 (a) and 2.5-7 (b) respectively. The non-linear model, while somewhat more complex than the SLV model, clearly does a superior job of capturing strain recovery.

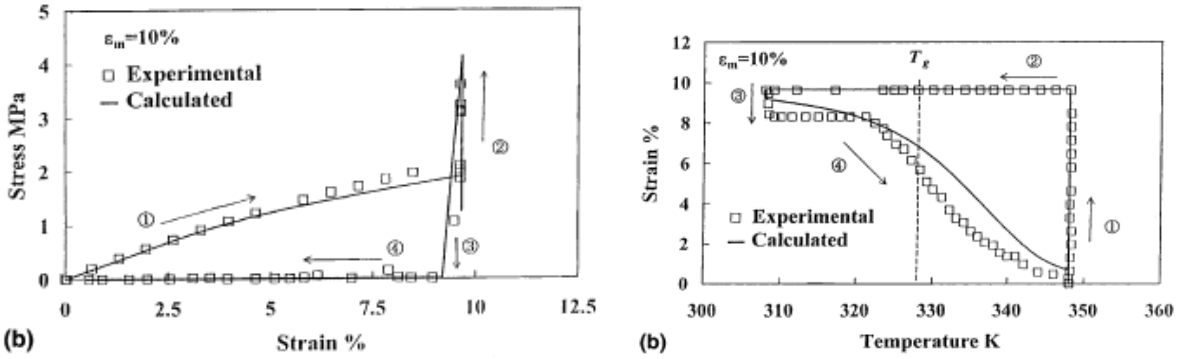

(a) (b)

Figure 2.5-7 Stress vs. Strain and Stress vs. Temperature Results of Non-Linear Model [25]

The stress vs. strain prediction becomes more accurate as the strain is increased because the relationship becomes less linear. The strain vs. temperature predictions follow the general shape of the experimental value but have more error during the relaxation part of the test. This particular aspect of the model could be modified to predict the aforementioned fill factor. This strategy reduces the number of real time experiments needed to determine the fill factor.

2.6 APPLICATIONS

The mechanical properties of SMPs described by the aforementioned studies are used to determine if the material is appropriate to any of a plethora of potential applications. This thesis will focus on morphing aircraft, but extensive developments of SMP based biomedical devices are worthy of mention [4, 15, 17, 23, 27]. One of these devices would be used to treat ischemic stroke victims. The intravascular device would be used to remove blood clots that cause the condition. The device utilizes an SMP programmed to cork screw when heated via an infrared laser. Figure 2.6-1 illustrates the process.

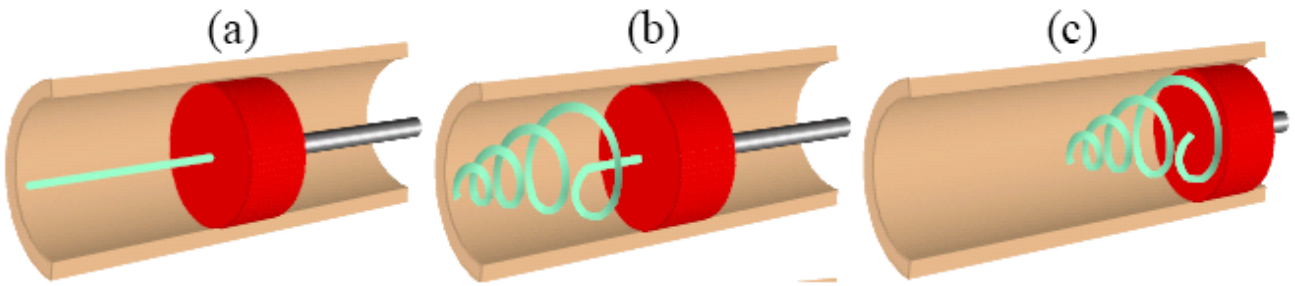

Figure 2.6-1. Depiction of SMP Thrombectomy Device. The device is inserted through blood clot (a), infrared heating returns the straight SMP to a memorized corkscrew (b) and is then retracted (c). [27]

Other biomedical devices include expandable stents for vascular reconstruction and self closing sutures for closing open wounds (Figures 2.6-2 and 2.6-3 respectively).

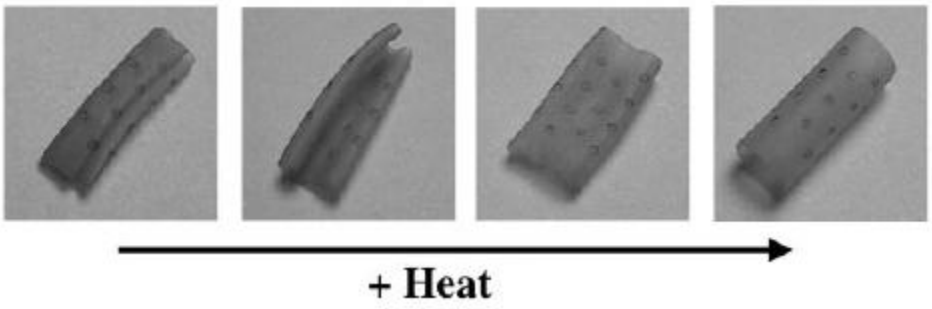

Figure 2.6-2 Cardiovascular Stent Created From SMP [17]

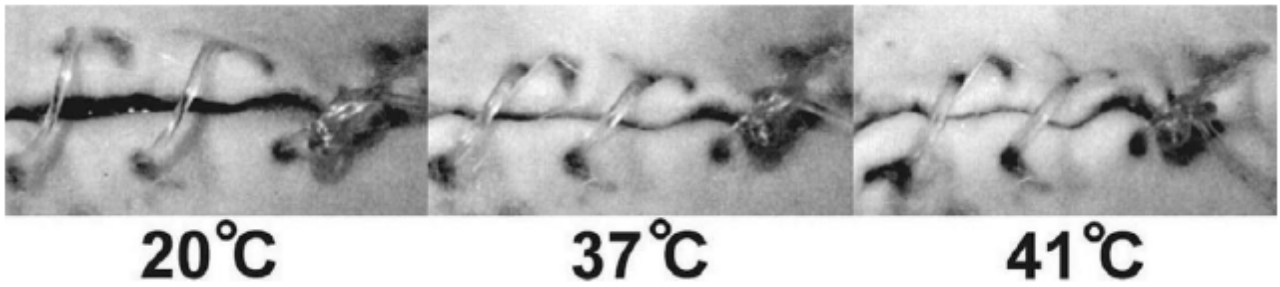

Figure 2.6-3 SMP Sutures [17]

2.7 THESIS OVERVIEW

This thesis will explore the fundamental mechanical properties of Veriflex® for application as a morphing aircraft skin. This novel styrene based SMP is intriguing because of its extraordinary stiffness range above and below T_g. However, it has yet to be fully characterized. The studies presented here are appropriate to the SLV expression (Equation 2.5-1). In addition, the understudied power consumption will be explored. From this basis preliminary studies of the suitability of this material in morphing aircraft will be presented.

3.0 EXPERIMENTAL SET UP AND PROCEDURES

This chapter details the experimental set ups and procedures followed during testing. Included in this section is the sample creation method as well as descriptions of various testing apparati. Table 3.1-1 summarizes all tests performed and the mechanical properties each test produces.

Table 2.7-1 Table of Experiments and Desired Properties

Experiment	Desired Mechanical Property
Tensile Test	Young's Modulus, Tensile Strength, Tensile Yield Strength
3-Point Bend Tests	Flexural Modulus, Flexural Strength, Flexural Yield Strength
Creep Tests	Creep Modulus
Analytical Heat Transfer*	Transition Time, Power Consumption
Heat Transfer Validation Experiment	Transition Time, Power Consumption

*Details in chapter 4

3.1 SAMPLE CREATION

The as-received Veriflex® SMP is in two separate parts that must be mixed together. The first part is a styrene based resin and the other is a hardener. A ratio of the two agents defined by the manufacturer is mixed together in a glass beaker by stirring. The stirring creates air bubbles that would have adverse effects during curing. To eliminate the bubbles, a medium vacuum of 27” of

mercury is pulled on the mixture for approximately 5 minutes. If large bubbles rise from the bottom of the mixture during this process, it is a sign that styrene is also being pulled from the sample. This is undesirable so the process is monitored and the vacuum is turned off if this begins to occur.

After the air bubbles have been removed from the sample, it is poured into a low carbon steel mold. For the tensile tests, a dog bone mold is used. The mold is 25mm deep and has a cross section width of 5 mm per ASTM D638. The inside surface of the dog bone mold has a surface finish of 32 micro inch roughness to ease the sample removal process. The mold employed for the creation of three point bend test specimens has inner dimensions of 80 mm x 10 mm wide x 31 mm and the inside walls of the mold have a 16 micro inch roughness rating. Before pouring, the walls of each mold are coated in a manufacturer supplied mold release agent to further ease sample removal after curing.

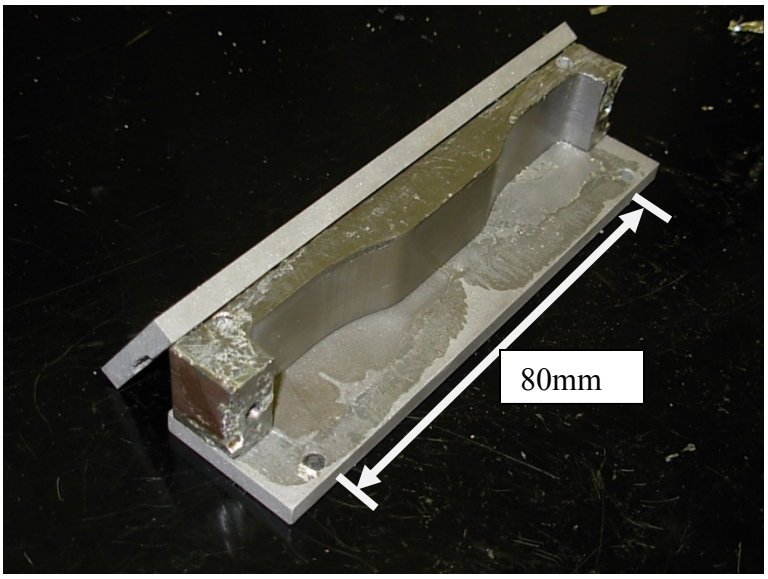

Figure 3.1-1. Dogbone Mold

The sample is cured in the mold for 37 hours and 15 minutes at 75ºC .This is 15 minutes longer than the manufacturer suggests. The added time is to allow the mold itself to heat up to the proper temperature, thus the sample will have a full 37 hours at the correct temperature.

When the curing process ends, the sample is removed from the mold by prying apart the steel pieces. Samples from the dog bone mold are cut into slices that are 3mm thick. This gives samples that have approximately a 3mm x 5 mm test section per ASTM D638.

Three point bend test samples are cut into 2mm thick by 80 mm long by 10 mm wide strips using a band saw. These dimensions follow ISO 178 standards that call for a length to thickness ratio of 20 for three point bend test specimens. In both sample cases, rough edges on the cut samples are sanded down using 200 grit sandpaper and then the sample is smoothed out using 60 grit sandpaper.

After cutting, the samples can be aged to steady state by 1 of 3 methods:

(1) Put the sample in a vacuum oven at 50ºC overnight.

(2) Subject the samples to 90ºC ambient conditions without a vacuum for 1 hour.

(3) Leave samples out in room temperature ambient surroundings for at least 1 week.

Of the three methods, the third is used to age each of the test samples prior to testing. The need for this aging step, previously unknown, has been established as part of this thesis research and will be described further in the results section.

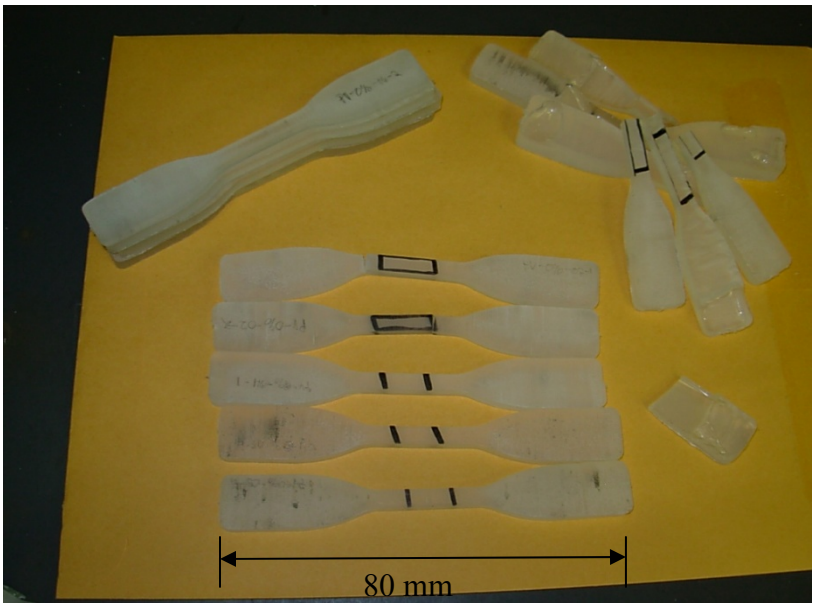

Figure 3.1-2. Dogbone Samples Marked for Extensometer

3.2 TENSILE TESTS

Tensile tests are conducted on a 5000 pound capacity screw driven load frame (MTI-5K) from Measurement Technology, Inc. The load frame in conjunction with a Messaphysik ME46-450 video extensometer yield load, stress, and strain data. It should be noted that displacement readings can be recorded directly from the load frame but this measurement is based solely on the screw position. The video extensometer is used to measure the strain of only the test section. This eliminates grip effects, thus providing more accurate results. This data is processed in a spreadsheet program in order to find the Young's modulus of the material above and below the glass transition temperature. A plot of stress versus strain is created for all tests above and below T_g and the Young's modulus is found by calculating the slope of the linear portion of the graph between 0.1% and 1.0% strains.

3.2.1 Cold SMP Tensile Tests

The "cold tests" are performed at room temperature. This is well below the 62ºC T_g, corresponding with the solid state illustrated by Figure 2.5-2. Tests employ the aforementioned load frame and a 250 pound capacity load cell. The load frame is programmed to tension the sample by stretching it at a rate of 4 mm/min. The tests are carried out until the sample yields.

3.2.2 Hot SMP Tensile Tests

The "hot tests" in tension are performed at 80ºC, corresponding with the rubbery state of Figure 2.5-2. These tests are conducted using the same load frame and load cell as the cold tests. A Bemco FTU3.0-100x600 UTM temperature and humidity control chamber is used with the load frame and load cell to control the ambient temperature. To insure that the samples are fully transitioned at the time of testing, every sample is put into the chamber for at least 10 minutes before it is subjected to testing.

3.3 THREE POINT BEND TESTS

The bend tests are performed using three point bend fixtures from Instron that are run by two different load frames. Cold tests are performed on the same load frame as the tensile tests but hot tests require more precision due to low deflection forces. The hot tests are performed on a smaller MTI 1000 pound capacity screw driven load frame. Temperature control for the hot tests is provided via the same chamber as the hot tensile tests. However, this chamber does not fit the

smaller load frame. As part of this research, an insert has been created to fit inside the chamber and around the load frame. The insert will be detailed in a later section.

The hot and cold bend tests require the use of two different load cells. When doing tests below the T_g of Veriflex®, a 250 pound load cell is used. However, when doing experiments above T_g, a 75 pound load cell is used to achieve the resolution appropriate to the lower forces required to displace the sample.

To measure the deflection of the samples during the testing, the Messaphysik ME46-450 video extensometer is used in conjunction with the load frame and chamber. A line is drawn lengthwise onto each cut sample with a black permanent marker so that the extensometer can track the movement of the bottom edge. As a stationary reference target, a piece of masking tape with a horizontal line drawn onto it is stretched between the lower anvils. The entire experimental set up can be seen in Figure 3.3-1 (a).

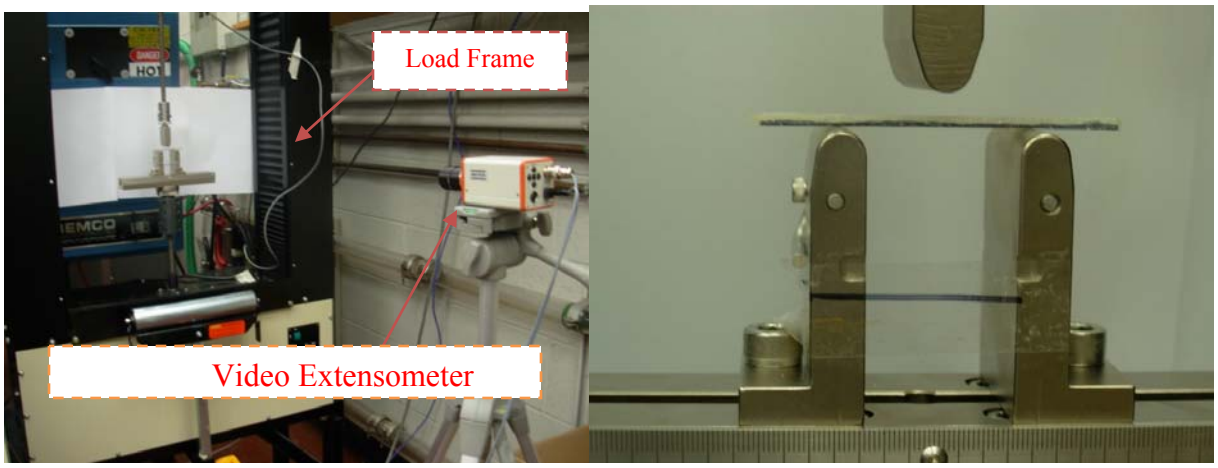

(a) (b)

Figure 3.3-1 Three Point Bend Test Set Up

The load and deflection data is then used to calculate the fiber stress and fiber strain in the material using Equation 3.3-1 and Equation 3.3-2 respectively. A plot of fiber stress versus

fiber strain is then created from the calculations. The flexural modulus is determined to be the slope of the linear region of this plot between 0.1 % and 1.0 % strains.

$$\sigma_f = \frac{3PL}{2bd^2} \qquad \textbf{(3.3-1)}$$

$$\varepsilon_f = \frac{6Dd}{L^2} \qquad \textbf{(3.3-2)}$$

Where P is the applied load, L is the distance between the lower anvils, D is the displacement, b is the width of the sample, and d is the thickness of the sample. As noted in Section 3.1, the sample has dimensions of 2 mm x 80 mm x 10 mm so b= 10 mm and d= 2 mm. The anvils are separated by L= 40 mm. This creates a length to thickness ratio of 20 which adheres to the ISO 178 three point bend test standard.

3.3.1 Cold SMP 3 Point Tests

As in the tensile test case (below T_g) "cold tests" are conducted in room temperature conditions at about 23º C. The load frame is programmed to move downward at a speed of 3.0 mm/min.

3.3.2 Hot SMP 3 Point Tests

Again mimicking tensile test procedures for "hot tests" (above T_g) in bending employ the temperature chamber, the chamber is used to create an ambient temperature of 80º C around the samples. To insure that the sample has completely reached 80º C, it is left in the hot chamber for at least 10 minutes before testing commences. The load frame is programmed to deflect the center of each specimen at a rate of 3.0 mm/min.

3.4 CREEP MODULUS TESTS

Cold State creep modulus tests are conducted using the same cold set up as the three point bend tests. Cold tests are run on the larger 5000 pound capacity load frame with the 250 pound capacity load cell. Each trial is run for 120 minutes with a constant force applied to the specimen mid span. The load frame is programmed to hold a 5 N force for the cold tests. Data from the tests are used to calculate fiber stress and fiber strain using Equation 3.3-1 and Equation 3.3-2. Subsequently, the creep modulus is calculated over the course of the test by taking the ratio of fiber stress to fiber strain as seen in Equation 3.5-1. In Equation 3.5-1, P is the applied load at the center of the sample, b is the width of the sample, d is the thickness of the sample and L is distance between the lower anvils. D is the deflection caused by load P. The creep modulus E_c is then plotted versus a logarithmic time scale.

$$E_c = \frac{PL^3}{4bDd^3} \qquad \textbf{(3.4-1)}$$

Due to resolution issues, neither load frame is used to conduct the hot state creep modulus tests. Instead, 0.1 grams of mass is hung from each sample for 2 hours. The mass is hung using a wire across the center of the sample and displacement is tracked using the video extensometer. This weight translates to a constant stress of about 60 Pa on the sample. From the displacement data and known constant force, the constant fiber stress and fiber strain are calculated via Equation 3.3-1 and Equation 3.3-2. The creep modulus is then found using Equation 3.4-1.

3.5 POWER CONSUMPTION AND TRANSITION TIME CALCULATION

3.5.1 Transition Time Baseline Test

In order to justify transition time calculations presented later in this thesis, a baseline test was conducted for comparison reasons. All calculations are conducted assuming a 2mm thick piece of Veriflex that is subjected to 80ºC ambient conditions. The baseline test is performed using a sample created with the bend test mold to best match this dimension. The sample is placed in the temperature chamber at 80ºC for three minutes and then subjected to a tensile test. Young's modulus is calculated from this test using the same techniques in the other tensile tests. This value will then be compared to the results from the hot tensile tests in order to determine if the material has indeed fully transitioned to its soft state in the allotted three minutes.

3.6 SET UP SUMMARY

Table 3.6-1 Equipment Used in Experiments

Equipment	Output Type	Resolution
MTI-5K Load Frame	Displacement	0.000127mm (0.000005 inches)
MTI-1K Load Frame	Displacement	0.000127mm (0.000005 inches)
Video Extensometer	Displacement	At 50 mm Axial Field of View < 0.3µm
Bemco FTU3.0-100x600 UTM	Temperature	± 0.5°C

4.0 EXPERIMENTAL RESULTS AND DISCUSSION

Early in testing, it was discovered that there is a period directly after curing where the SMP would slowly harden as time passed. As illustrated in Figure 4.0-1, this variation can be substantial with early samples, displaying a modulus as low as 200 MPa versus aged samples which display a modulus as high as 700 MPa. This is attributed to the presence of a residual monomer remaining after the curing process that acts as a plasticizer and impedes cross link development. Over time, this monomer evaporates out of the SMP until a steady state is reached and the stiffness becomes constant. Of the three methods of monomer removal stated in Section 3.1, leaving the samples in room temperature ambient conditions is chosen because the elevated temperature methods have a risk of causing oxidation in the sample.

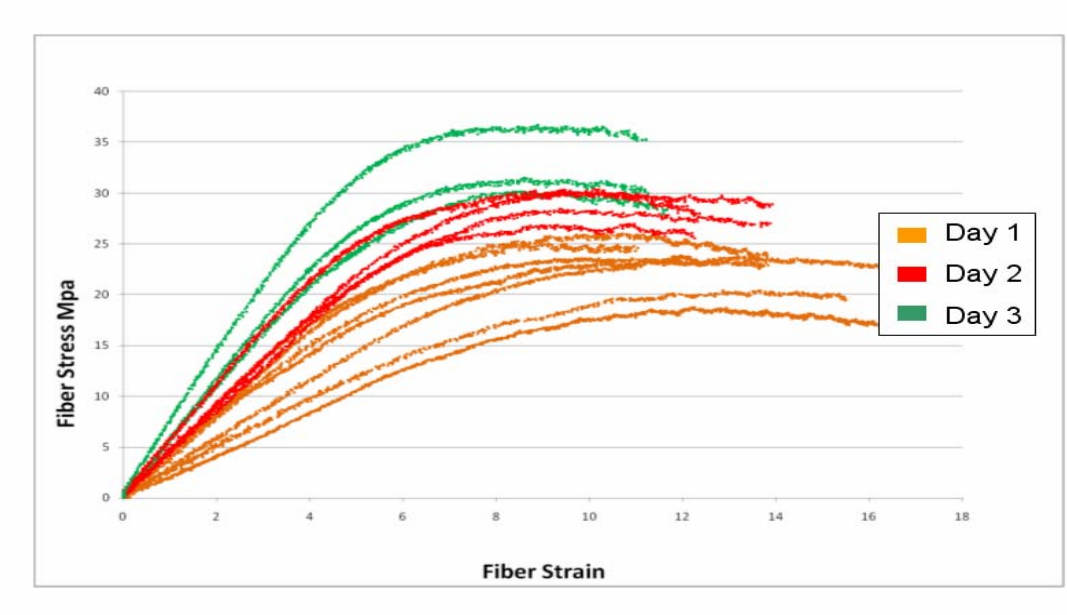

Figure 4.0-1 Variation of Early Results of Cold Three Point Bend Tests

This experimental observation is a significant finding. All tests reported in the following sections are appropriately aged. At the conclusion of this chapter, summary tables of experimental results that include 95% confidence intervals are presented.

4.1 TENSILE TEST RESULTS

A typical result of the cold state tensile test can be seen in Figure 4.1-1. Results of every test can be seen in Appendix A. The stress versus strain curves of four tensile tests conducted at 23ºC yield an average Young's modulus of nearly 1010 MPa with a 95% confidence interval of +/- 58 MPa. The tensile yield strength is calculated to be about 19.5 MPa and the tensile ultimate strength is approximately 19.1 MPa.

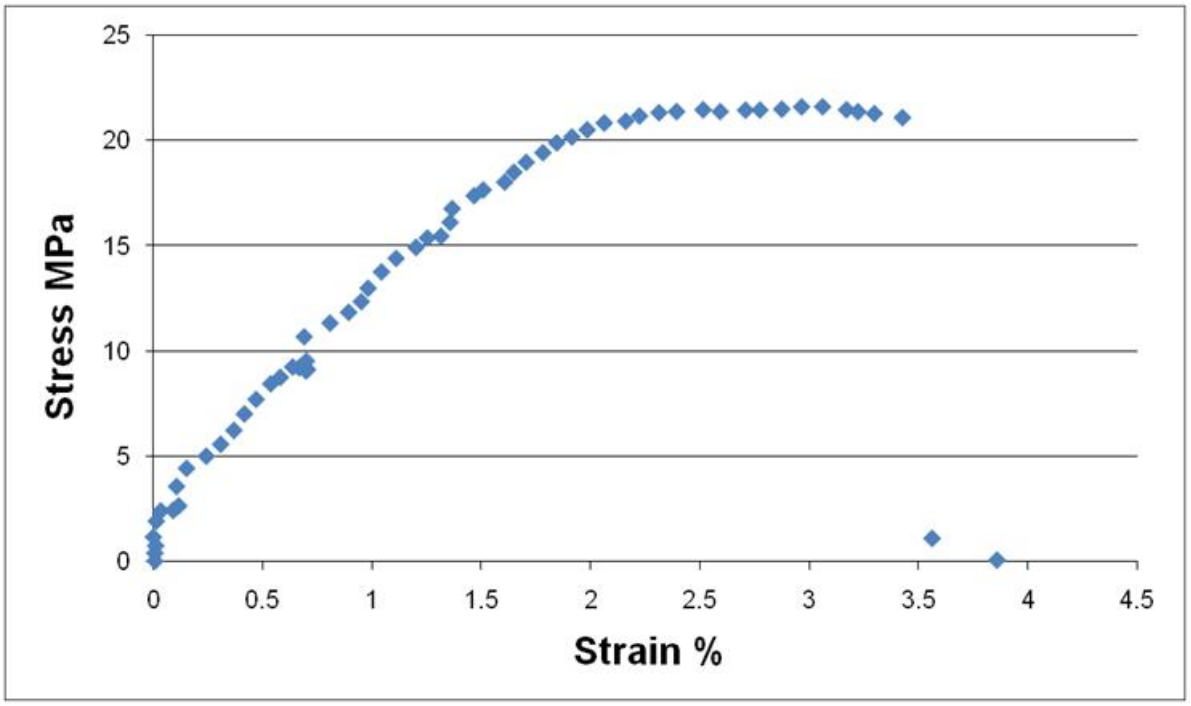

Figure 4.1-1 Typical Stress vs. Strain Result of Cold Tensile Test With Data Smoothing

A typical plot of the hot state tests can be seen in Figure 4.1-2. The stress versus strain plots of six hot tests give a mean Young's modulus of about 2.6 MPa and a tensile strength of 0.6 MPa. There is no yield stress above T_g. A comparison of the hot and cold tensile tests will be made in the discussion section of this thesis.

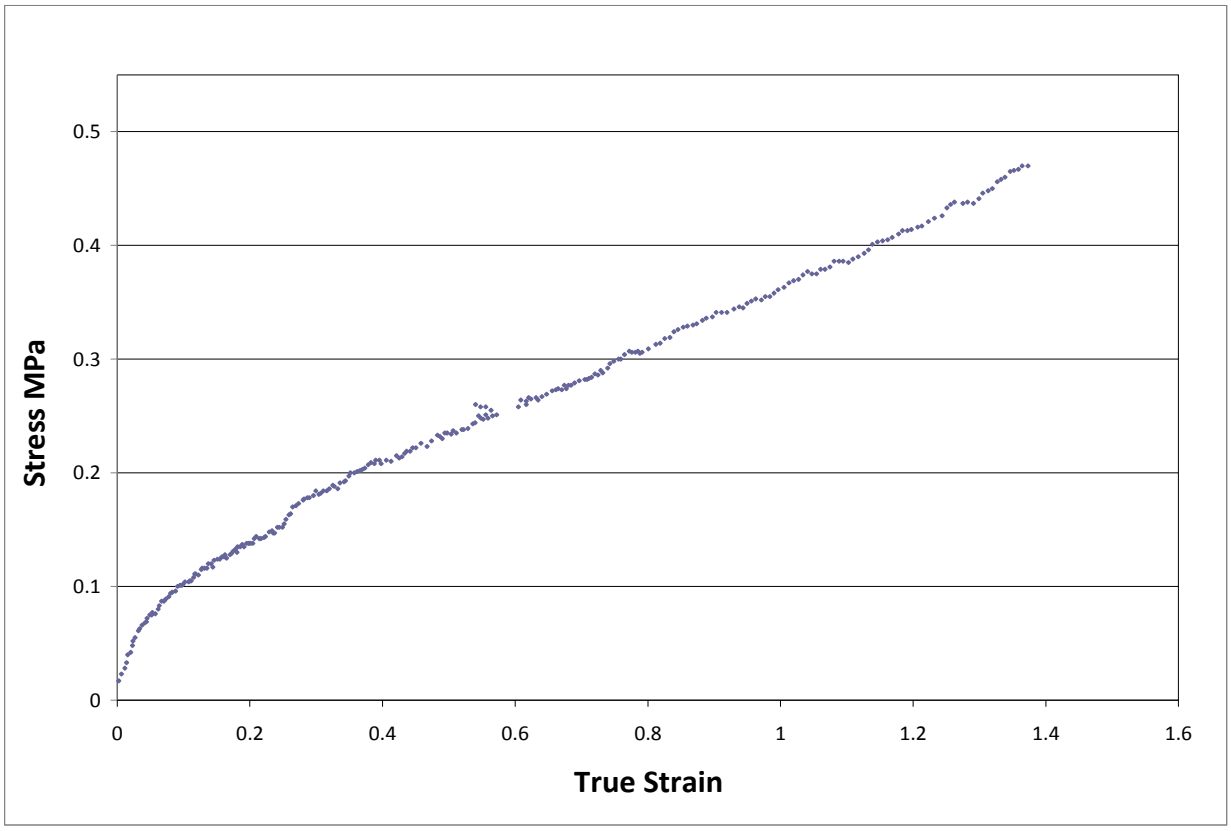

Figure 4.1-2 Typical Stress vs. Strain Plot of Hot Tensile Tests

4.2 THREE POINT BEND TEST RESULTS

Figure 4.2-1 shows a typical result of the three point bend tests of the SMP while in its cold state at 23ºC. The resulting flexural modulus from five samples is about 700 MPa and the flexural strength is approximately 37 MPa. The flexural ultimate strength could not be calculated because the samples slipped between the anvils before breaking.

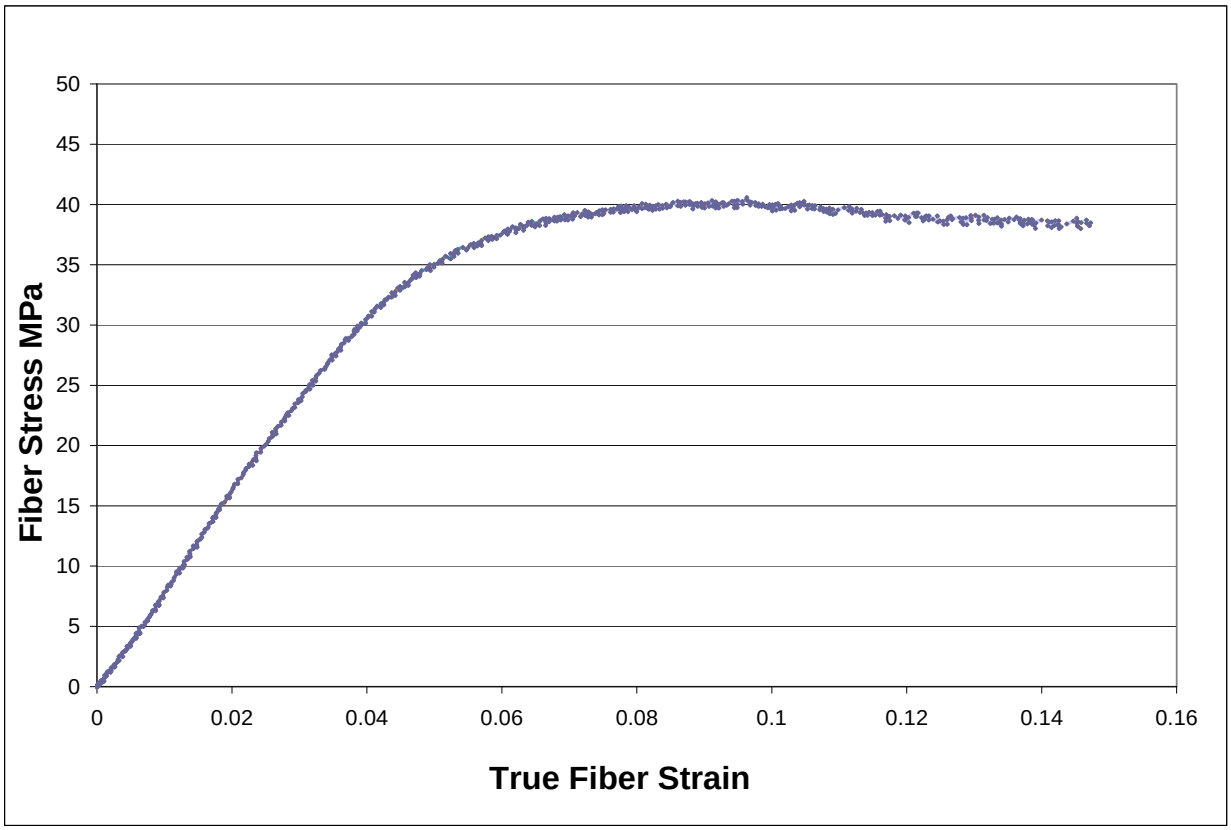

Figure 4.2-1 Typical Result of Fiber Stress vs. Fiber Strain for Cold Bend Tests

The results of the hot state testing can be seen in Figure 4.2-2. At 80ºC, the material exhibits a flexural modulus of approximately 7 MPa and a flexural strength of 0.2 MPa. Once again, the flexural ultimate strength could not be found because the samples slip between the lower anvils before failure.

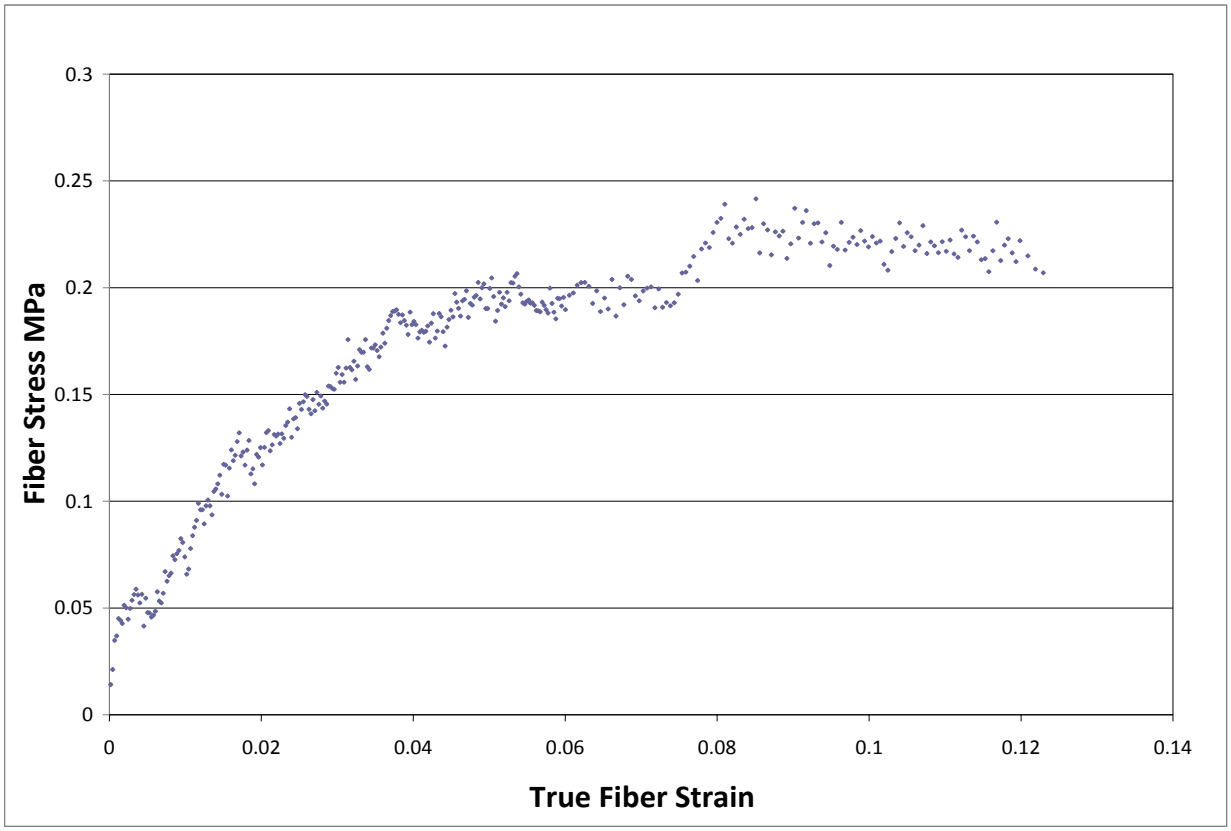

Figure 4.2-2 Typical Result of Fiber Stress vs. Fiber Strain for Hot Bend Tests

4.3 TENSILE AND THREE POINT BEND TEST RESULT DISCUSSION

The contrast in modulus values between hot and cold state tests is expected. The tensile tests show the Young's modulus decreases 99.7% after the SMP is heated above its glass transition temperature. A similar decrease is seen in the three point bend tests. The SMP's flexural modulus decreases 99.0 % when it is heated above the glass transition temperature. The change in tensile modulus is similar to the transitions exhibited by the two polyurethane SMPs mentioned in the literature review section of this thesis. Those SMPs saw modulus decreases of 98.8% (from 750 MPa to 8.8 MPa) and 99.8% (from 620 MPa to 1 MPa). These large scale

decreases in modulii show that the material does indeed function as expected. Heating Veriflex® above its glass transition temperature allows the material to withstand much larger strains because of a reduction in both tensile and bending stiffness.

Tensile and flexural strength values also see a similar decrease in value after transitioning between hot and cold tests. Tensile tests show that the SMP exhibits a 98.3% decrease in tensile strength when transitioned from the cold to hot states. Three point bend test yield the same type of decrease with a 99.4% decrease in flexural strength.

The discrepancy between the results for the SMP's cold state Young's modulus and flexural modulus is most likely created because of the physical properties of the SMP. Under tension, polymer chains will become aligned and make the material stiffer. However, under out-of-plane bend loading, the polymer chains will not align and stiffen the SMP. This tension-induced polymer chain alignment is likely the reason that the tensile modulus is found to be greater than the flexural modulus. The alignment will enhance the tensile modulus but does not affect the flexural modulus.

4.4 CREEP MODULUS TEST RESULTS

An average result from the cold state creep testing can be seen in Figure 4.4-1 and Figure 4.4-2. In each test, the creep modulus decreases over time at a relatively constant rate. The tests have creep modulii that fall in a range of about 200 MPa throughout testing. The spikes and gaps in both figures are caused by the load frame pausing its motion when it hits the specified load, and then restarting once the material creeps and the load decreases. Upon restarting, the load frame

must overcome its own internal friction in its ball screws and lurches forward slightly causing the load to jump briefly.

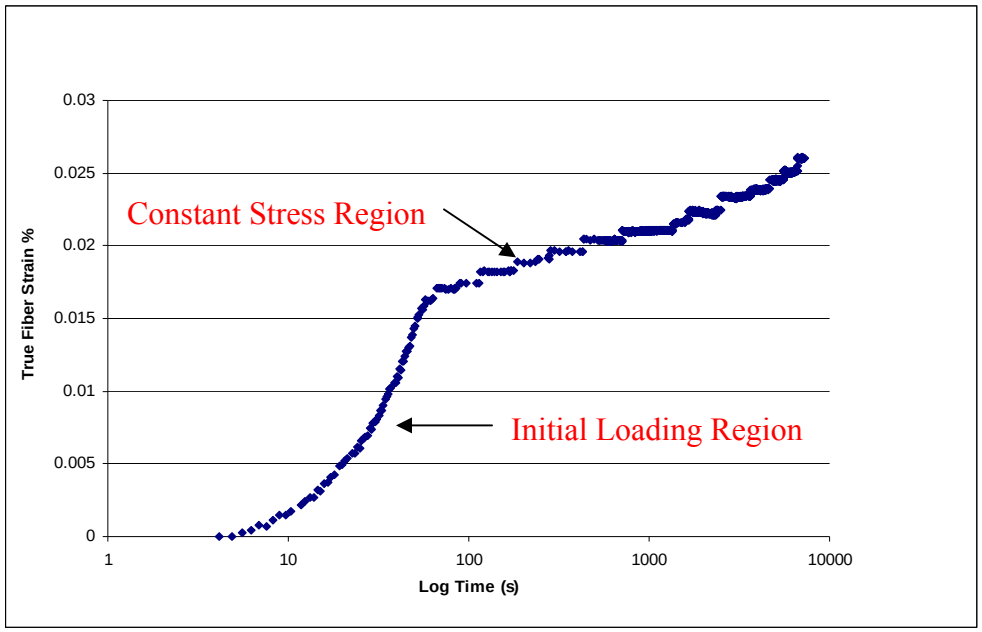

Figure 4.4-1 Typical Result of True Fiber Strain vs. Log Time for Cold State Creep Test

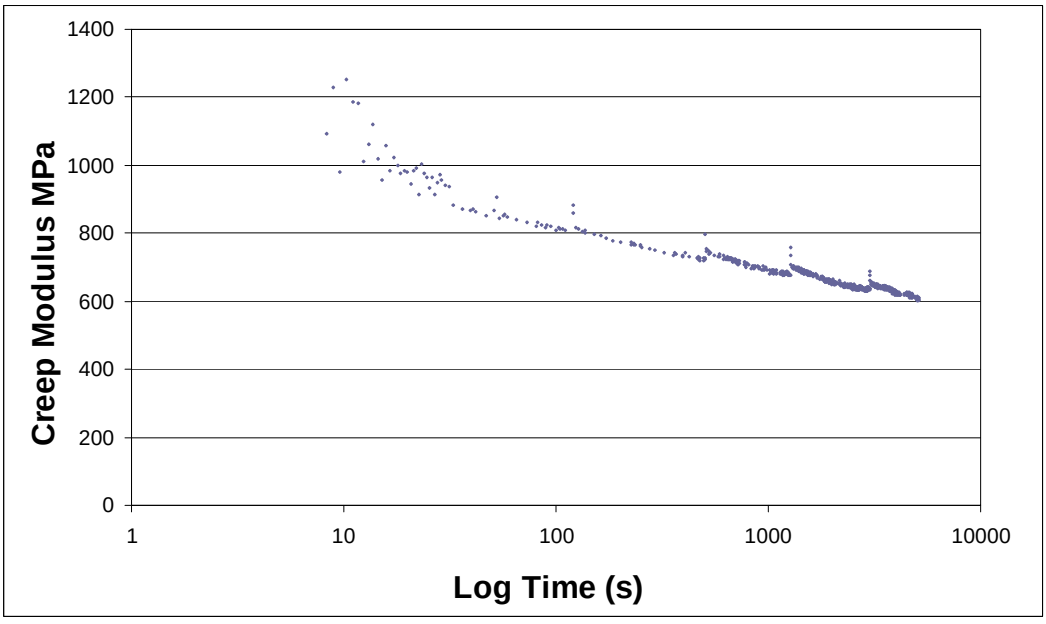

Figure 4.4-2 Typical Result of Creep Modulus vs. Log Time Scale for Cold Creep Tests

Typical results of hot state creep testing can be seen in Figure 4.4-3 and Figure 4.4-4. The four hot state creep tests conducted all fall within a reasonable range. After about 200 seconds, all creep modulus values fell within the small range of 1 Pa of one another.

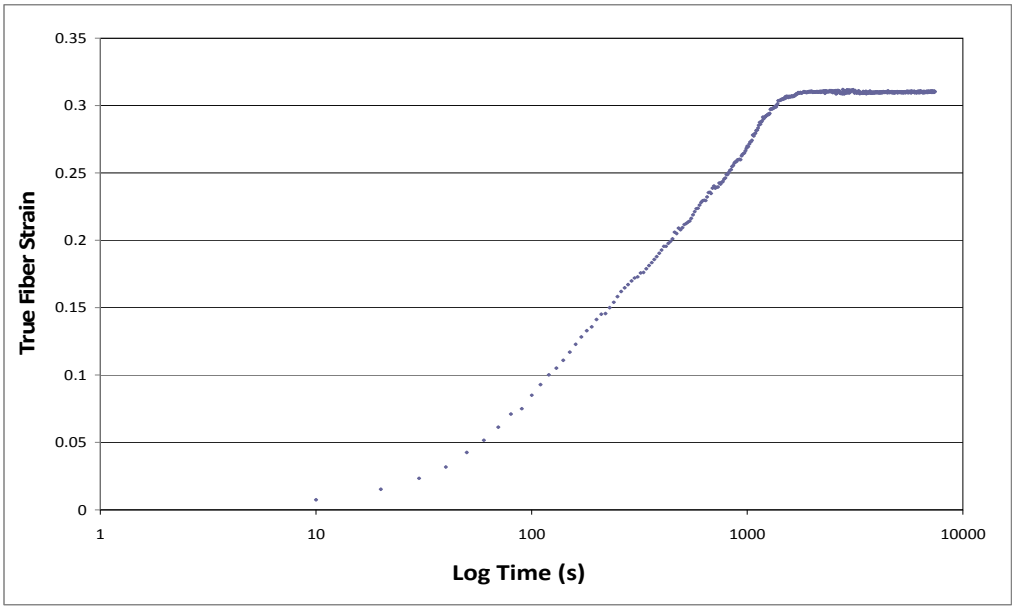

Figure 4.4-3 Typical Result of True Fiber Strain vs. Log Time for Hot State Creep Tests

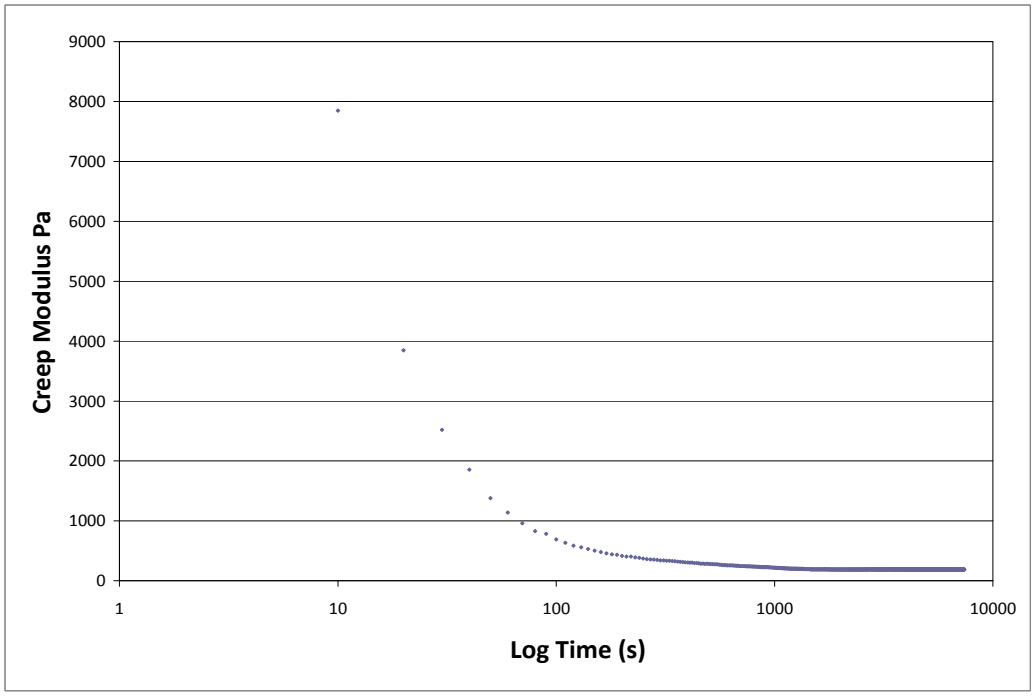

Figure 4.4-4 Typical Result of Creep Modulus vs. Log Time Scale for Hot Creep Tests

The most important thing to notice from creep testing is that the material does indeed creep while in its cold state. The increase in fiber strain over time signifies an increase in deflection while under the constant stress. In terms of the material's potential use as a morphing aircraft skin, this is undesirable. During flight, the skin will be subject to a constant out of plane aerodynamic stresses. If the material creeps during a sustained flight, it will have a significant effect on a plane's performance. Therefore, a strategy may need to be developed to mitigate this particular material property during the morphing aircraft design process.

Not surprisingly, Veriflex® creeps more in its hot state than it cold state. The cold state creep tests show a typical decrease of about 33% in creep modulus over the 2 hour duration of the tests while the hot state tests show a typical decrease of over 50%. The lower hot state Young's Modulus allows for greater strains over time which creates larger decreases in the creep modulus over time than in cold state tests. While excessive creep may become problematic, the hot state will only be exposed to aerodynamic loads over short increments of flight. The material will only be in its hot state while it is actively morphing. After morphing is completed, the material will immediately be transitioned back to its cold state. Hot state creep characteristics are therefore less problematic in application than the cold state creep performance.

4.5 APPLICATION OF RESULTS TO SLV MODEL

Using the experimental results, it is possible to determine every coefficient in the SLV model presented earlier in Equation 2.5-1. The model can be used to predict the stress-strain of the SMP by plugging in the appropriate coefficients and solving the differential equation. Values for

Young's modulus, E, were determined from tensile test results. The viscosity and retardation time parameters, λ and μ, can be found using creep test data.

The Young's modulus parameter definition is very straight forward. If the SLV model is to be used for cold tests, the modulus calculated from cold tensile tests (1010 MPa) is to be inserted into the equation. Similarly, the hot tensile test's calculated modulus (2.6 MPa) would be inserted into Equation 2.5-1.

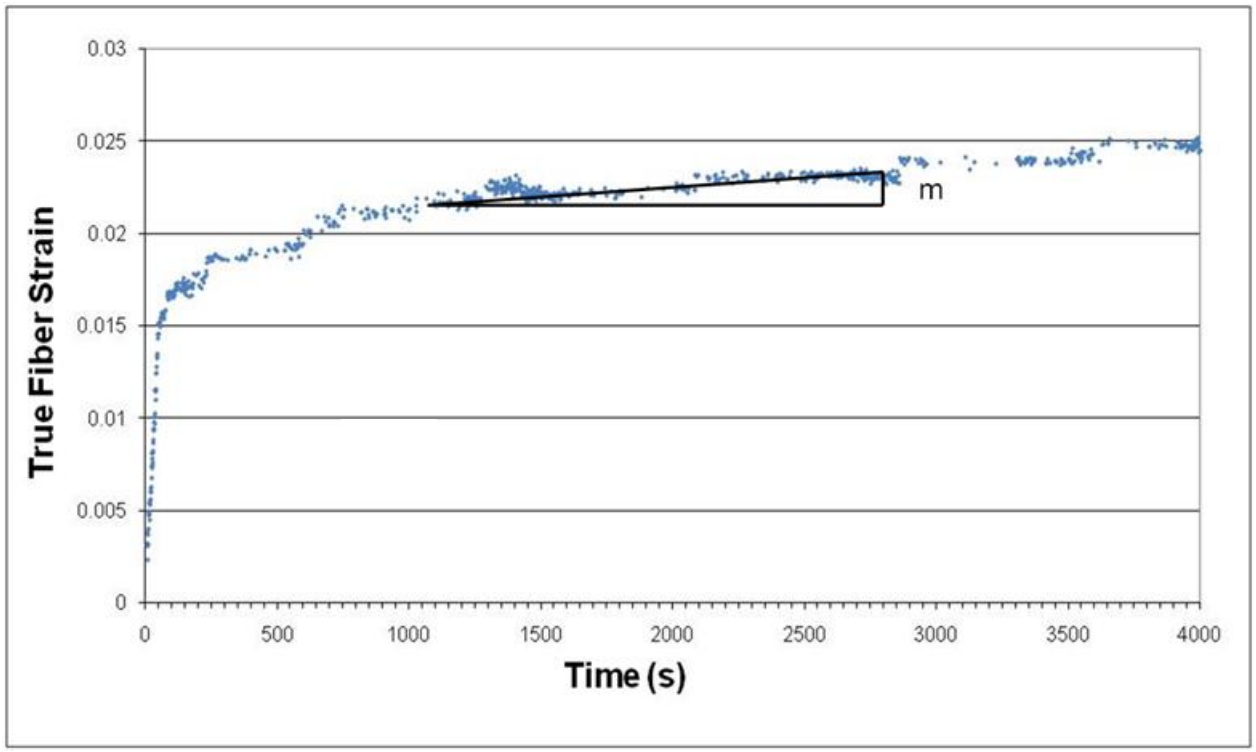

4.5-1 Determining Viscosity Time From Experimental Results

The viscosity parameter can be found from the strain versus time plot from creep tests. The zero shear viscosity is found by multiplying reciprocal of the slope of the steady state linear region of the strain versus time curve by the constant stress applied during the creep test. This is illustrated in Figure 4.5-1 and Equation 4.5-1. The cold state creep tests yield a mean viscosity

of about 170 GPa·s while the hot state creep tests yield a mean viscosity of approximately 6.6 MPa·s. These values would be substituted into Equation 2.5-1 as the μ parameter.

$$\mu = \frac{1}{m}\sigma \tag{4.5-1}$$

Retardation time is estimated via Equation 4.5-2. Where E is the experimentally determined Young's modulus for the SMP and μ is the viscosity calculated from the strain versus time plot. So, for the cold state, values of 1010 MPa and 170 GPa·s would be substituted into Equation 4.5-1 for E and μ respectively. This leads to a calculated retardation time of approximately 1650 s for the cold state. Similarly, for the hot state, values of 2.6 MPa and 6.6 MPa·s are used in Equation 4.5-1 for E and μ respectively. Subsequently, the hot state retardation time is calculated to be about 2.5 s.

$$\lambda = \frac{\mu}{E} \tag{4.5-2}$$

For the most part, the calculated values for viscosity and retardation time seem to be reasonable. The hot state retardation time seems fairly low at first glance but the cold state calculations fall very close to values found in a previous study of a different SMP [30]. The study reported values of 200 GPa·s and 2000 s for the viscosity and retardation time of a polyurethane SMP in its cold state. However, the same study yielded hot state values of 0.7 GPa·s and 77 s for viscosity and retardation time.

The difference in the hot state viscosity and retardation time values calculated in this study and the aforementioned study [30] could result from several factors. The most fundamental of these is that the studies were done on different SMPs. This thesis focuses on a polystyrene SMP while the previous study used a polyurethane SMP. The polystyrene SMP is a relatively new material with a much wider performance gradient than the older polyurethane

SMPs. So, it is very possible it simply is less viscous in its hot state thus resulting in a higher ductility and a much lower retardation time. Veriflex®'s manufacturer does not report any viscosity numbers so it cannot be said for sure that this is the case.

A second possible reason for the low retardation time stems from experimental factors. A previous study of Veriflex® has reported a Young's modulus as low as 0.2 MPa in the hot state [6]. This is a bit lower than the 2.6 MPa hot state modulus found in this thesis. A lower stiffness would result in a higher retardation time if it were used in Equation 4.5-2.

The values found for Young's modulus, viscosity, and retardation time can be plugged into the SLV model (Equation 2.5-1) to predict how the SMP would perform under various loading, strain, and temperature conditions. The model would have to be solved analytically or numerically in order to produce sought after results. This thesis will not pursue the solution any further as it is beyond the mission of this work.

4.6 POWER CONSUMPTION AND TRANSITION TIME CALCULATION RESULTS

4.6.1 Analytical Result

In order to evaluate the transition time, the SMP is considered to be an infinite slab of 2mm thickness. Since most of the experiments are done with ambient heating, calculations are made by setting the outside surfaces of the slab at 80ºC. It is then calculated how long it will take for the center of the slab to reach 75ºC. 75ºC is chosen because it is not necessary for the material to be heated all the way to 80ºC for it to transition into its soft rubbery state. The center of the SMP

just needs to be comfortably above the glass transition temperature of 62ºC. It is also assumed that the material starts out at room temperature, so the center starts at 23ºC.

Several material properties are required to perform the transient heat conduction calculation. Based on Cornerstone Research Group's published material properties and values typically used for the heat transfer coefficient of air, the following values are used as constants:

Table 4.6-1 Constants Used in Heat Transfer Calculations

Constant	Description	Value
K	Conductivity	$0.17\,W/m°K$
ρ	Density	$920\,kg/m^3$
C_p	Specific Heat	$1800\,J/kg°K$
h_{air}	Convection Heat Transfer Coefficient	$25\,W/m^2°K$

From these parameters, the Biot number and coefficient of thermal expansion are calculated per Equations 4.5-1 and 4.5-2.

$$B_i = \frac{hL}{K} = 0.15 \qquad \textbf{(4.6-1)}$$

$$\alpha = \frac{K}{\rho C_p} = 102.7 \bullet 10^{-9}\ m^2/s \qquad \textbf{(4.6-2)}$$

where L is the distance to the point of interest. In this case L=1mm because we are assessing the center of the beam. Also because we are calculating at the center of the beam, the dimensionless parameter ζ=0. Next the relative heat flow out of the slab is calculated using Equation 4.5-3.

$$\frac{Q}{Q_i} = 1 - \left(\frac{t_{ave} - t_f}{t_i - t_f} \right) \qquad \textbf{(4.6-3)}$$

Substituting in the values t_{ave}=75C, t_i=23C, and t_f=80C results in $\frac{Q}{Q_i}$=0.912. The actual heat flow into the slab can then be calculated with Equation 4.5-4.

$$\frac{Q}{A} = L\rho C_p \left(t_i - t_f \right) \frac{Q}{Q_i} \qquad \textbf{(4.6-4)}$$

This results in $\frac{Q}{A}$ = -86 kJ/m^2 for one side of the slab; for both sides, $\frac{Q}{A}$ = -172 kJ/m^2. The negative value means that this amount of heat is flowing *into* the slab.

To calculate the time it takes for the center of the slab to reach 75ºC, the Fourier number must be found using a chart of heat flow in an infinite slab as a function of time and thermal resistance. This chart can be seen in Figure 4.4-1.

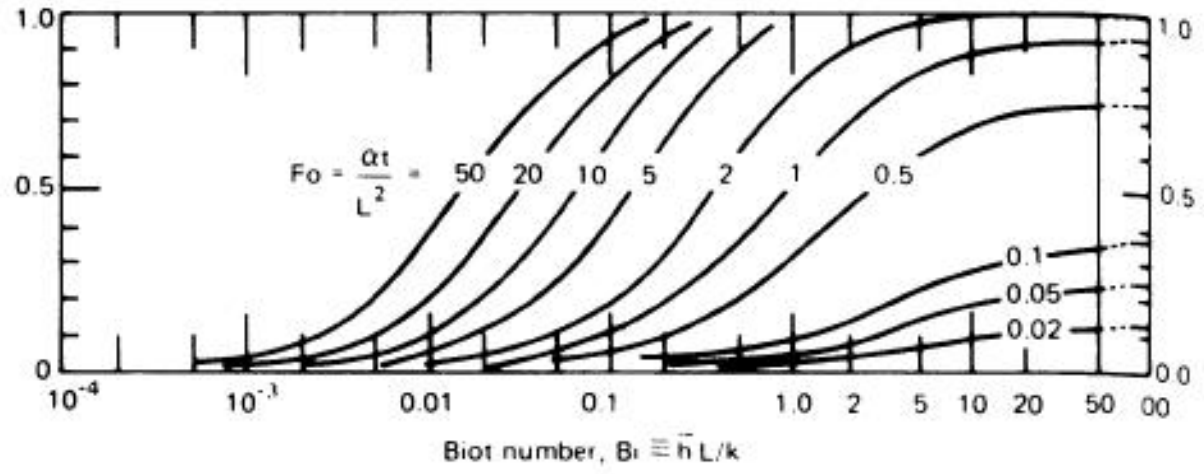

Figure 4.6-1 Heat Flow of an Infinite Slab as a Function of Time and Thermal Resistance [31]

Using the predetermined values of the Biot number, Bi, and relative heat flow, it is found that the Fourier number is about 18. Subsequently, by using the definition of the Fourier number in Equation 4.5-5, we can find the time the transition takes.

$$Fo = \frac{\alpha \tau}{L^2} \qquad \textbf{(4.6-5)}$$

or

$$\tau = \frac{FoL^2}{\alpha} = 175s$$

So it will take almost three minutes for the center of the slab to reach 75ºC if both the top and the bottom are exposed to 80ºC ambient conditions.

4.6.2 ANSYS Result

A thermal analysis is also conducted in the ANSYS finite element analysis program. This analysis is conducted by creating a two dimensional area with the dimensions of 40mm long by 2 mm thick. The meshed area can be seen in Figure 4.4-2. These dimensions are chosen because they match the cross section of the samples used in three point testing. The proper material properties are inputted into the program and the program is set up to subject the area to an ambient temperature load of 80°C. The program is then run until the sample reaches steady state. In post processing, the centerline temperature of the area is plotted against time to determine how long it takes the center of the area to reach 75°C.

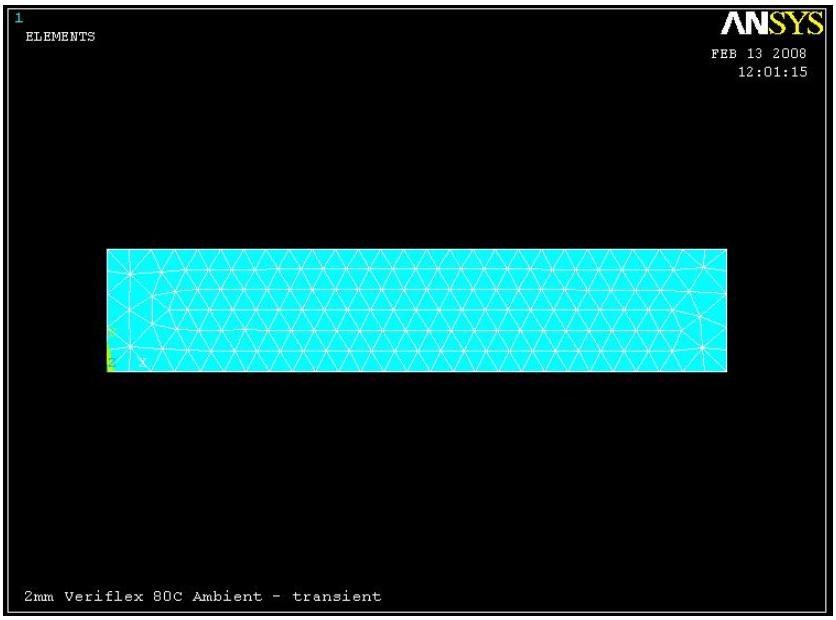

Figure 4.6-2 Meshed 2D Area for ANSYS Analysis

The results of the transition time analysis performed in ANSYS can be seen in Figure 4.4-3. The graph of centerline temperature versus time for a 2mm thick by 40mm long sample of Veriflex® shows that the material will take about 180 seconds to reach approximately 75ºC. This corresponds very closely to the analytical result of 175 seconds. The relationship between the analytical and ANSYS results will be further explored in the Comparison and Discussion section.

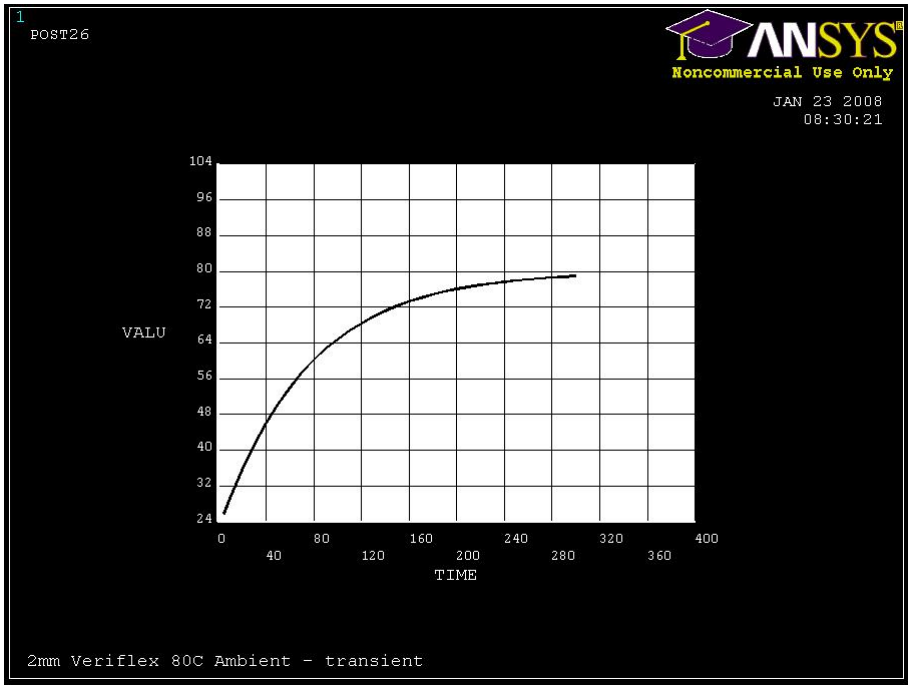

Figure 4.6-3 Centerline Temperature of 2 mm Thick SMP in ANSYS

4.6.3 Transition Time Calculation Validation Experiment

While the agreement between the analytical and numerical studies is promising, a simple experiment is also conducted as validation. After three minutes in the temperature chamber at 80ºC, the SMP exhibits a Young's modulus of 2.07 MPa. This corresponds closely with the hot tensile tests mean modulii which allow ten minutes to reach thermal equilibrium.

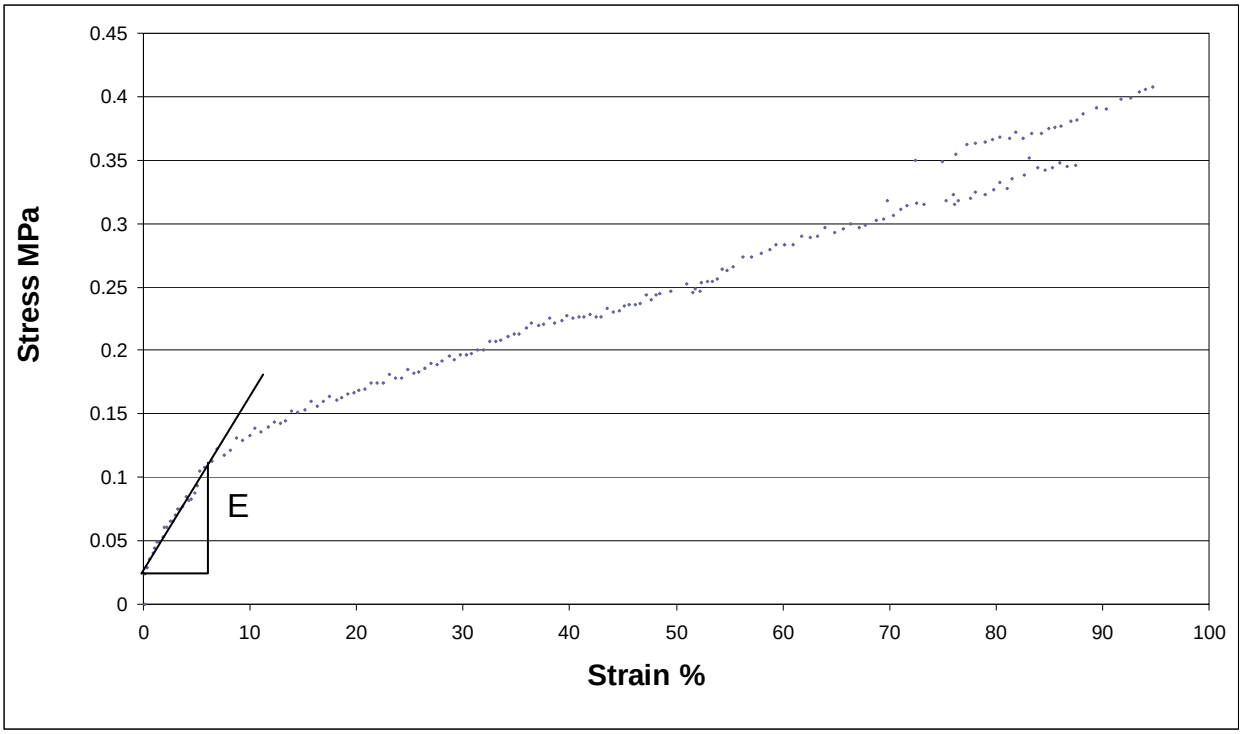

Figure 4.6-4 Result of 3 Minute Transition Time Baseline Test. Resulting Modulus Corresponds With Hot State Tensile Tests.

4.6.4 Power Consumption

The power requirement to transition a 2mm x 10 mm x 40 mm strip of Veriflex® can be calculated using results from the ANSYS transition time calculations. The centerline temperature versus time data is used to determine the heat transfer rate at each point in time using Equation 4.5-6.

$$Q = KA\frac{(T_1 - T_2)}{s} \qquad \textbf{(4.6-6)}$$

In the equation, Q is the heat transfer rate, K is the conductivity of Veriflex® ($0.17 {}^{W}\!/_{m°K}$), A is the surface area of the strip (400 mm^2), T_1 is the temperature at the outside surface, T_2 is the centerline temperature, and s is the distance to the centerline of the strip. The plotted results of heat transfer versus time can be seen in Figure 4.5-6. The plot shows that the heat transfer rate is about 3.5 Watts after 180 seconds. 180 seconds is the time it takes the center of the material to reach approximately 75ºC as calculated by the ANSY simulation in Section 4.5-2.

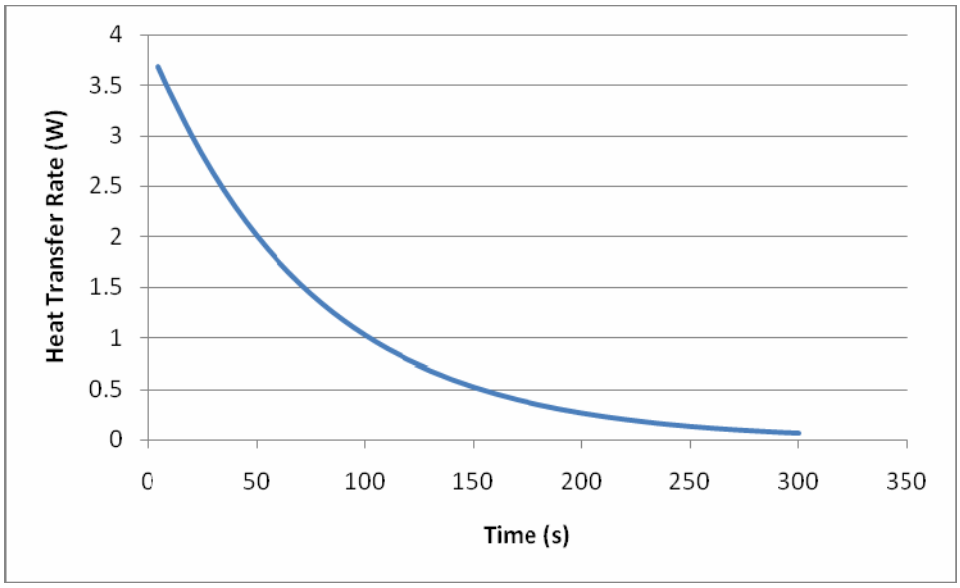

4.6-5 Heat Transfer Rate Versus Time From ANSYS Results

The amount of energy required to transition the SMP is calculated by finding the area under the heat transfer versus time curve. Since the curve is created with data points, the trapezoidal rule must be used to calculate this area. The trapezoidal rule can be seen in Equation 4.5-7

$$A = (t_2 - t_1)\left(\frac{f(t_2) + f(t_1)}{2}\right) \qquad \textbf{(4.6-7)}$$

Where A is the area of a particular trapezoid t_1 and t_2 are the times at the ends of the trapezoid and $f(t_1)$ and $f(t_2)$ are the values of the heat transfer at times t_1 and t_2. The energy required for transition is the sum of all the trapezoids that create the heat transfer versus time curve. This is calculated to be 252 J.

4.7 RESULTS SUMMARY

The results from all of the mechanical tests can be found in this section. For each value, the mean of the tests is given along with a 95% confidence interval. Tensile test results are presented in Table 4.6-1 and three point bend test results are presented in Table 4.6-2.

Table 4.7-1 Results and Confidence Intervals for Tensile Tests

	Cold State Tensile Test	Hot State Tensile Test
Young's Modulus MPa	1010 +/- 58	2.63 +/- 1.20
Tensile Strength MPa	20 +/- 2.69	0.61 +/- 0.08
Tensile Ultimate Strength MPa	19 +/- 2.46	N/A

Table 4.7-2 Results and Confidence Intervals for Three Point Bend Tests

	Cold State 3 Point Bend Test	Hot State 3 Point Bend Test
Flexural Modulus MPa	700 +/- 37	6.84 +/- 1.71
Flexural Strength MPa	37 +/- 2	0.23 +/- 0.03
Flexural Yield Strength MPa	N/A	N/A

5.0 CANDIDACY AS MORPHING AIRCRAFT SKIN

5.1 GENERAL THOUGHTS AND CONCERNS

The large scale changes in Young's and flexural modulii that Veriflex® shows when it is transitioned from its hard to soft state act as a double edged sword when it comes to the morphing aircraft application. While the material is in its hard state, it is likely that it is strong enough to support the out of plane loads that it will endure while in flight. Similarly, the material's soft state allows it to withstand the very large deformations required if it is to be used as a morphing aircraft skin. However, in reality, the wing will not instantly change from one configuration to the next. It will take time for the mechanical mechanisms to shift the wing from one shape to the next. During this time, the material's ductility in the soft rubbery state can certainly handle the in-plane morphing strains, but there may be a problem when it comes to supporting the out-of-plane aerodynamic loads. This chapter addresses this challenge via the creation of a 3D wing section model that uses Veriflex® as the skin. The model is then run through the finite element analysis program ANSYS Workbench with the SMP in different states.

Another concern regarding the morphing aircraft application is finding a suitable method to heat the SMP above its glass transition temperature while it is being used as a wing skin. While it is fairly simple to use ambient heat to induce a transition in the laboratory environment,

this method would be impractical to use on an entire aircraft wing. A UAV's wing will have a suface area on the scale of square meters as opposed to the square millimeter sections used in experiments. Also, only the inside of the skin could be heated using ambient temperatures because the outside surface will be exposed to open air flow during flight. These issues create challenging problems in the design of an actual morphing wing with an SMP skin.

5.2 ANSYS WING SECTION MODEL

The 3D wing section model is created using the Solidworks computer aided design program. The wing section utilizes a NACA 0110 airfoil because of its common use in general aviation designs. A 2mm thick SMP skin is wrapped around two supporting airfoils that are distanced 152 mm (6 in) apart. The design is intended to mimic a small section of a larger wing. In order to create an entire wing, several wing sections would be placed in succession and a wing spar would run through the sections as a support. The wing section can be seen in Figure 5.2-1.

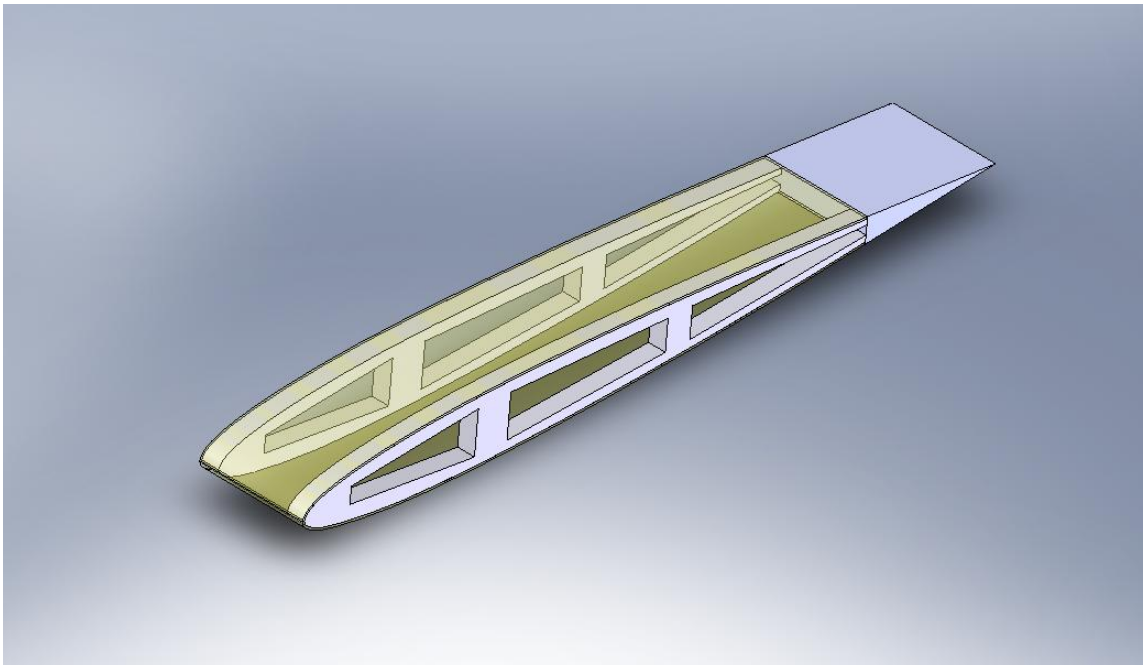

Figure 5.2-1 Solidworks Model of SMP Wing Section

Four different scenarios are considered. Each scenario uses the same wing section but adjustments are made to the mechanical properties of the wing skin to represent the SMP in two cold states and one hot state. Two cold states are chosen because of the discrepancy between the Young's modulus value found through experiments of 1010 MPa and the reported value of 1241 MPa. Both modulus values are set as parameters and simulated for comparison reasons. The third and fourth scenarios use two hot state Young's modulus values. The first modulus value is 2.6 MPa, which was found during experimentation. The second modulus value of 0.2 MPa was found in a previous study [6]. The SMP's manufacturer does not report a hot state modulus value.

During each simulation, a pressure of 400 pounds per square foot (0.0192 MPa) is applied to the upper surface of the wing section. This value is chosen because it is the maximum pressure sustained by NextGen Aeronautics' MFX-1 during its successful test flight [7]. Also, the two airfoils are assigned mechanical properties of 2024 aluminum because of its common use

in aircraft applications. The airfoils are then defined as fixed supports while the wing skin remains flexible.

The results for the vertical deflection caused by the pressure in the two cold states can be seen in Figure 5.2-2 and Figure 5.2-3. The 1240 MPa model shows a maximum downward deflection of 1.9 mm. The 1010 MPa deflects considerably more with a maximum displacement of 2.3 mm downward. This result shows that the Young's modulus of the material is a factor in deciding if this material can be used in morphing aircraft applications. As expected, an approximate 20% decrease in modulus produces an additional 20% of deflection in the wing skin. Because the cold state modulus measurements in this work have a reasonable standard deviation and are in relative agreement with another set of experiments [6], it is asserted that 1010 MPa is an accurate measurement. However, in light of the significant effect of the curing method unveiled in this thesis (Section 4.0), it is hypothesized that the manufacturer's reported modulus of 1240 MPa arises from a different cure process. Therefore it is important that the SMP's material properties are highly consistent between manufactured and cured batches; sources of these variations may warrant further detailed study.

In addition, this model does not address creep. However, by considering 2 modulii in the above, some assertions may be made regarding the effect of creep. Namely, an approximate 20% increase in deflection. Because the creep tests indicate an effective change of another 20%, the increased deflection due to creep could be expected to be of this order.

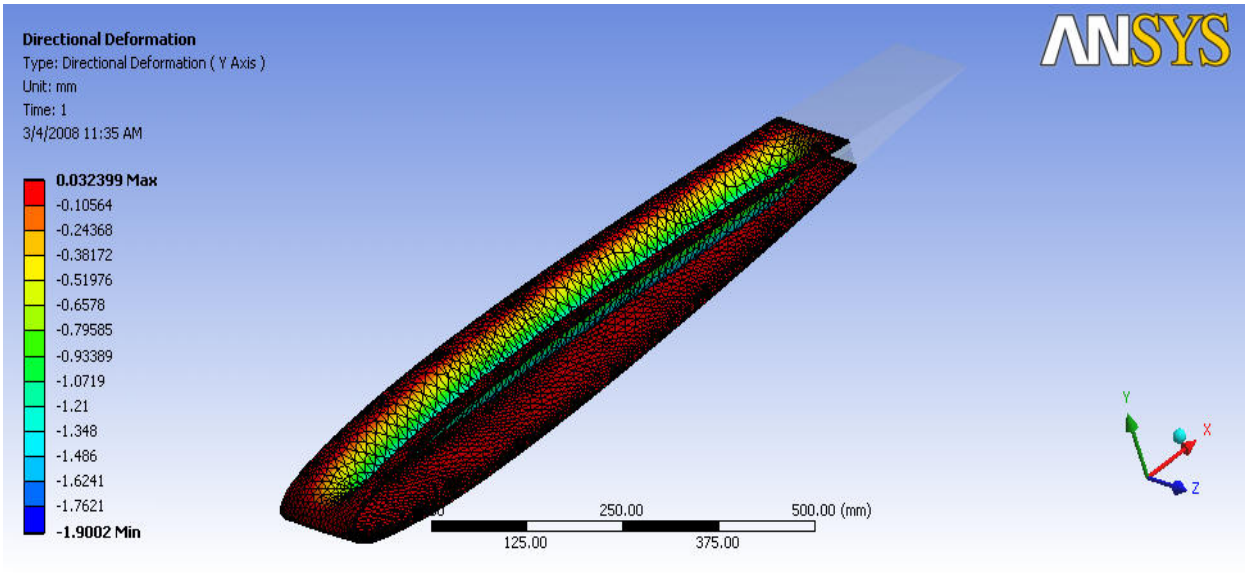

Figure 5.2-2 ANSYS Workbench Results for Deflection of 1240 MPa Modulus Wing Section

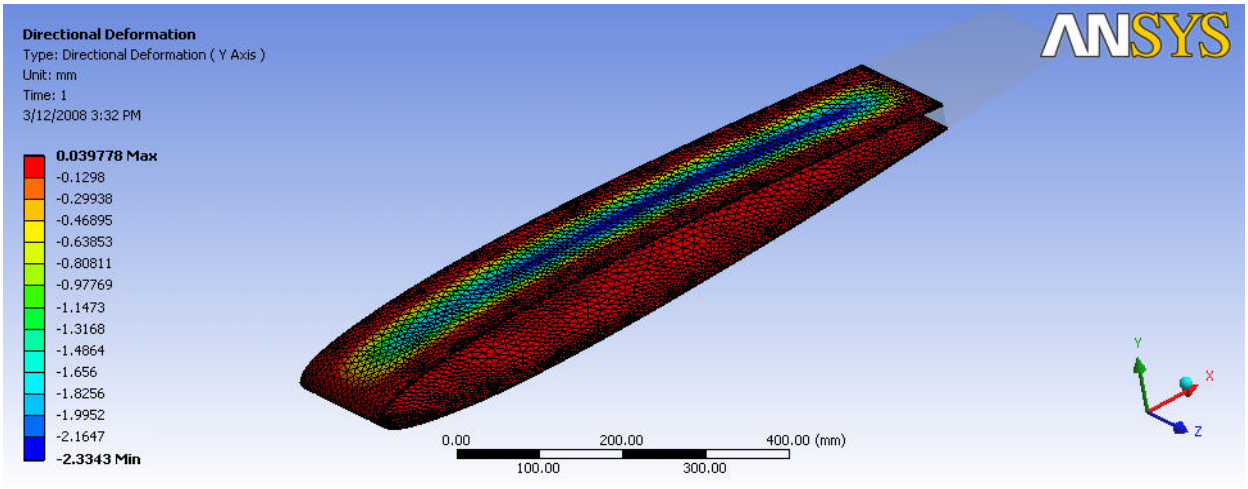

Figure 5.2-3 ANSYS Workbench Results for Deflection of 1010 MPa Modulus Wing Section

The stresses in the models are fairly consistent. Figure 5.2-4 and Figure 5.2-5 show the Von Mises stress distribution in the two models. Both instances saw nearly identical maximum Von Mises stress values of about 9.4 MPa. This is as expected for this load-control model.

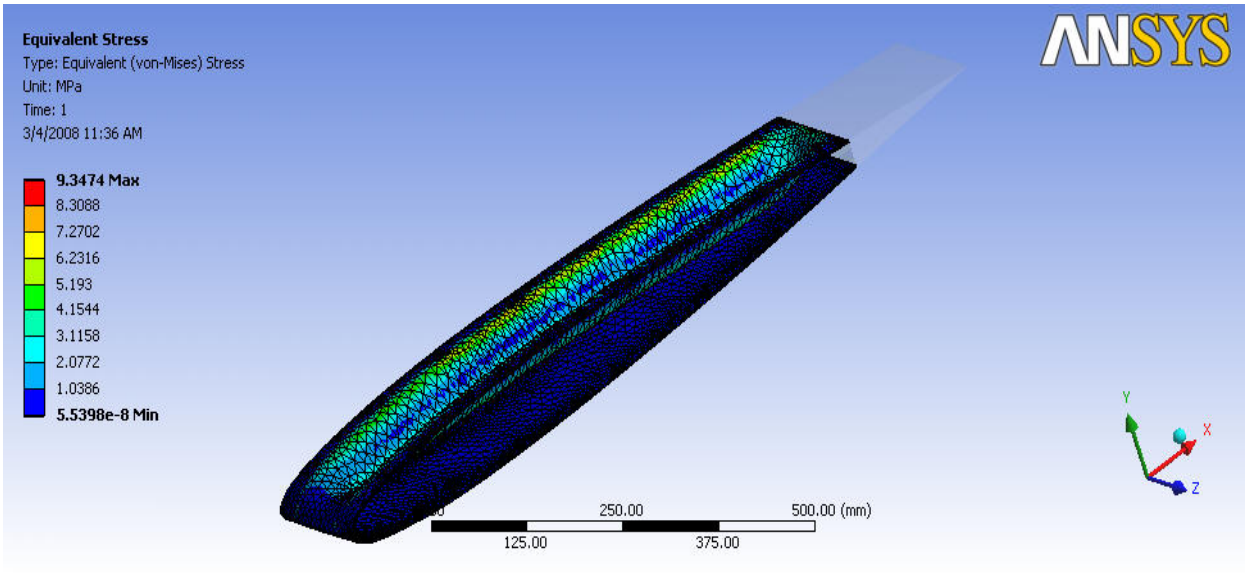

Figure 5.2-4 ANSYS Workbench Results for Von Mises Stress of 1240 MPa Modulus Wing Section

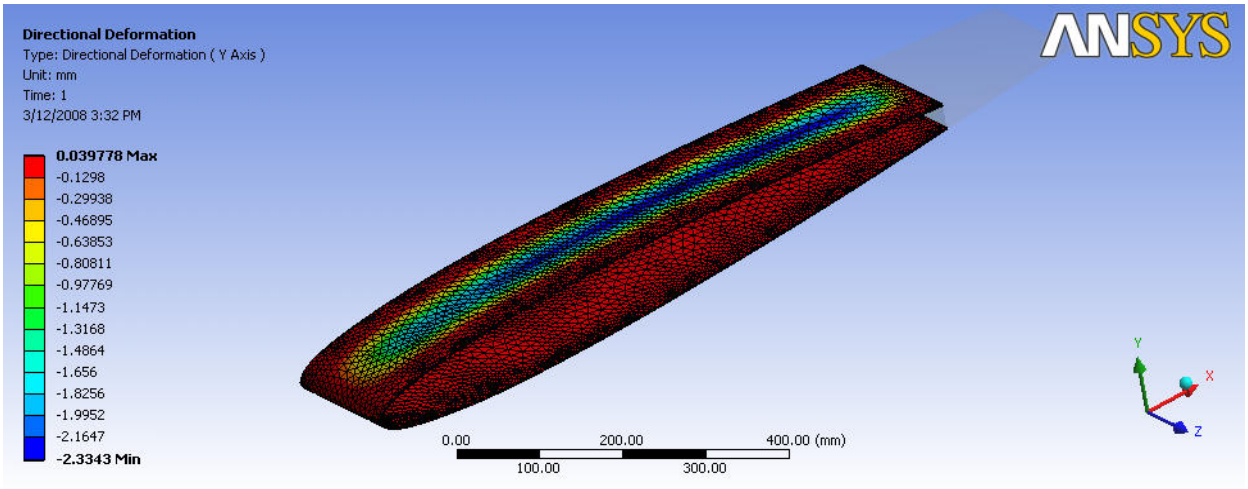

Figure 5.2-5 ANSYS Workbench Results for Von Mises Stress of 1010 MPa Modulus Wing Section

The final scenario considered the wing section in its soft state. This simulation produced expected results of very large scale deformations in response to this out-of-plane load. The deformations are so large that the program's solver could not produce reliable results. This is consistent with the anticipated need for a reinforcing structure noted in Chapter 2.

An alternate version of the wing section design is therefore proposed. In this case, a support structure is introduced that is compliant during in-plane morphing deformation, but

comparatively rigid in response to out-of-plane aerodynamic loads is proposed: a polyurethane honeycomb structure (Figure 5.2-6). The new model is then imported into ANSYS Workbench where the same three test cases are simulated again.

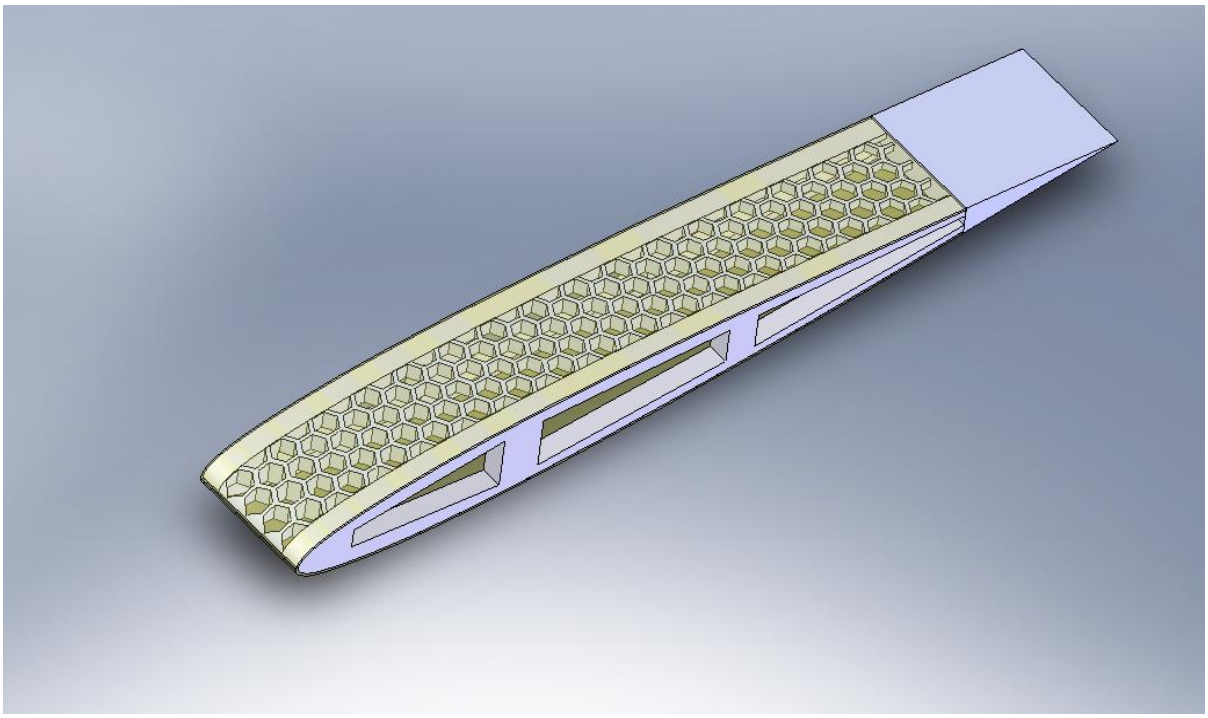

Figure 5.2-6 Second Wing Section Version With Honeycomb Support

The displacement and Von Mises stress distributions for the 1240 MPa and 1010 MPa models can be seen in Figure 5.2-7 and 5.2-8 respectively. As expected, the addition of the honeycomb support decreases the maximum vertical deflection and maximum Von Mises stress in both cases. The 1240 MPa model sees a maximum deflection of 0.5 mm and a maximum stress of 4.3 MPa. The 1010 MPa also improves with maximums of 0.6 mm and 4.1 MPa for deflection and stress respectively; it is reasonable to assume that the maximum deflection for this case under creep conditions increases to 0.7 mm.

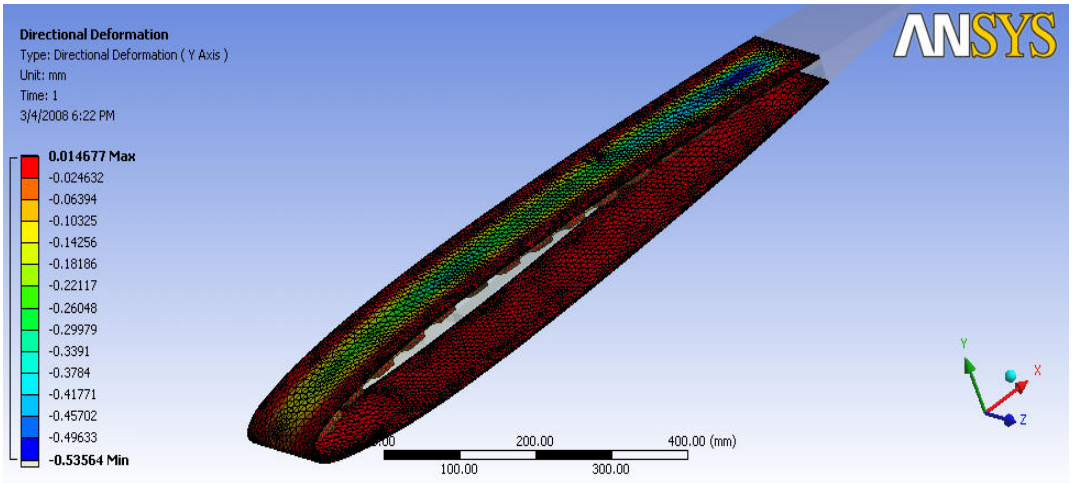

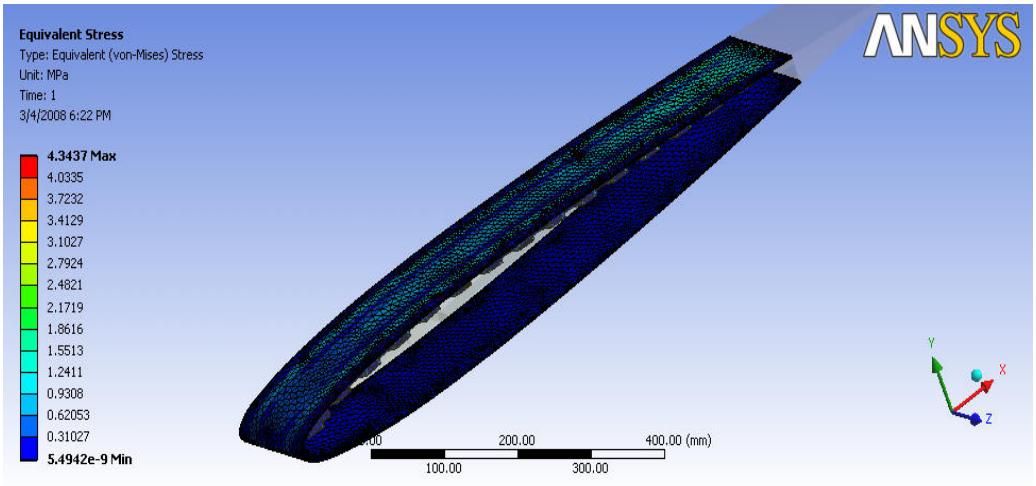

Figure 5.2-7 Displacement and Stress Results for 1240 MPa Redesigned Wing Section

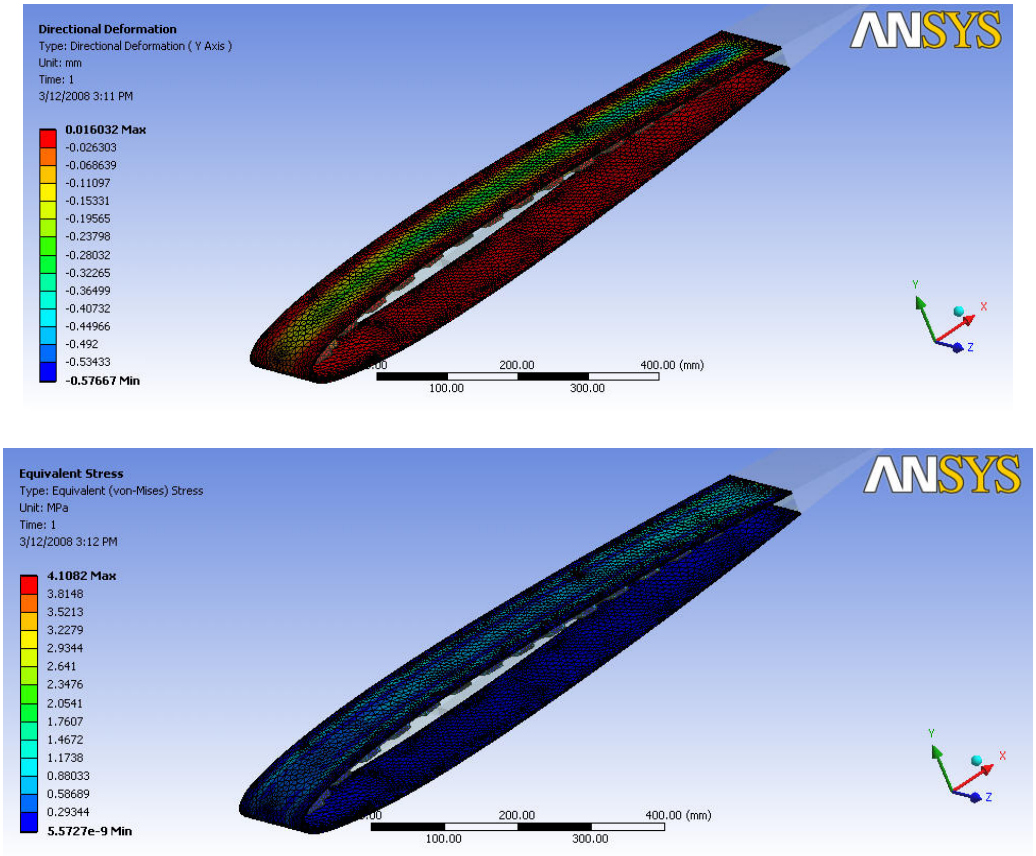

Figure 5.2-8 Displacement and Stress Results for 1010 MPa Redesigned Wing Section

The true test for the redesign is if it properly supports the skin when the skin is in its hot state. The deflection results of the soft state 0.2 MPa simulation can be seen in Figure 5.2-9. This model sees a maximum deflection of about 23.9 mm. This maximum is however localized at the very ends of the wing section as seen in Figure 5.2-10. On the top surface, typical deformation is on the order of 7-10 mm. The Von Mises stress distribution also shows improvement over the unsupported first design. Figure 5.2-11 shows that the maximum Von Mises stress in this model is about 8.2 MPa.

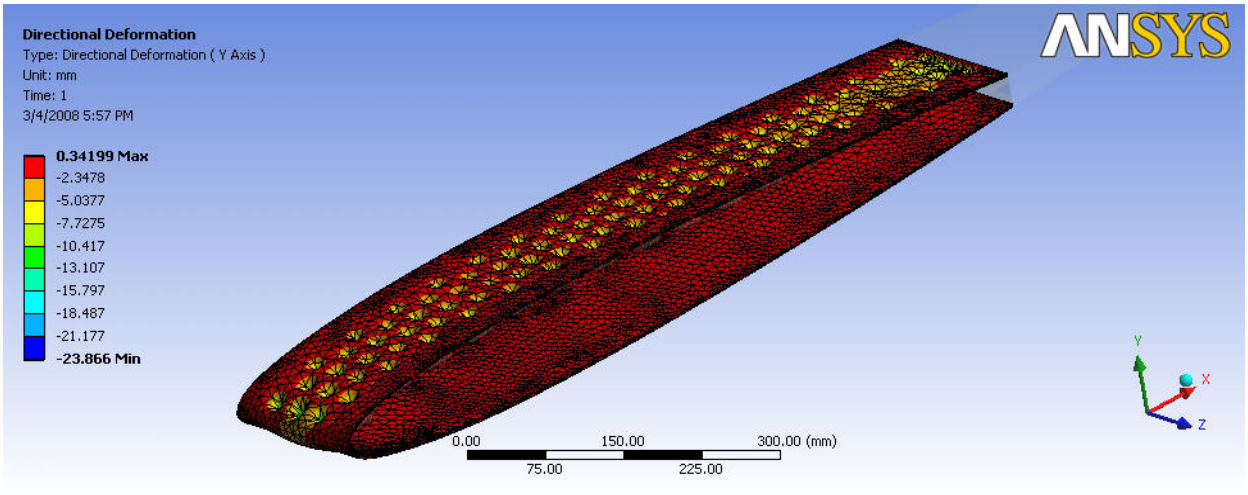

Figure 5.2-9 Displacement Results for 0.2 MPa Redesigned Wing Section

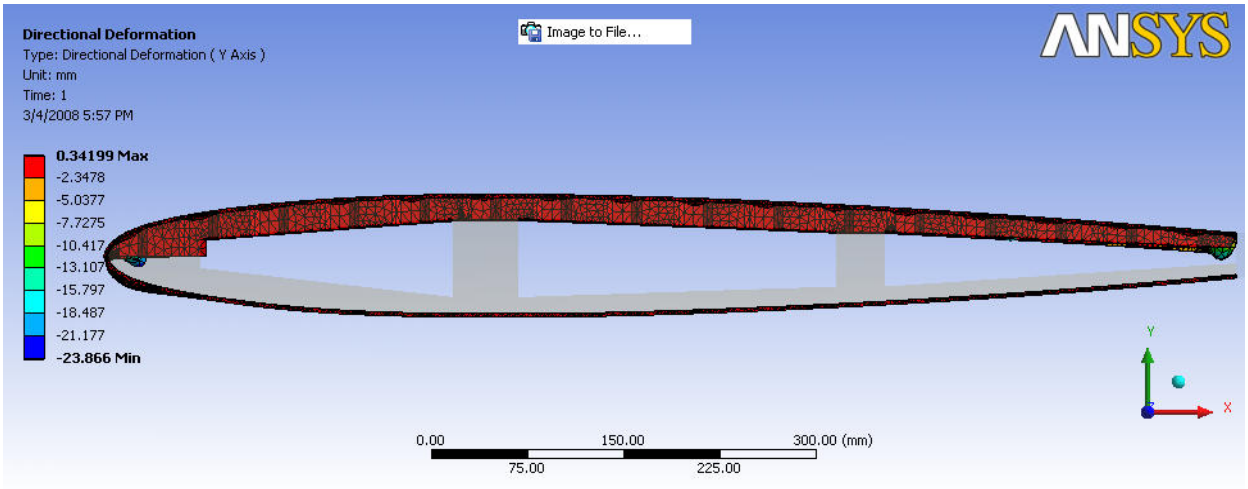

Figure 5.2-10 Front View of Displacements in 0.2 MPa Redesigned Wing Section

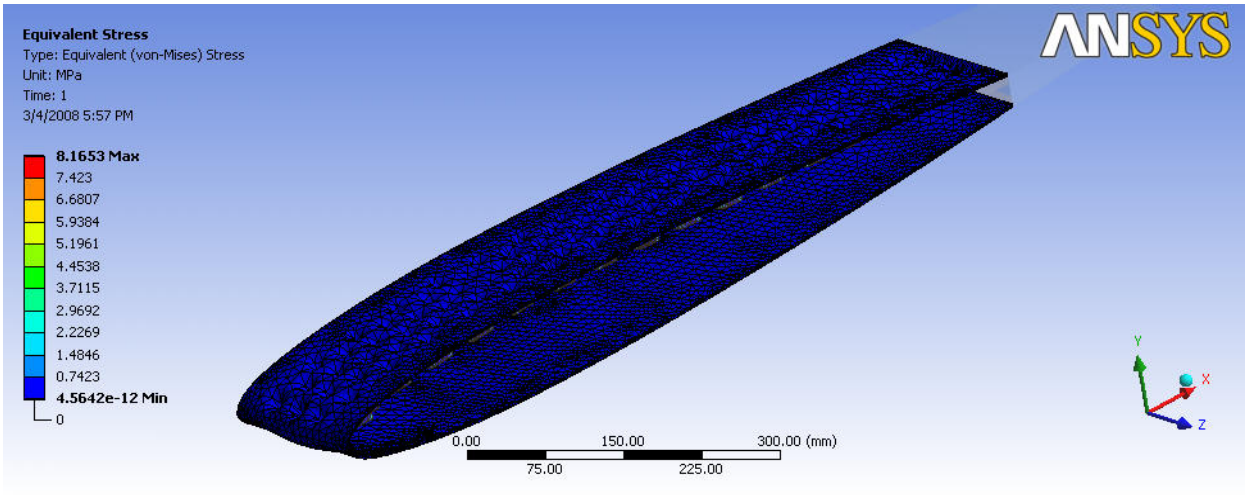

Figure 5.2-11 Von Mises Stress Results for 0.2 MPa Redesigned Wing Section

The 2.6 MPa hot state simulations see much better results. As seen in Figure 5.2-12, the 2.6 MPa wing section has a maximum deflection of about 3.3 mm due to the surface pressure. This deflection causes a maximum Von Mises stress of about 6.1 MPa in the skin (Figure 5.2-13). The ten fold increase in modulus between the first and second hot state simulations creates large deflection differences. The 2.6 MPa skin deflects over 20 mm less than the 0.2 MPa skin. Once again, modulus proves to be a very large factor for design considerations. Moreover, in light of the significant difference between the modulus reported here and elsewhere [6], particular care has been taken here. It is asserted that the measurement reported here is appropriate because: (1) Similar variations between hot state and cold state are observed in the bend tests and (2) Similar variations between hot state and cold state are observed in other SMPs.

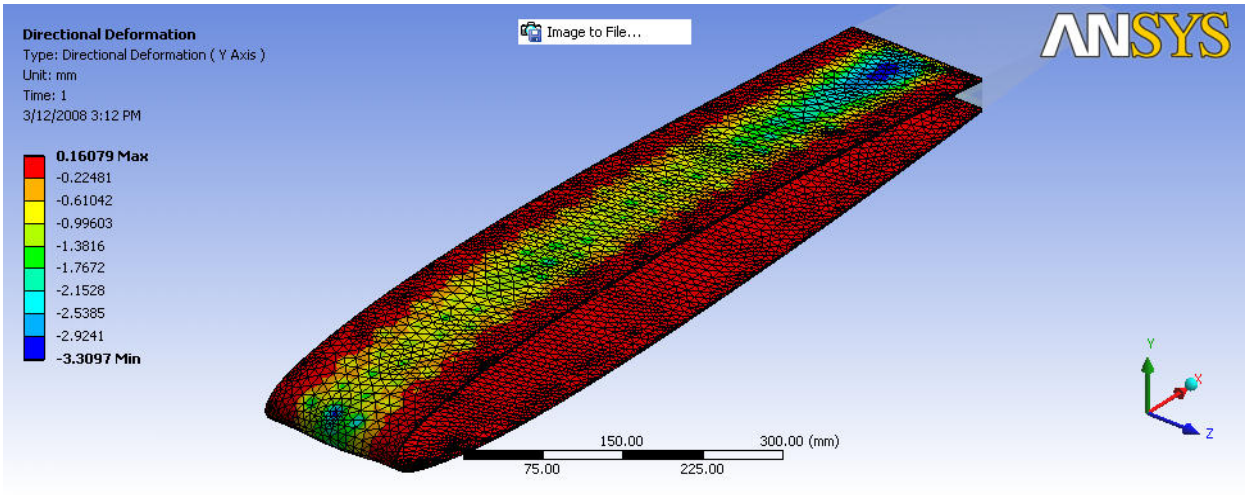

Figure 5.2-12 Displacement Results for 2.6 MPa Redesigned Wing Section

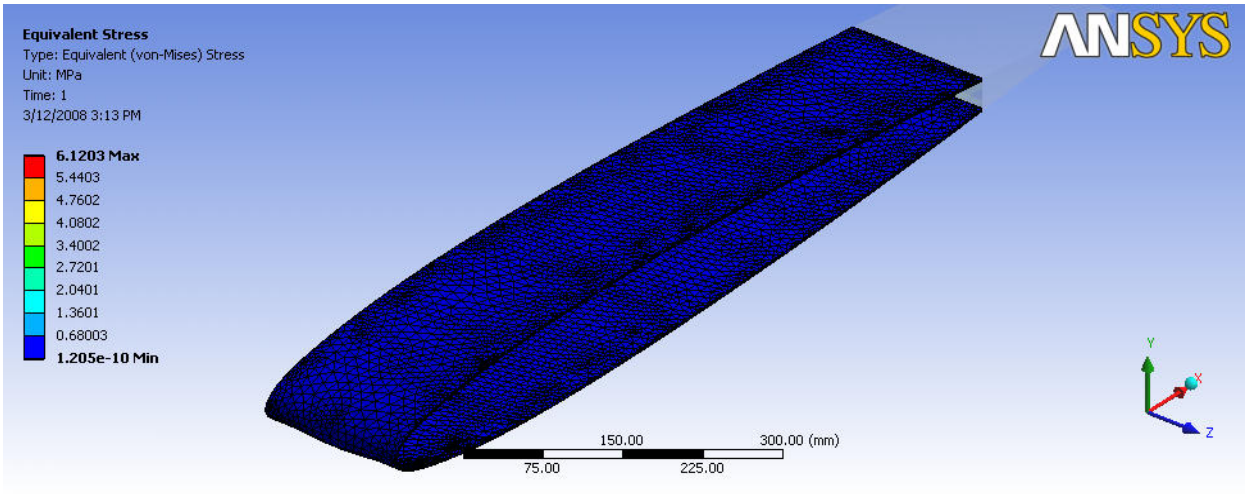

Figure 5.2-13 Displacement and Von Mises Stress Results for 2.6 MPa Redesigned Wing Section

The redesigned, honeycomb supported wing section is not an ultimate solution to the problem of supporting the skin in its soft state. However, it does show that with some ingenuity, a proper support system can be created. The polyurethane honeycomb adds some support to the wing and will allow for some span wise extension of the wing section. Determining the exact amount the polyurethane honeycomb would allow the wing section to expand is outside of the scope of this thesis.

5.2.1 Wing Candidacy Closing

Combining experimental characterization results with actual UAV loading conditions in an FEA analysis demonstrates both the potential and challenges of using Veriflex® as a morphing skin. There are some design challenges that need to be addressed but it should not be completely discounted as a candidate. For instance, creative substructure design could minimize out-of-plane deflections while it is in its soft state and the hard state should be able to easily handle aerodynamic loads. In addition it should be noted that the cold state is the nominal state, while the hot state is solely a short transient state. The most significant challenge in the cold state will be mitigating the unexpected creep revealed in this thesis. It should also be recognized that the material itself may be redesigned. For example, doping the Veriflex® with a small percentage of a stiffer inactive resin could increase the soft state stiffness and minimize cold state creep.

The next significant issue is how to heat the skin while it is in a wing in flight. Instead of making the entire skin with SMP, a future wing design will need to minimize the amount of SMP by only using it in key places that require area changes. This would decrease the amount of energy needed to transition the SMP because it would lower the overall volume of the material in the wing. Also, an alternative heating method needs to be created. Ambient heating is not nearly efficient enough and would be nearly impossible to implement in a full scale wing. One possible solution would be to use flexible strip heaters placed against the SMP. The strip heaters would apply heat directly to the surface of the SMP which is more effective then free convective ambient heating.

6.0 CONCLUSION

6.1 CONTRIBUTIONS

This thesis provides further mechanical characterization for Shape Memory Polymers. The mechanical properties found in this study can be used in a range of fields to determine if SMPs are an appropriate material in a variety of applications. In particular, the potential use of SMPs as a morphing aircraft skin is explored in depth by experimentally determining flexural response of Veriflex® and creating a wing section using the material as a skin.

The flexural and creep testing presented by this work are some of the first of their kind for SMPs and, in particular, Veriflex®. Previous efforts have focused on axial loading and the temperature response of the material. This effort, mainly considers out of plane loading by using a three point bend test set up to determine the flexural modulus and creep response.

Also explored is the transition time for the material and how much energy is required to achieve this transition. Through both experimental and analytical methods, a transition time for a certain thickness of Veriflex® is determined. Data from transition time calculations is then used to determine the energy requirement. This data can be used to determine the practicality of using the SMP in applications where transition time and the availability of power are issues.

From this thesis, one should be able to duplicate tensile, flexural, and creep testing on SMPs. This includes, but is not limited to, sample preparation and test data post processing.

Also, a requirement for aging test specimens is introduced and discussed. This illustrates the importance of consistency in the sample creation and curing of SMPs.

6.2 DIRECTIONS FOR FUTURE WORK

There has been some research conducted with Veriflex® that involved promoting anisotropies by aligning its polymer chains [6]. Aligning the polymer chains in the direction of axial strain produced drastic increases in the material's Young's modulus. Anisotropies may also affect Veriflex®'s performance while subjected to flexural loading. In order to fully understand this material's potential as a morphing aircraft skin, further attention should be paid to this particular phenomenon.

There should also be studies that examine the transitional temperature range of SMPs. This research uses temperatures that are comfortably outside of Veriflex®'s transitional range in order to make sure the material has completely transitioned from its hard to soft state. However, the transitional range should still be explored. SMPs need to be characterized at a spectrum of temperatures in order to insure they function properly in a multitude of devices and environments.

A major obstacle to Veriflex®'s use in a variety of applications is how to heat the material. In order to increase the application readiness of Veriflex®, a low energy method of heating must be discovered. Inductively heating SMPs by embedding them with magnetically or electrically conductive materials may be an answer to the problem. Future efforts should involve research into heating methods like embedding in addition to characterization studies.

APPENDIX A

TENSILE TESTS RESULTS

This appendix contains experimental results for tensile tests in the form of plots. In certain cases, there are also comments explaining notable characteristics of the plots. Each plot shown is the result of testing an individual sample once.

A.1 COLD TENSILE TEST RESULTS

All of the cold tensile test results shown in this appendix are unfiltered so they exhibit a large amount of noise. The noise is most likely due to mechanical and interface problems with the larger load frame.

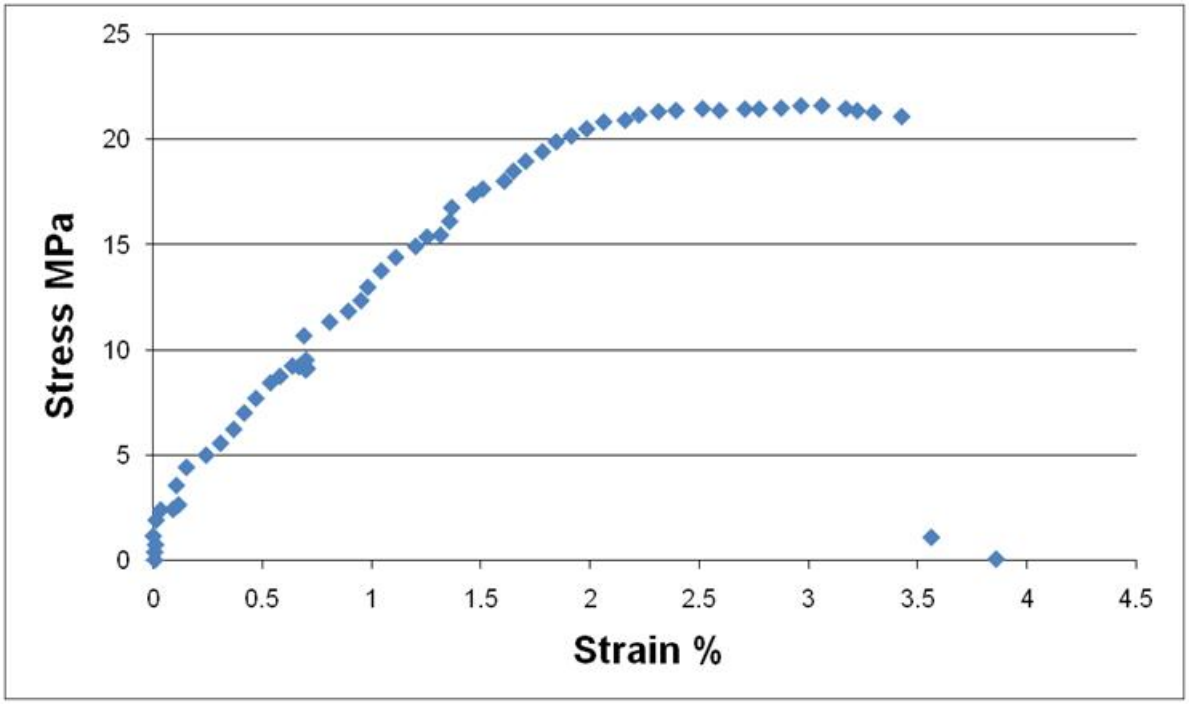
Stress MPa
25
20
15
10
5
0
0
0.5
1
1.5
2
2.5
3
3.5
4
4.5
Strain %

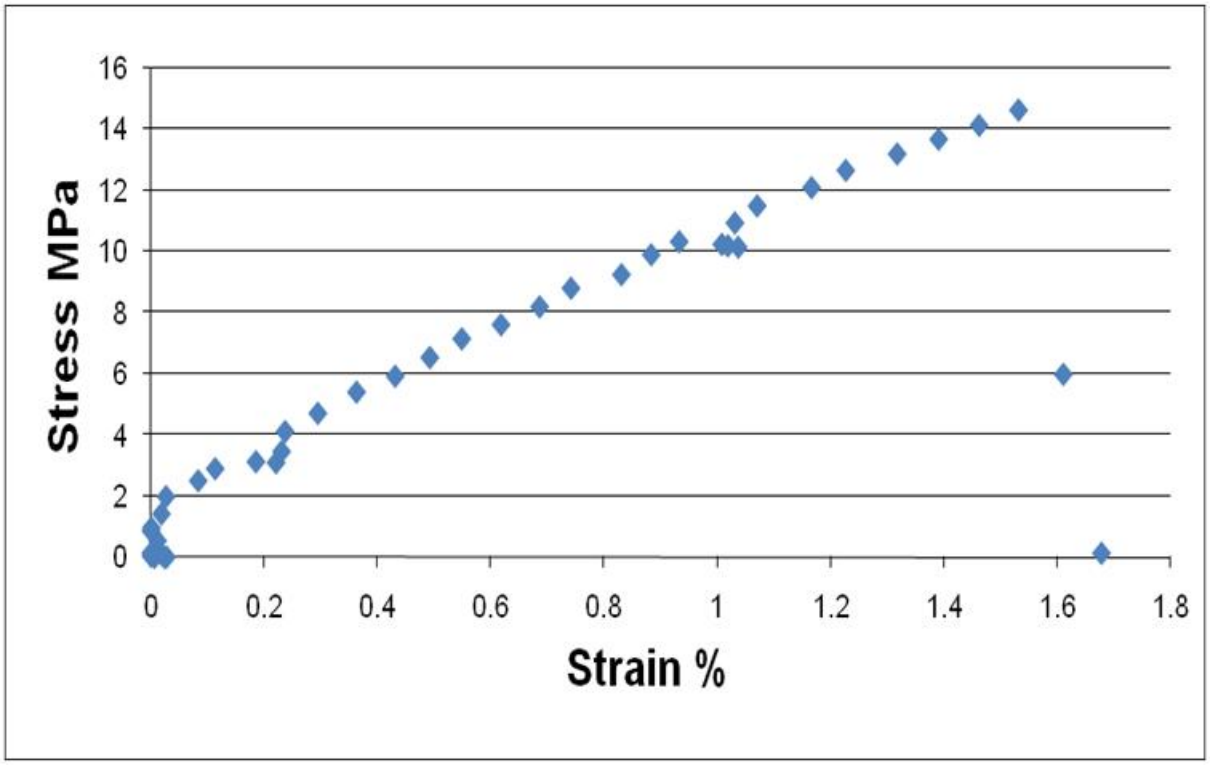
Stress MPa
16
14
12
10
8
6
4
2
0
0
0.2
0.4
0.6
0.8
1
1.2
1.4
1.6
1.8
Strain %

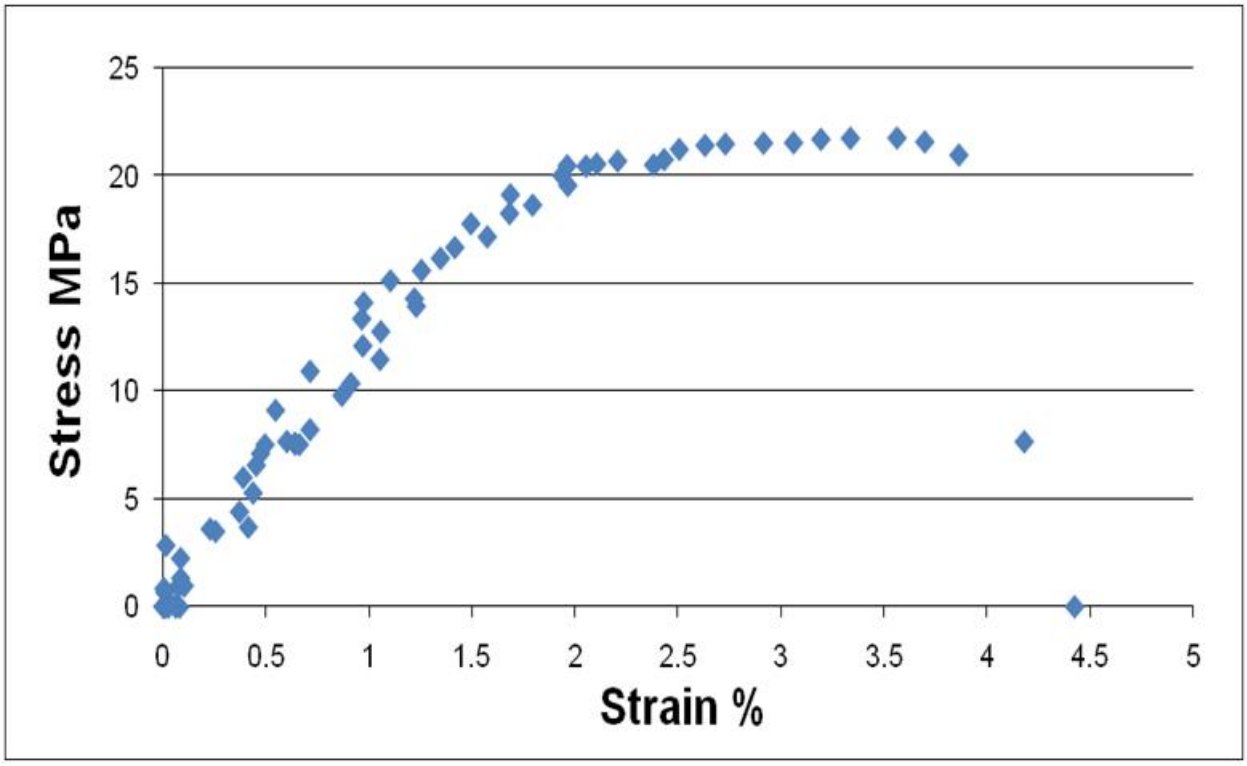
Stress MPa
25
20
15
10
5
0
0
0.5
1
1.5
2
2.5
3
3.5
4
4.5
5
Strain %

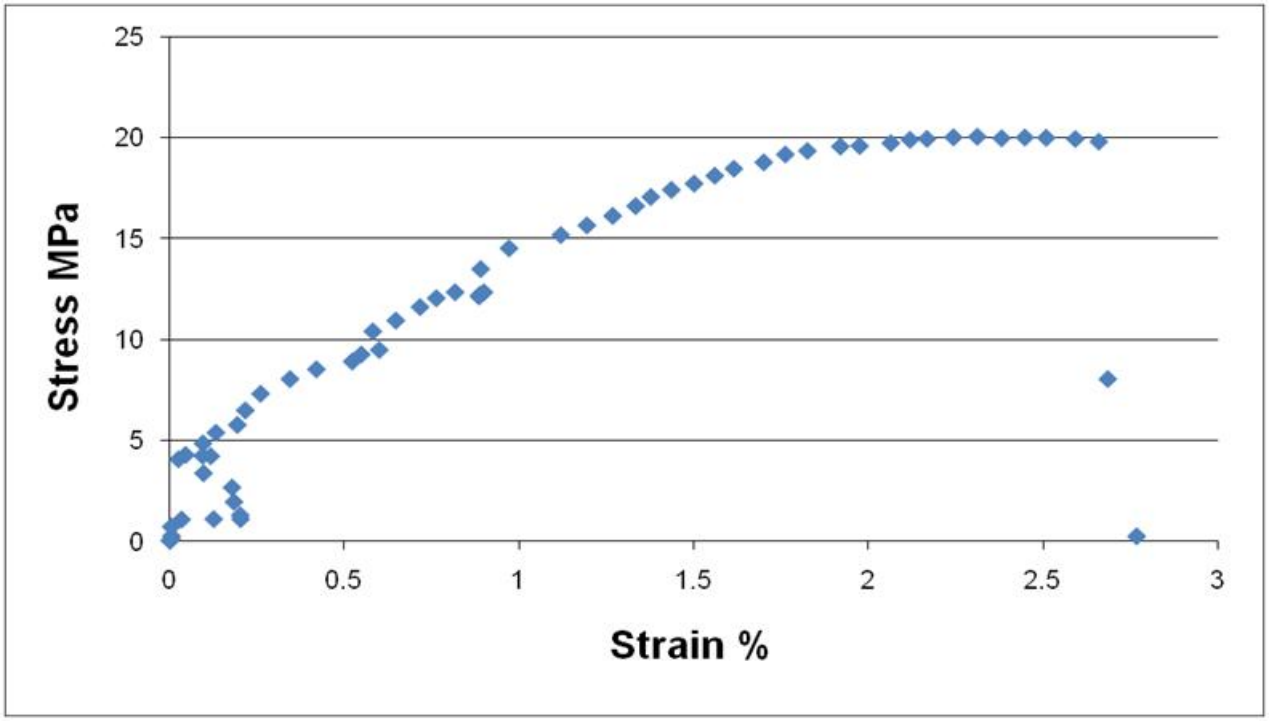
Stress MPa
25
20
15
10
5
0
0
0.5
1
1.5
2
2.5
3
Strain %

A.2 HOT TENSILE TEST RESULTS

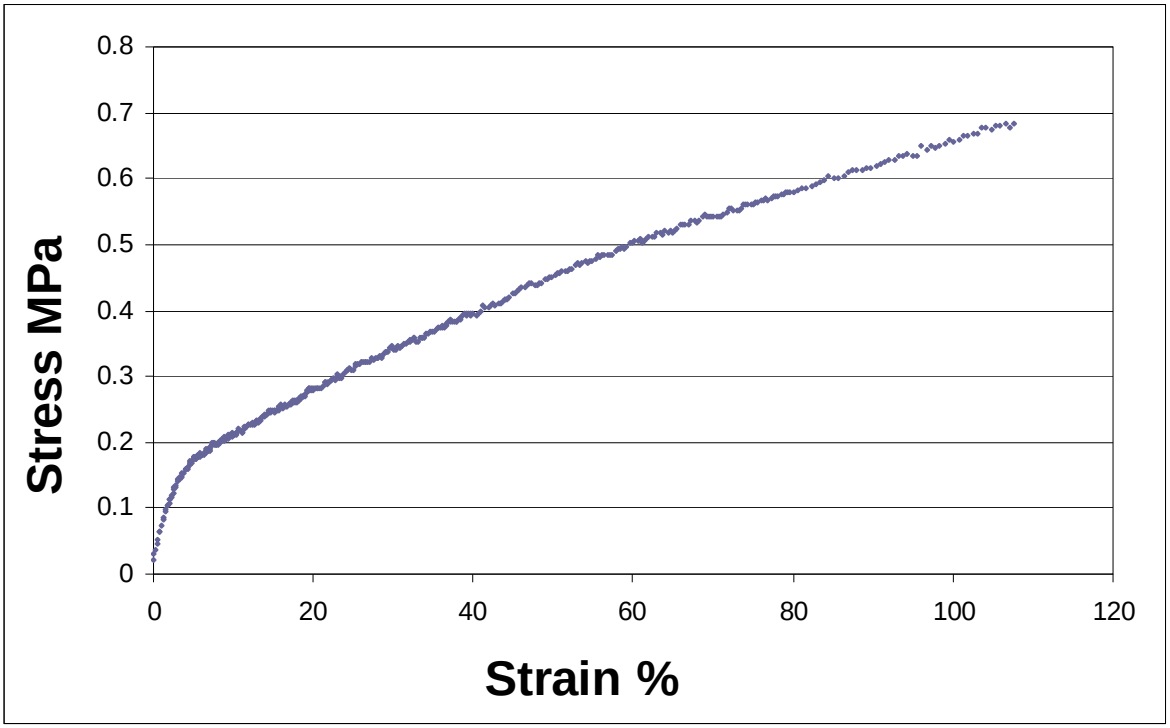

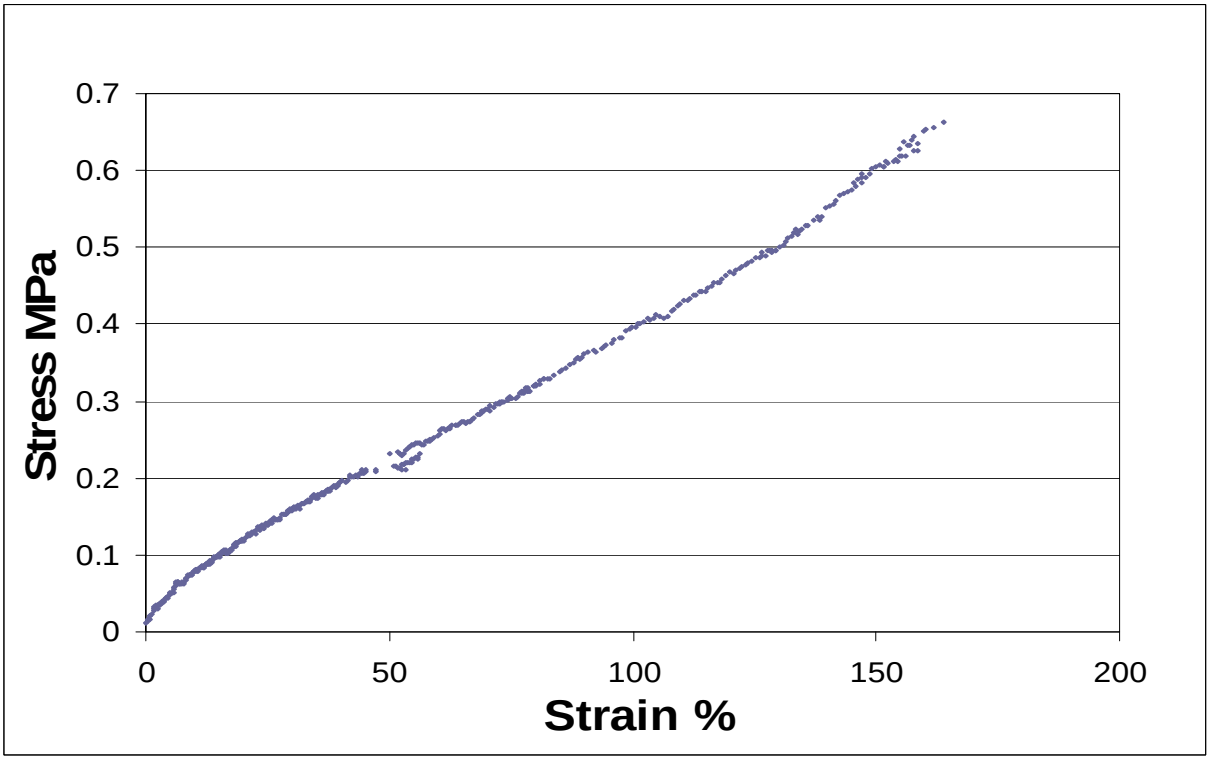

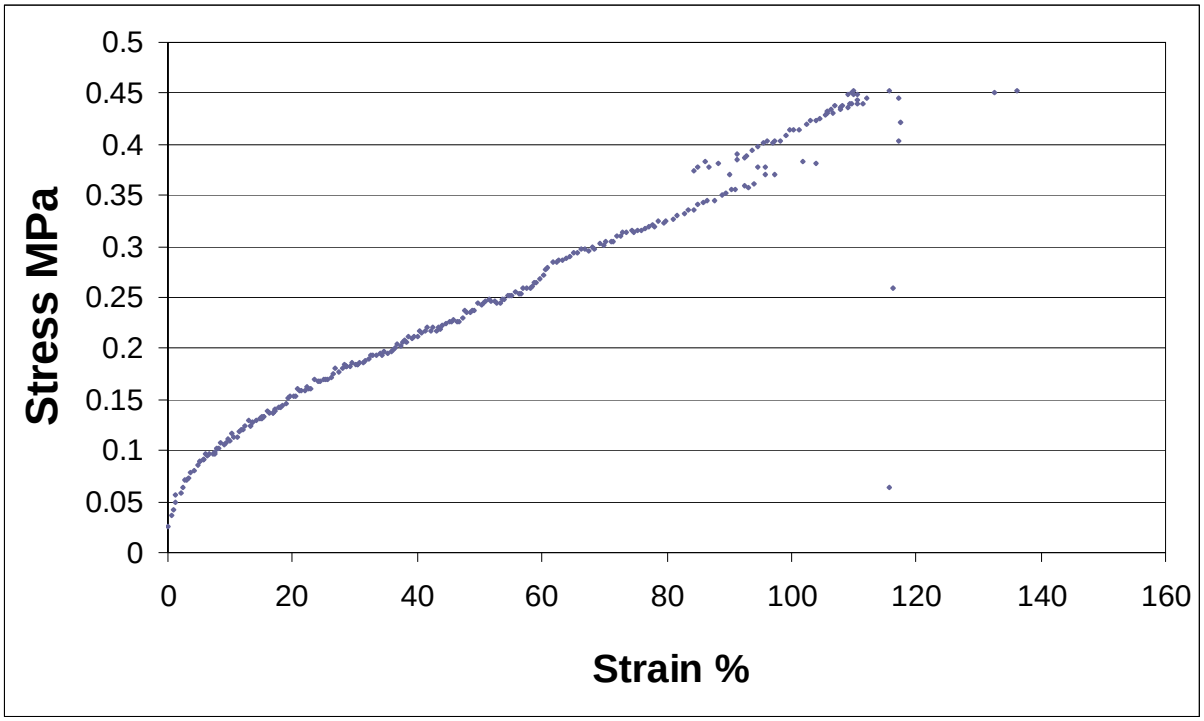
Stress MPa
0.5
0.45
0.4
0.35
0.3
0.25
0.2
0.15
0.1
0.05
0
0
20
40
60
80
100
120
140
160
Strain %

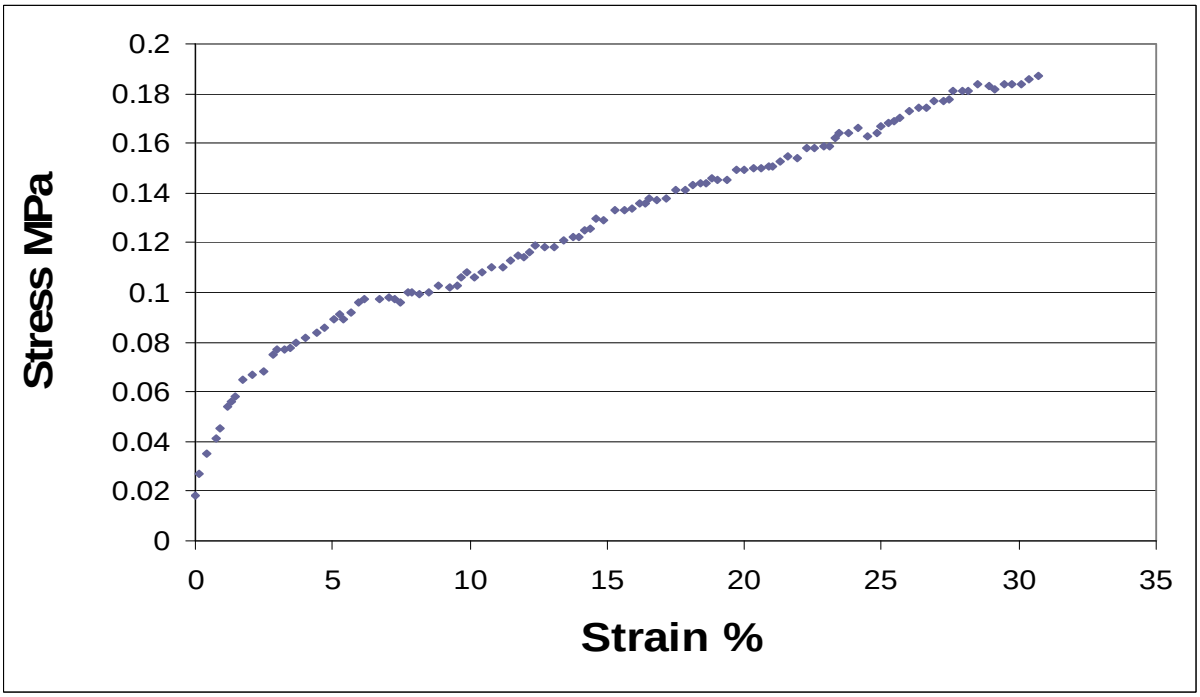
Stress MPa
0.2
0.18
0.16
0.14
0.12
0.1
0.08
0.06
0.04
0.02
0
0
5
10
15
20
25
30
35
Strain %

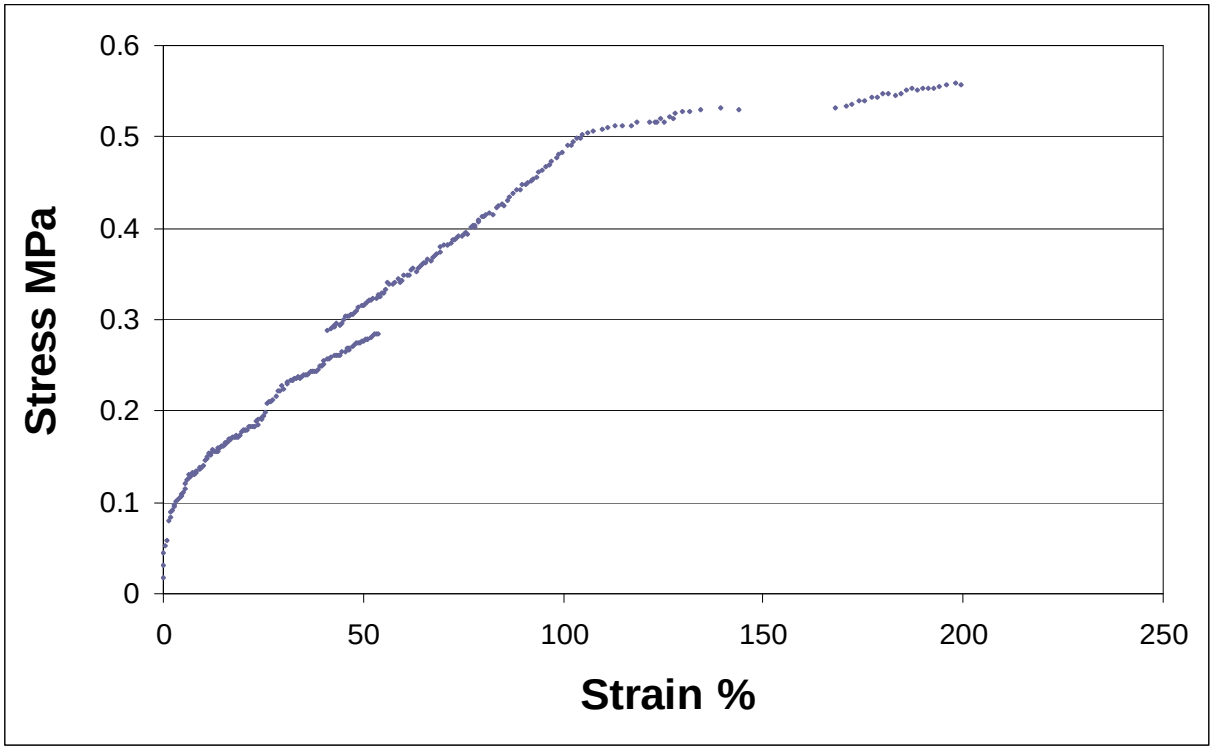
Stress MPa
0.6
0.5
0.4
0.3
0.2
0.1
0
0
50
100
150
200
250
Strain %

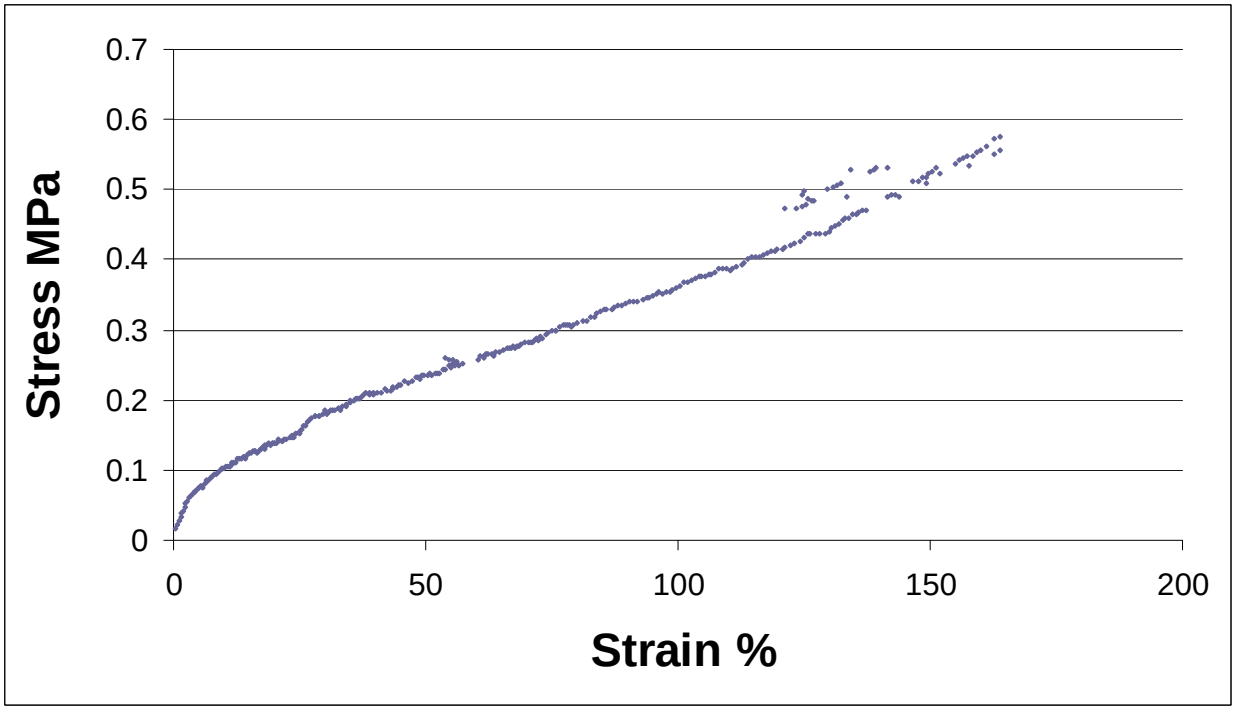
Stress MPa
0.7
0.6
0.5
0.4
0.3
0.2
0.1
0
0
50
100
150
200
Strain %

APPENDIX B

THREE POINT BEND TESTS RESULTS

This appendix contains experimental results for three point bend tests in the form of plots. In certain cases, there are also comments explaining notable characteristics of the plots. Each plot shown is the result of testing an individual sample once.

B.1 COLD BEND TEST RESULTS

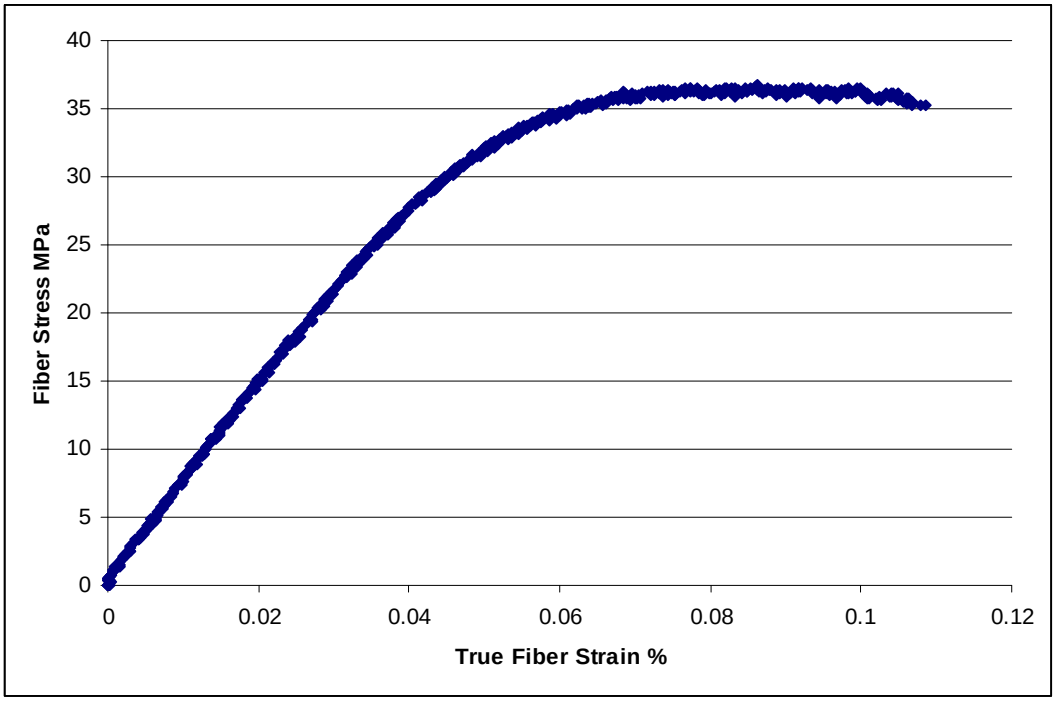

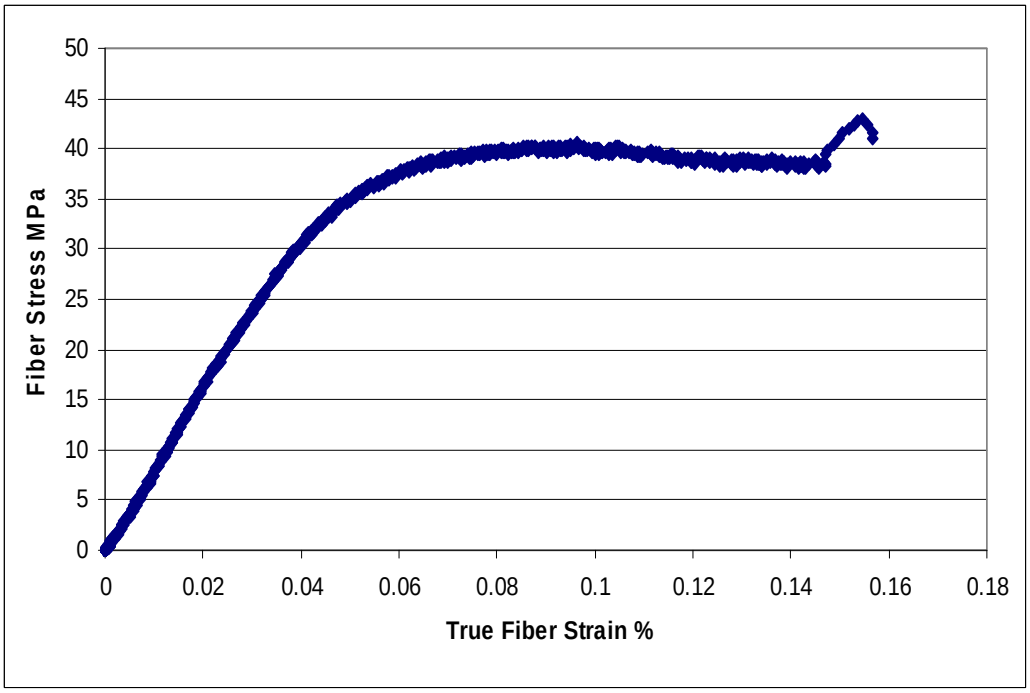

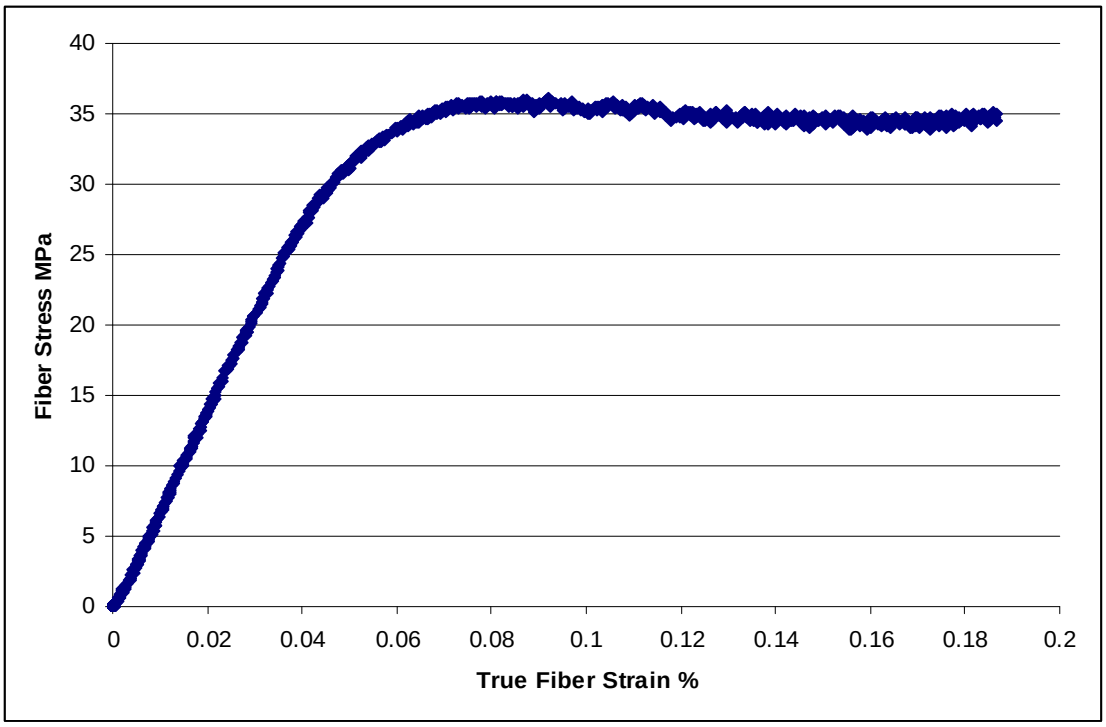
40
35
30
25
20
15
10
5
0
Fiber Stress MPa
0
0.02
0.04
0.06
0.08
0.1
0.12
0.14
0.16
0.18
0.2
True Fiber Strain %

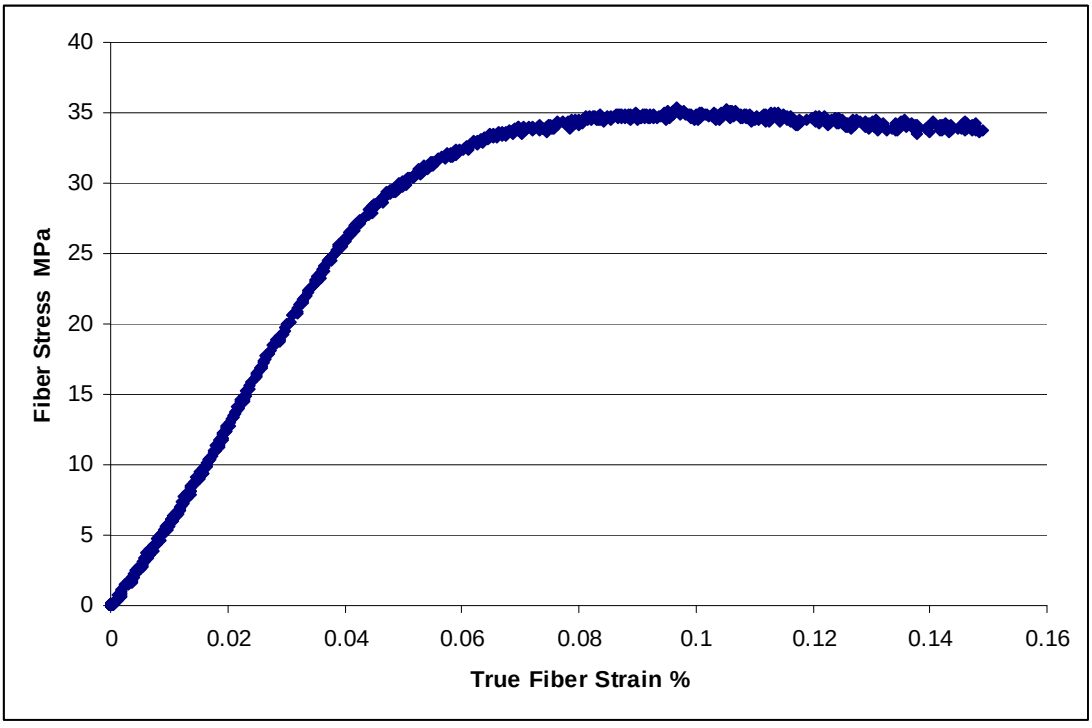
40
35
30
25
20
15
10
5
0
Fiber Stress MPa
0
0.02
0.04
0.06
0.08
0.1
0.12
0.14
0.16
True Fiber Strain %

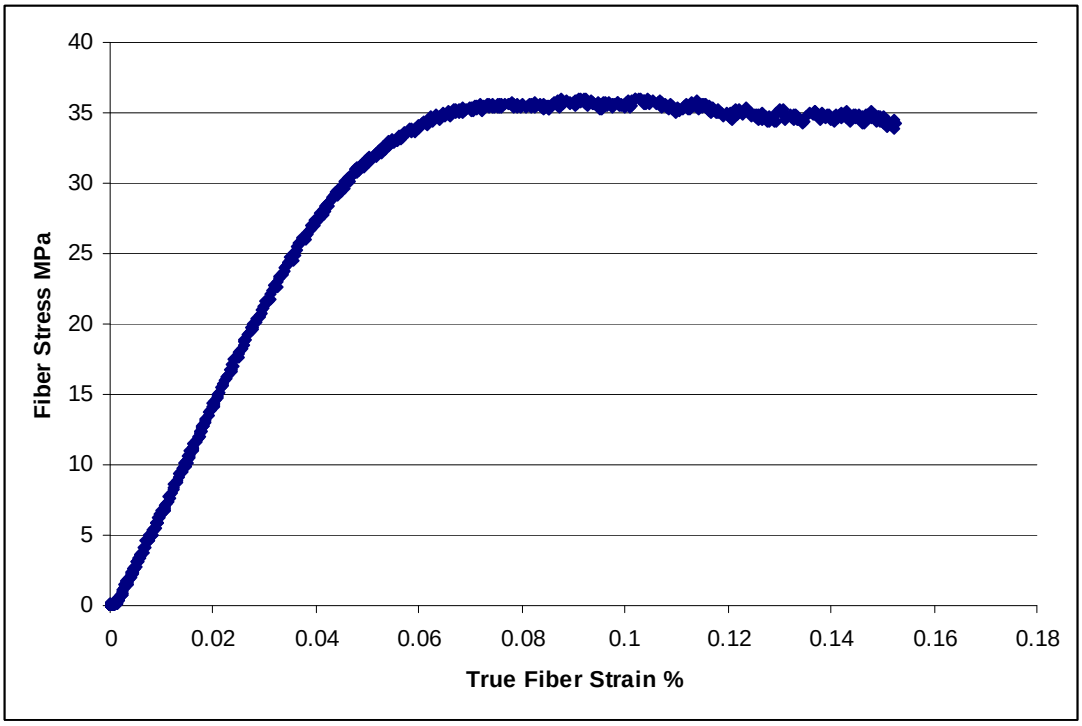
40
35
30
25
20
15
10
5
0
Fiber Stress MPa
0
0.02
0.04
0.06
0.08
0.1
0.12
0.14
0.16
0.18
True Fiber Strain %

B.2 HOT BEND TEST RESULTS

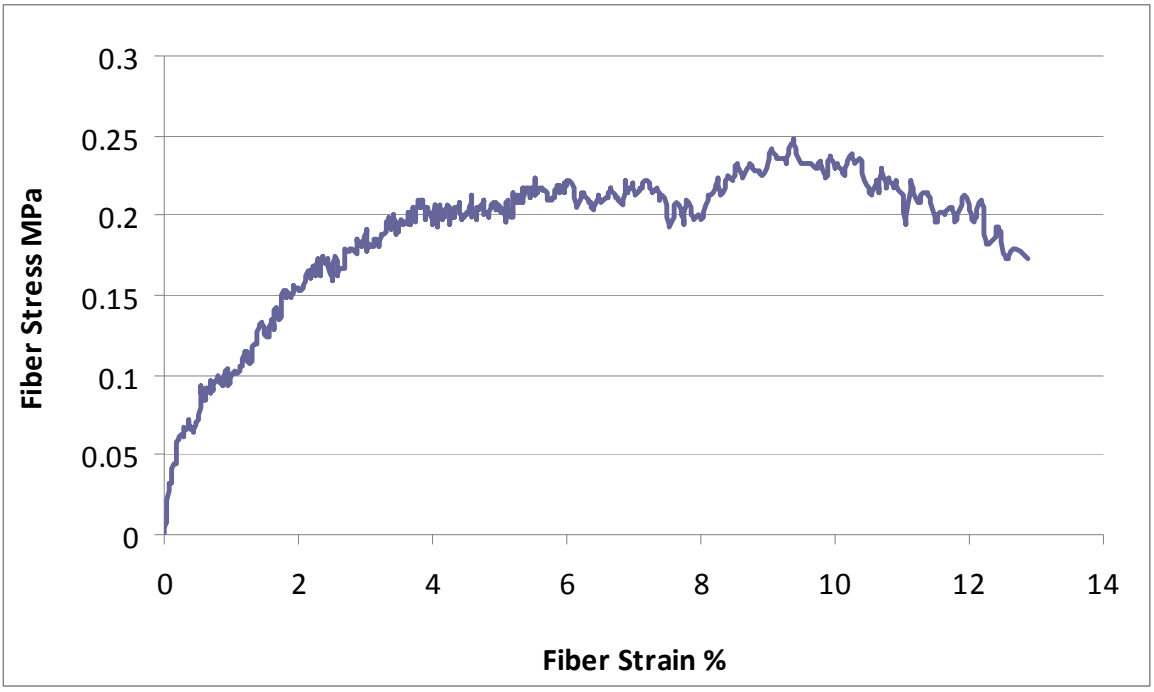

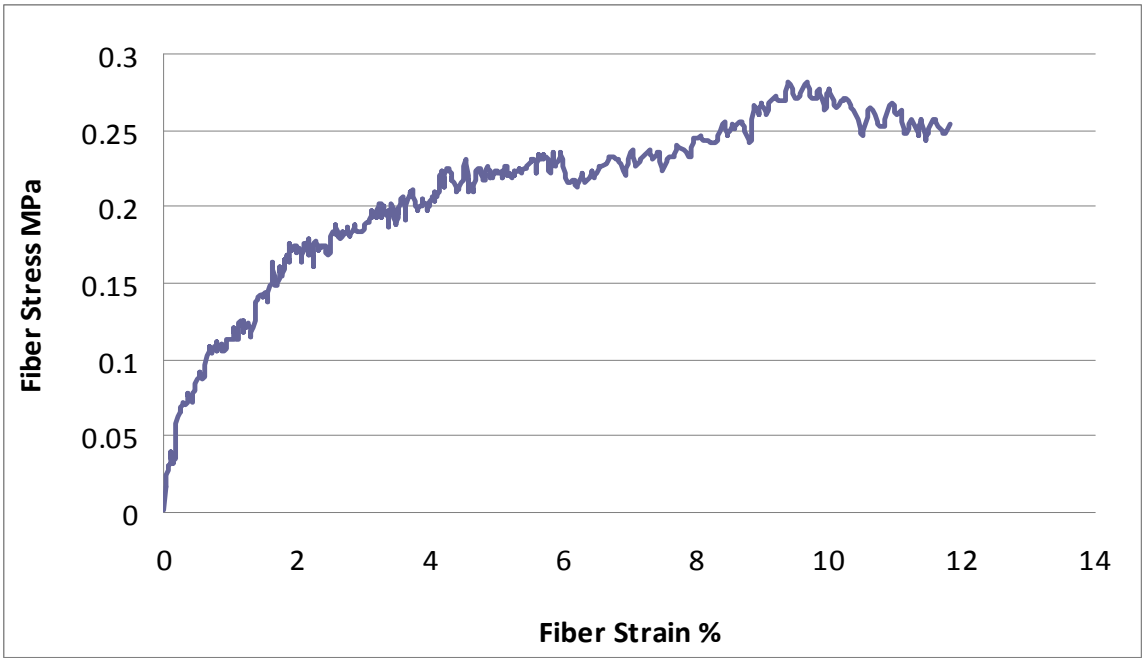

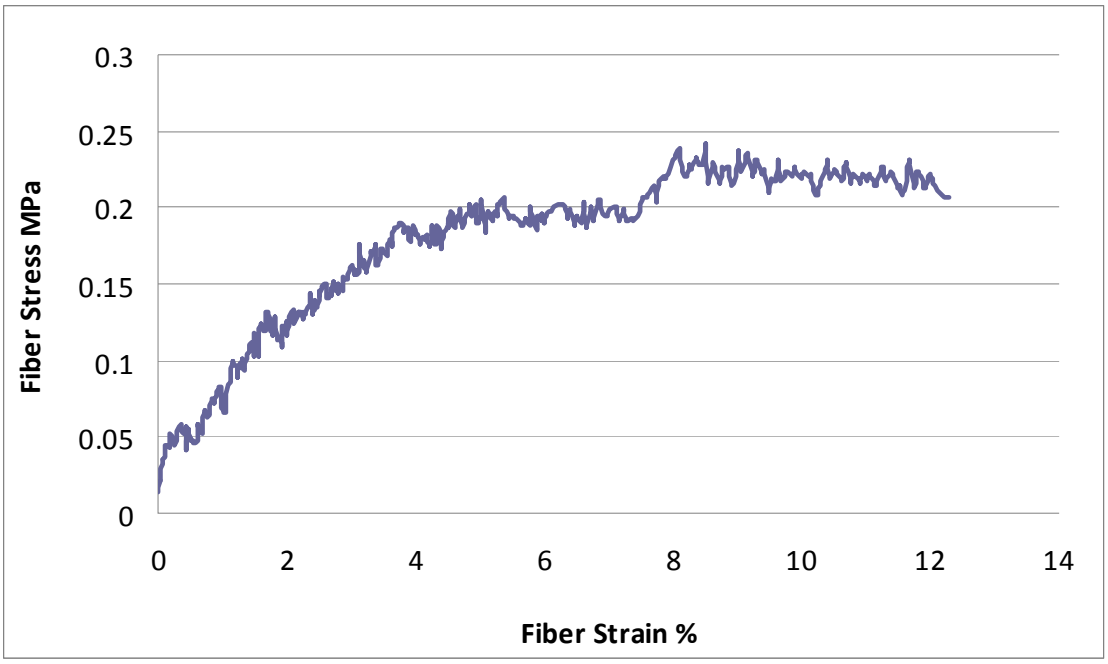
0.3
0.25
0.2
0.15
0.1
0.05
0
Fiber Stress MPa
0
2
4
6
8
10
12
14
Fiber Strain %

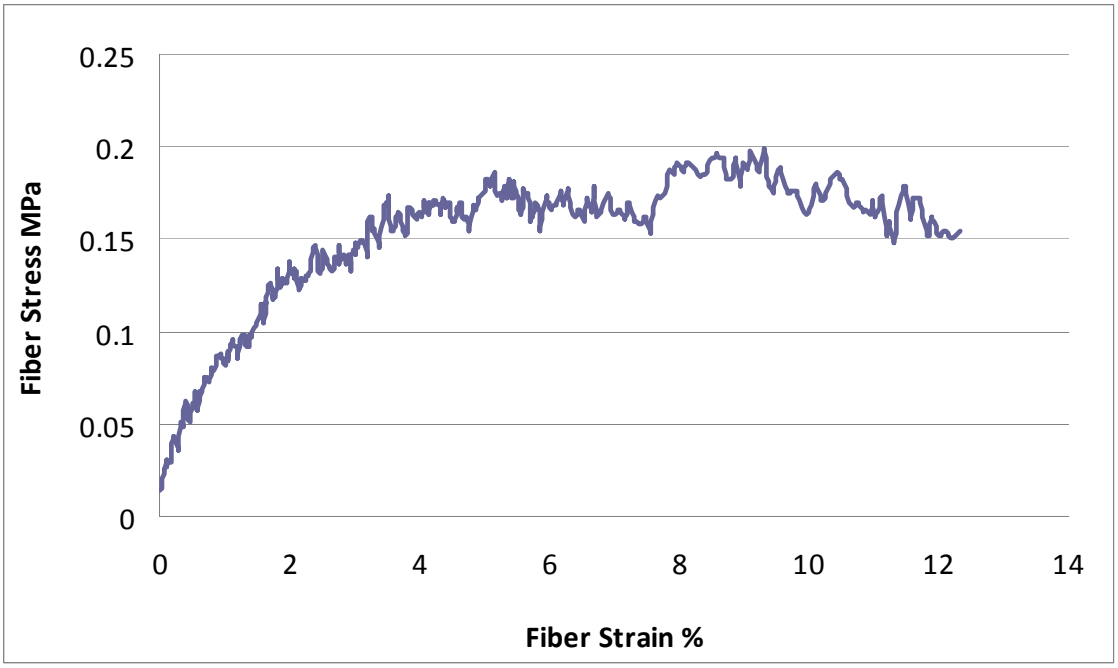
0.25
0.2
0.15
0.1
0.05
0
Fiber Stress MPa
0
2
4
6
8
10
12
14
Fiber Strain %

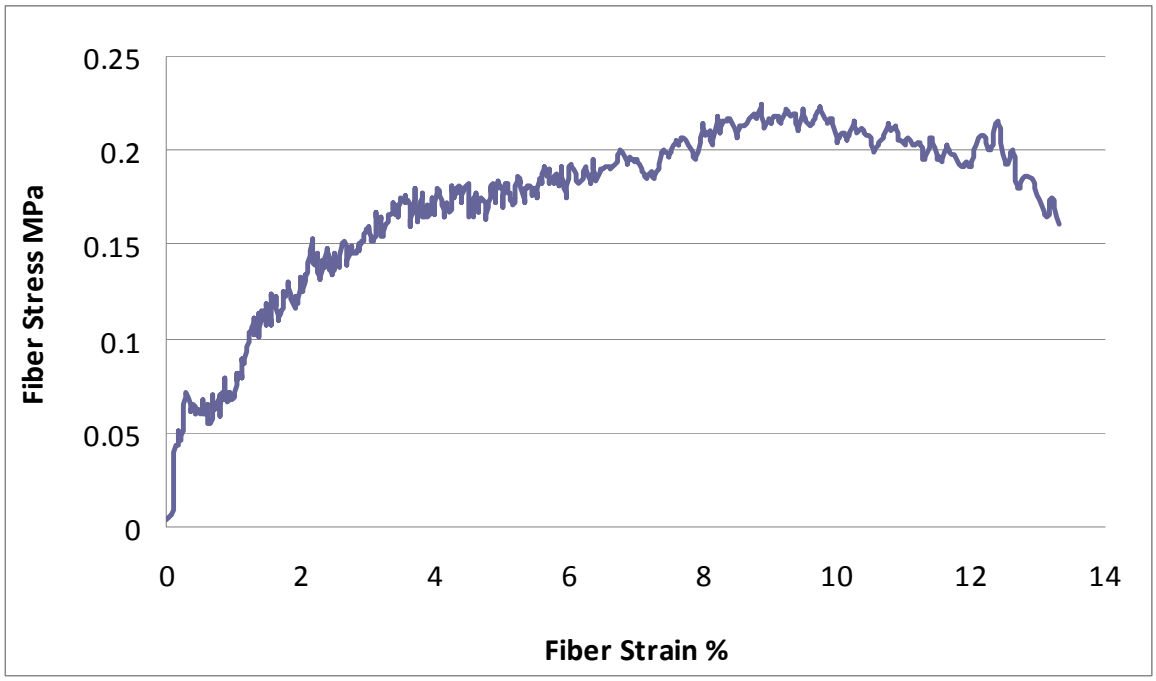
0.25
0.2
0.15
0.1
0.05
0
Fiber Stress MPa
0
2
4
6
8
10
12
14
Fiber Strain %

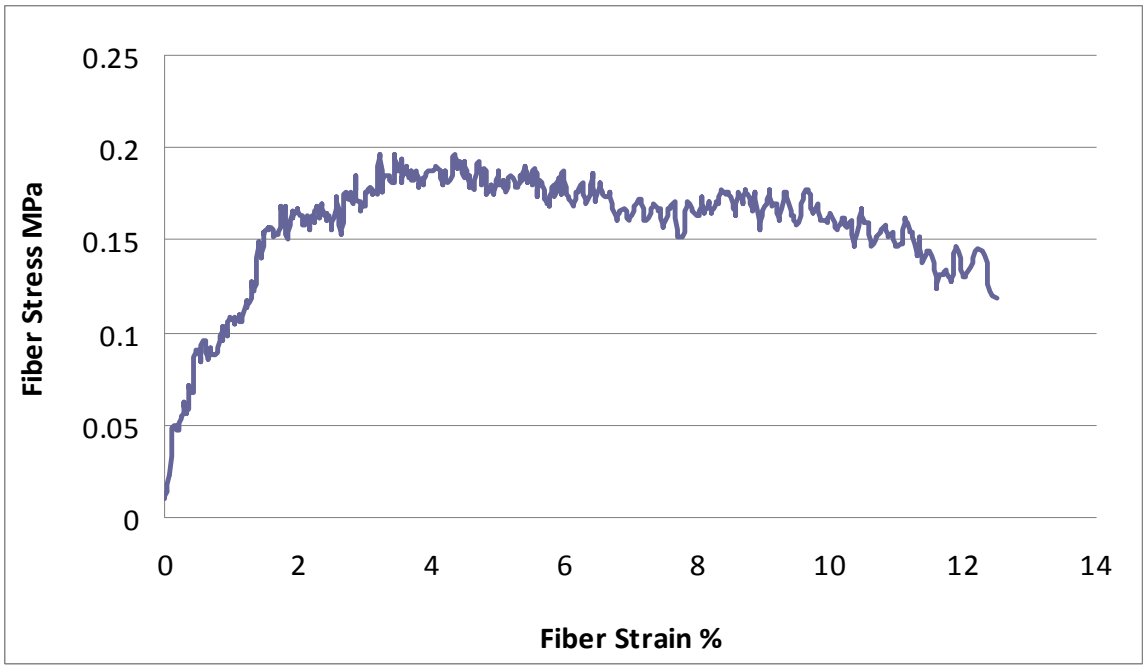
0.25
0.2
0.15
0.1
0.05
0
Fiber Stress MPa
0
2
4
6
8
10
12
14
Fiber Strain %

APPENDIX C

CREEP TESTS RESULTS

This appendix contains experimental results for creep tests in the form of plots. In certain cases, there are also comments explaining notable characteristics of the plots. Each plot shown is the result of testing an individual sample once.

C.1 COLD CREEP TEST RESULTS

C.1.1 Strain vs. Log Time

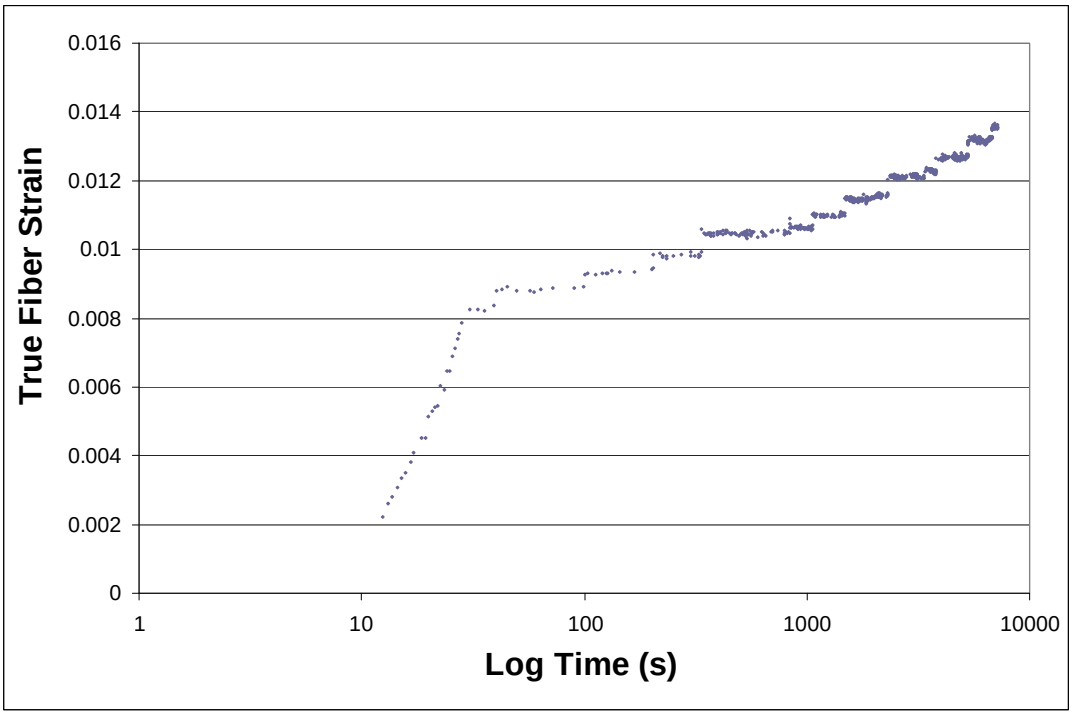

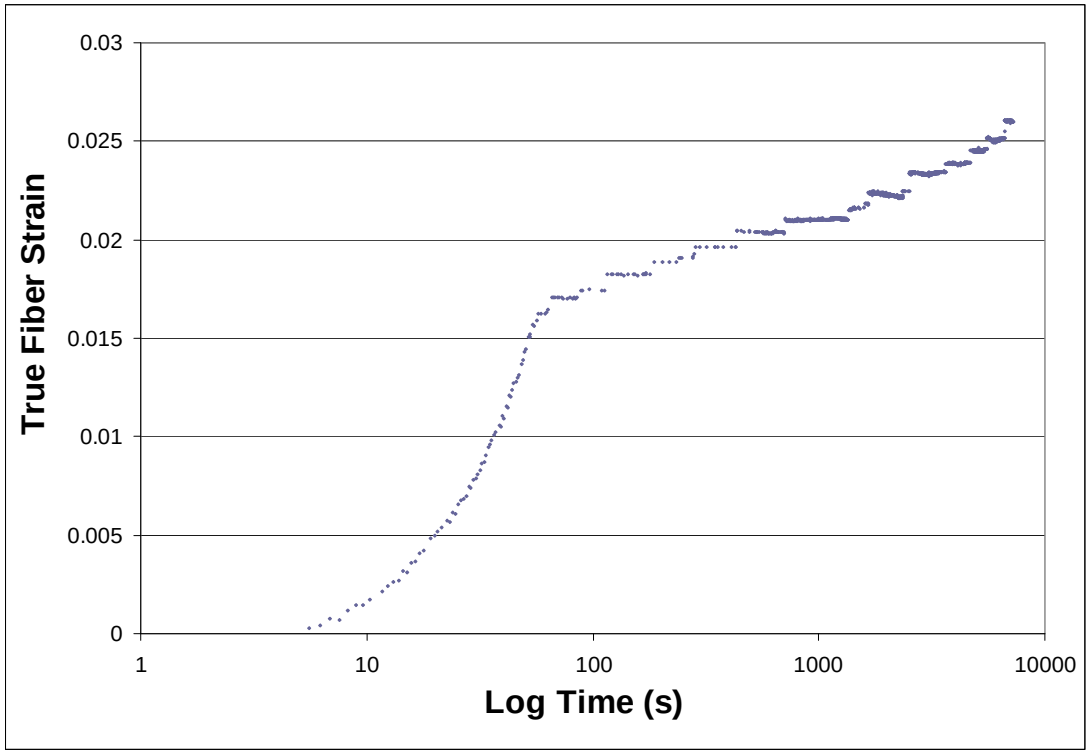
True Fiber Strain
0.03
0.025
0.02
0.015
0.01
0.005
0
1
10
100
1000
10000
Log Time (s)

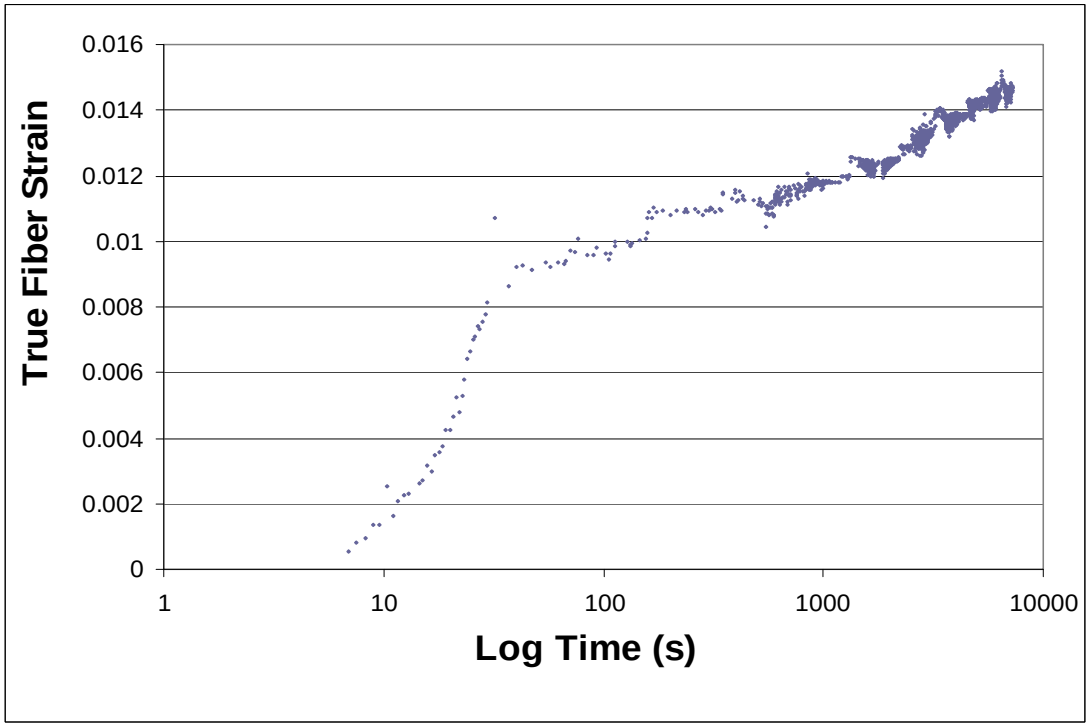
True Fiber Strain
0.016
0.014
0.012
0.01
0.008
0.006
0.004
0.002
0
1
10
100
1000
10000
Log Time (s)

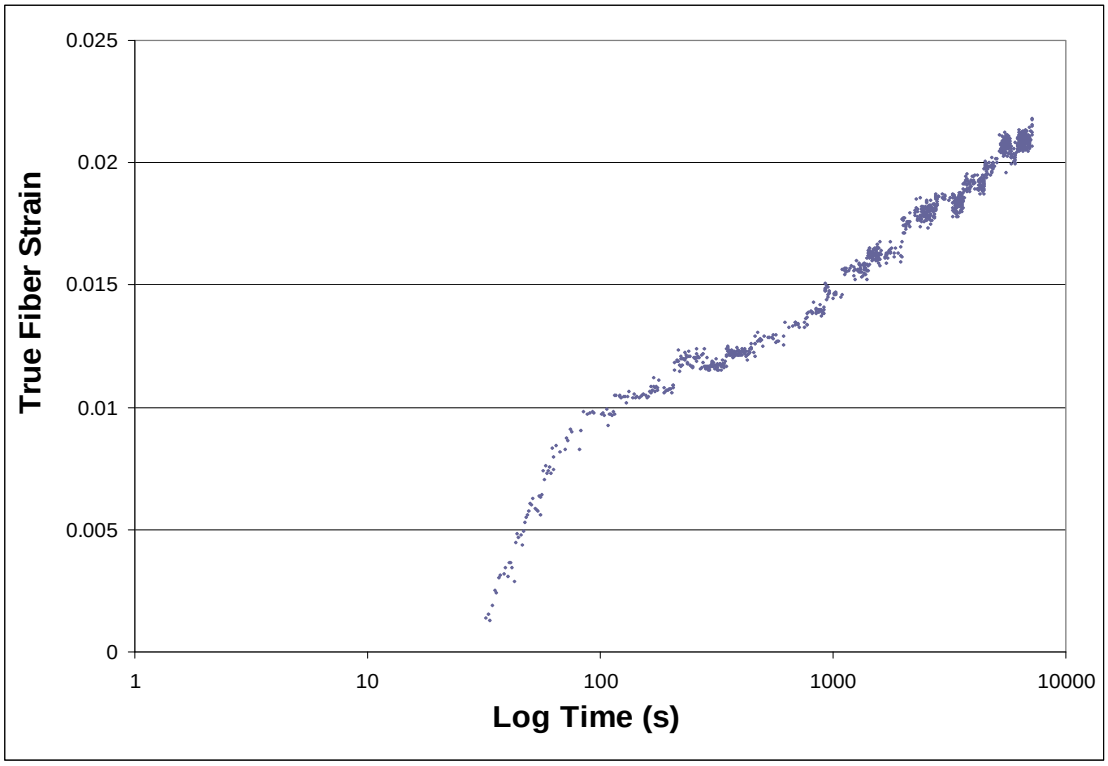
0.025
0.02
0.015
0.01
0.005
0
True Fiber Strain
1
10
100
1000
10000
Log Time (s)

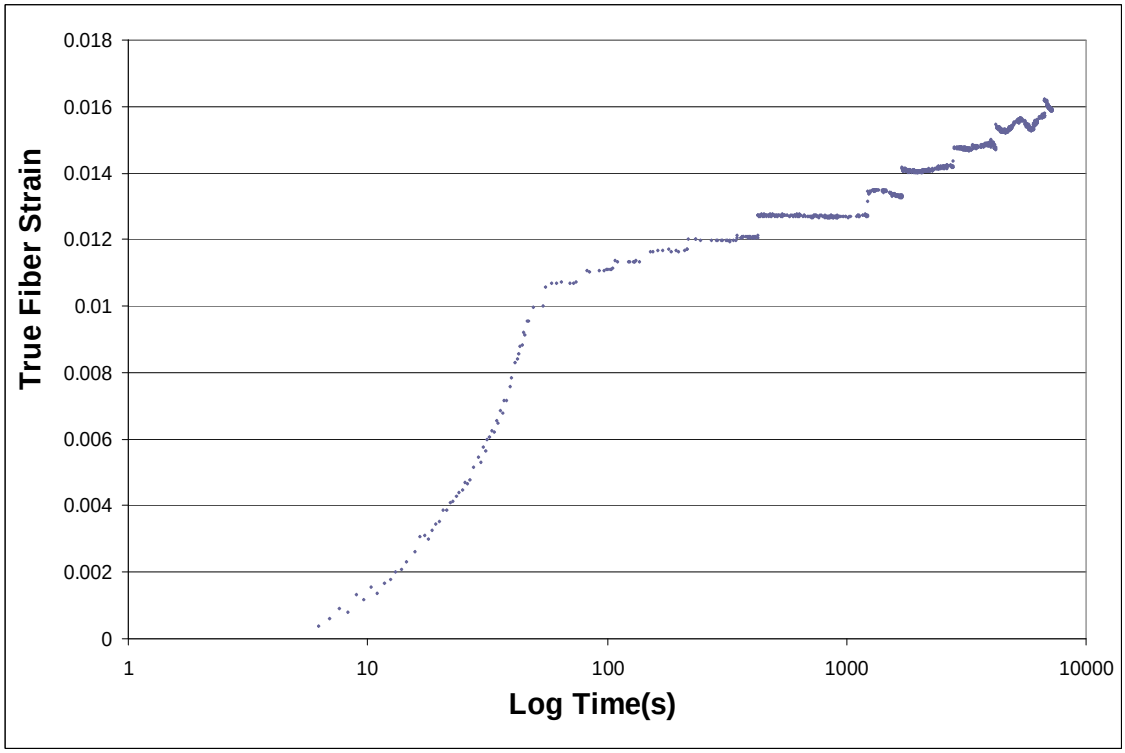
0.018
0.016
0.014
0.012
0.01
0.008
0.006
0.004
0.002
0
True Fiber Strain
1
10
100
1000
10000
Log Time(s)

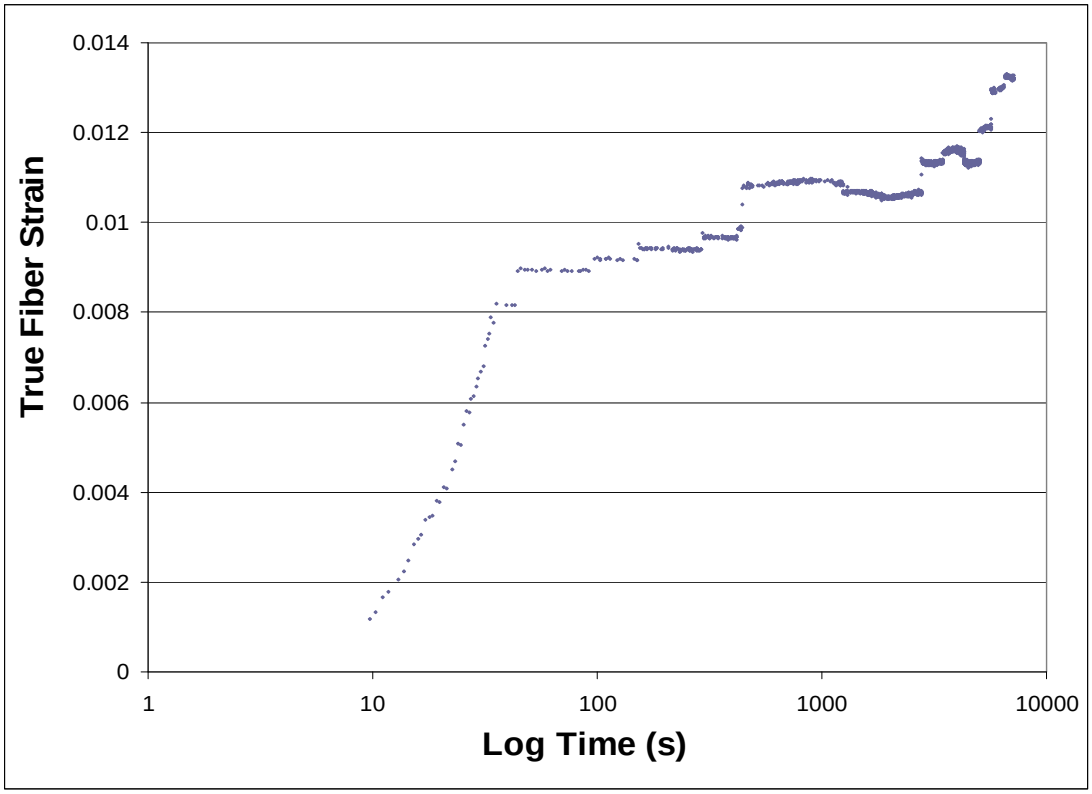
True Fiber Strain
0.014
0.012
0.01
0.008
0.006
0.004
0.002
0
1
10
100
1000
10000
Log Time (s)

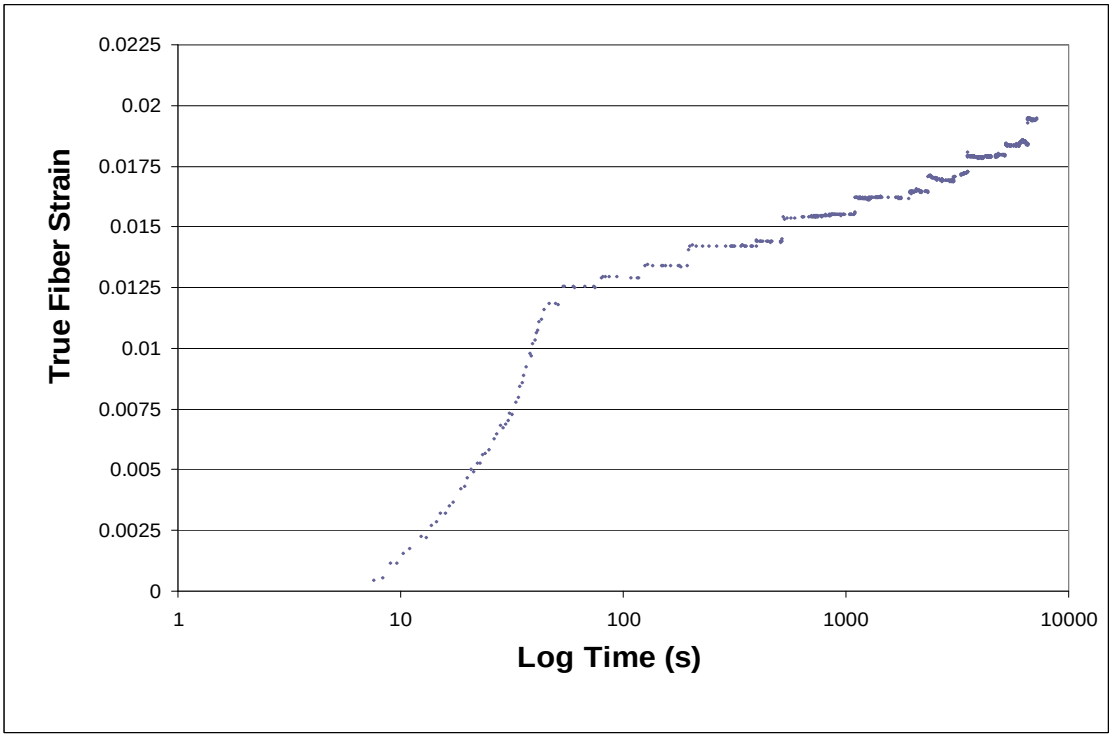
True Fiber Strain
0.0225
0.02
0.0175
0.015
0.0125
0.01
0.0075
0.005
0.0025
0
1
10
100
1000
10000
Log Time (s)

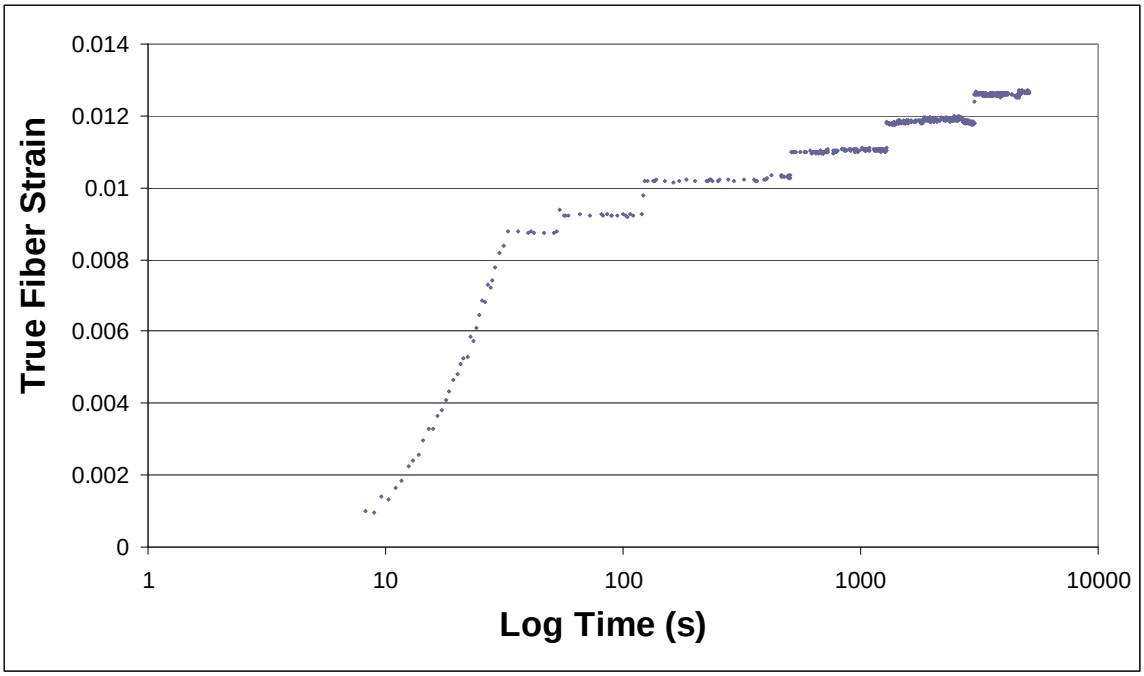
True Fiber Strain
0.014
0.012
0.01
0.008
0.006
0.004
0.002
0
1
10
100
1000
10000
Log Time (s)

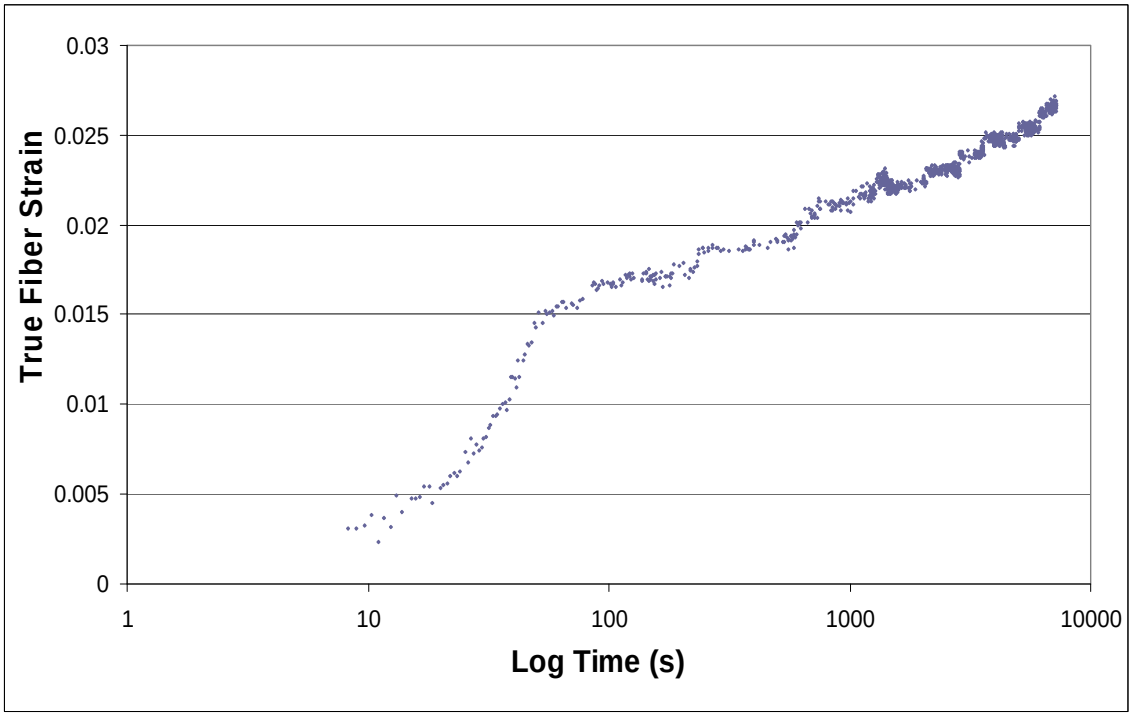
True Fiber Strain
0.03
0.025
0.02
0.015
0.01
0.005
0
1
10
100
1000
10000
Log Time (s)

C.1.2 Creep Modulus vs. Log Time

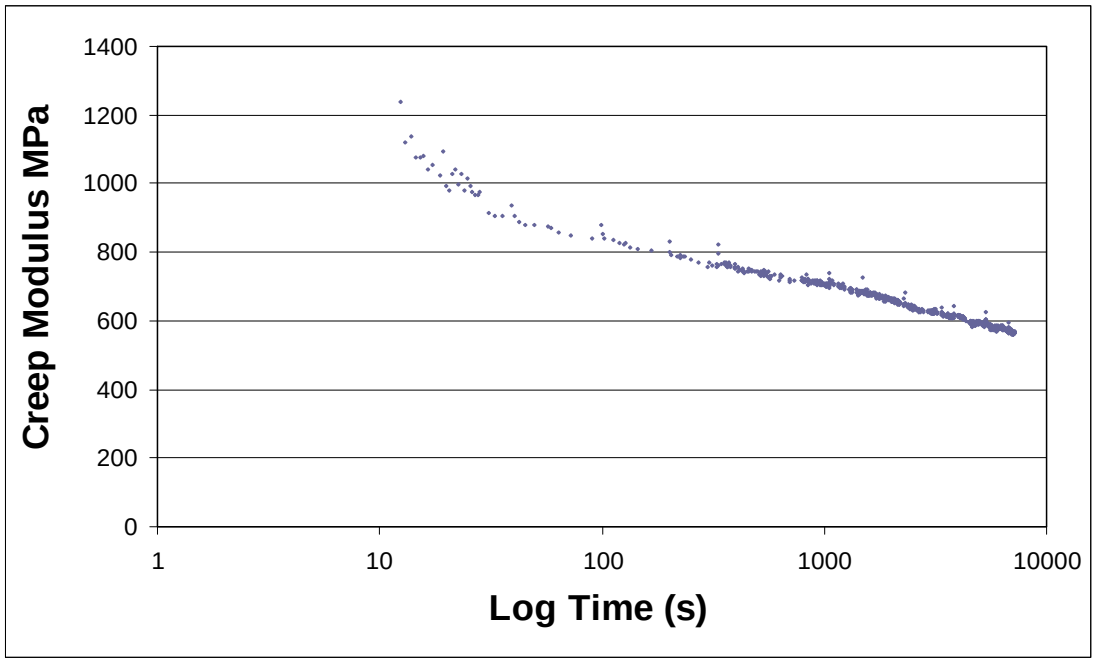

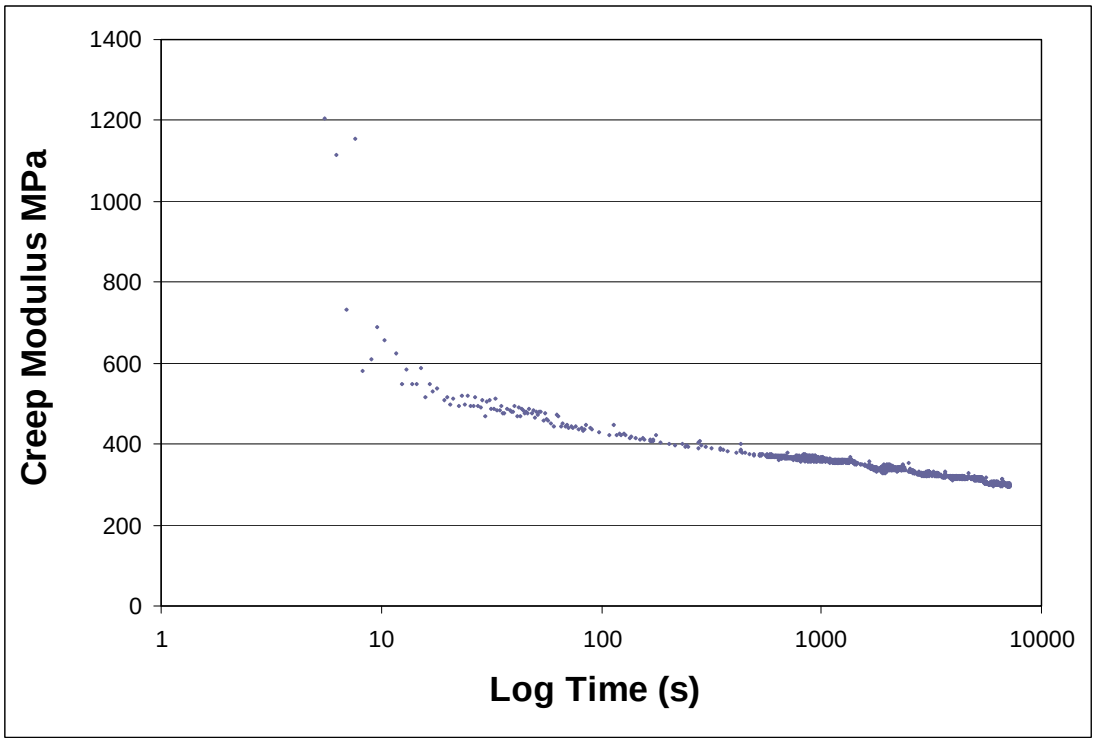

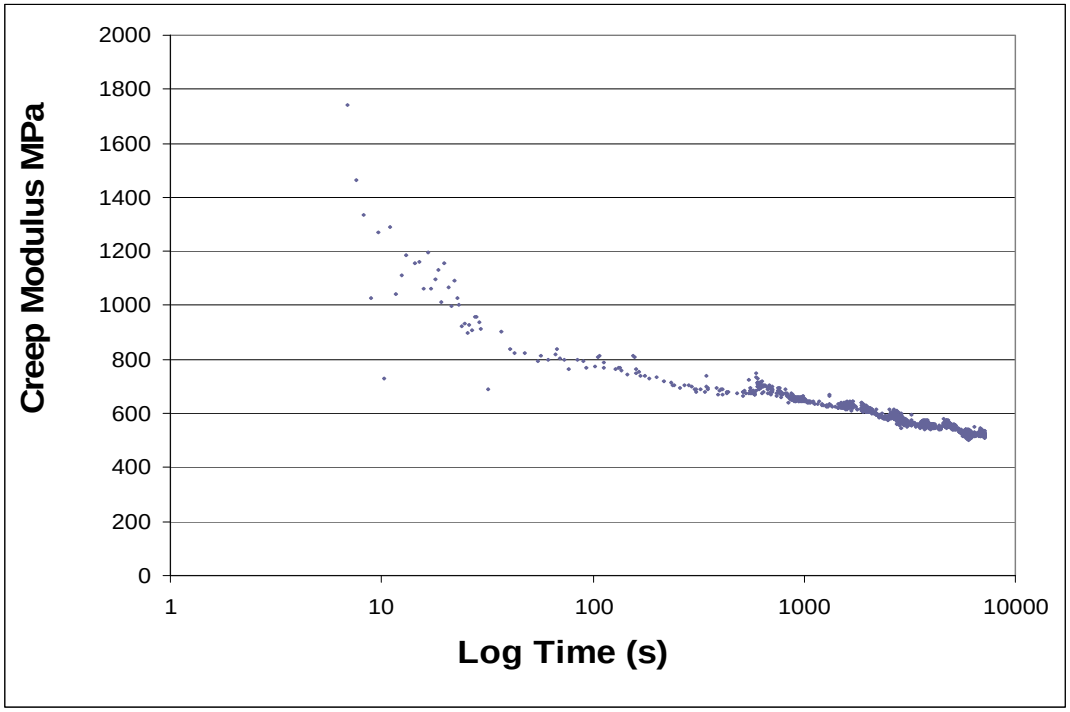
Creep Modulus MPa
2000
1800
1600
1400
1200
1000
800
600
400
200
0
1
10
100
1000
10000
Log Time (s)

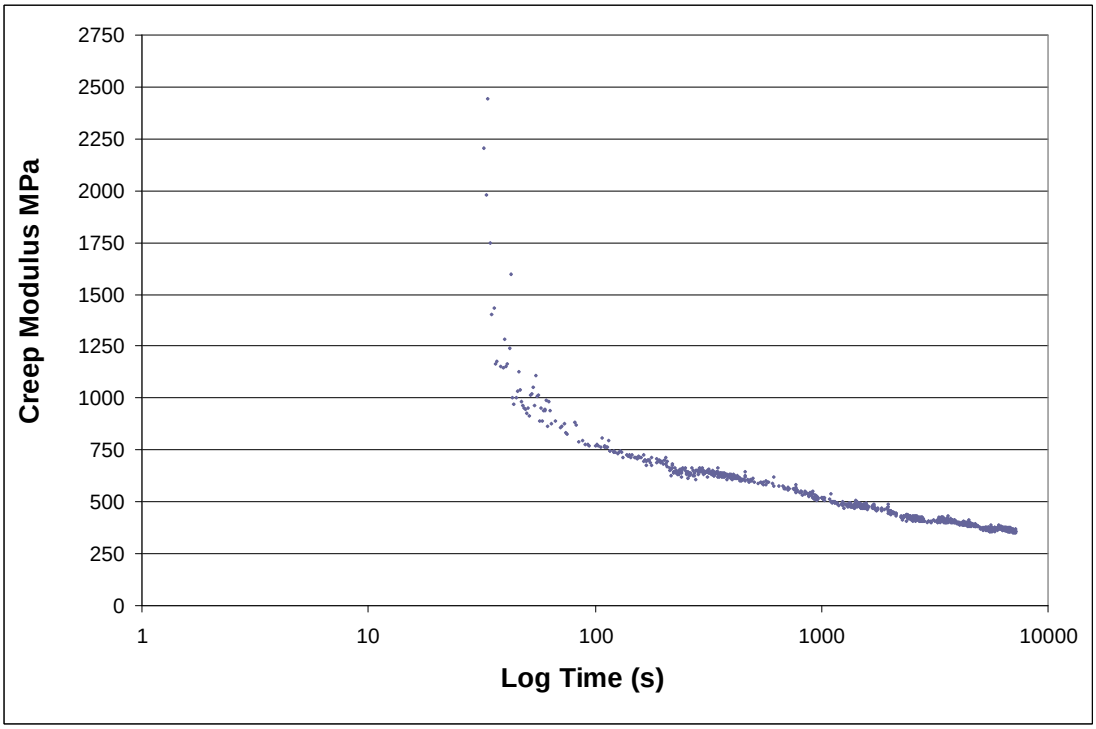
Creep Modulus MPa
2750
2500
2250
2000
1750
1500
1250
1000
750
500
250
0
1
10
100
1000
10000
Log Time (s)

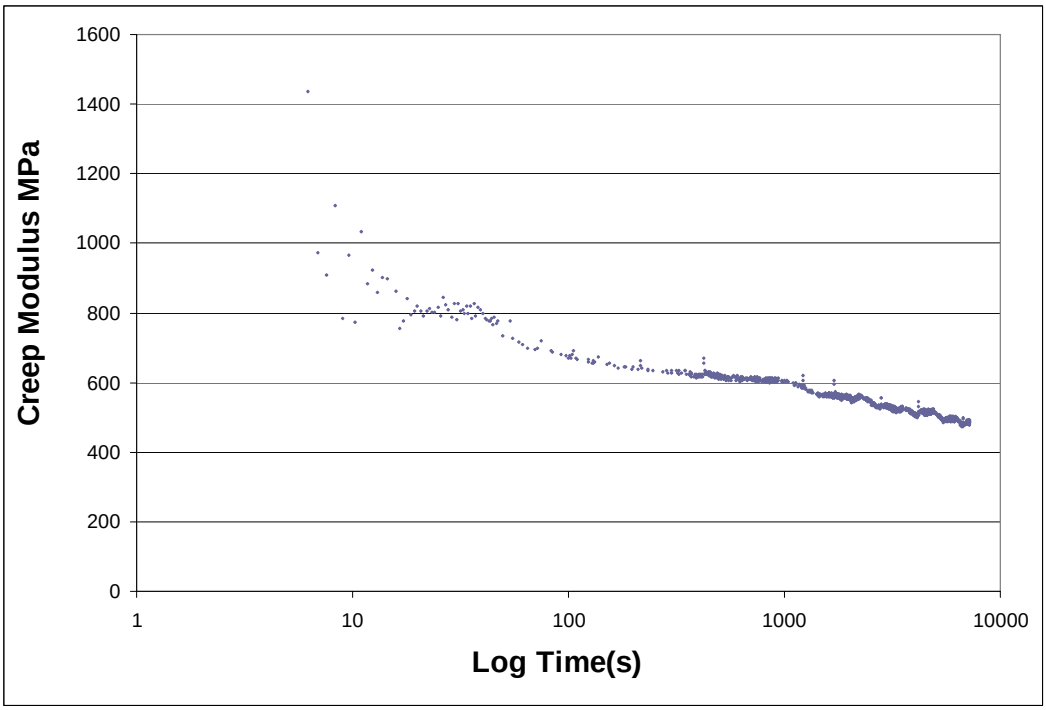
Creep Modulus MPa
1600
1400
1200
1000
800
600
400
200
0
1
10
100
1000
10000
Log Time(s)

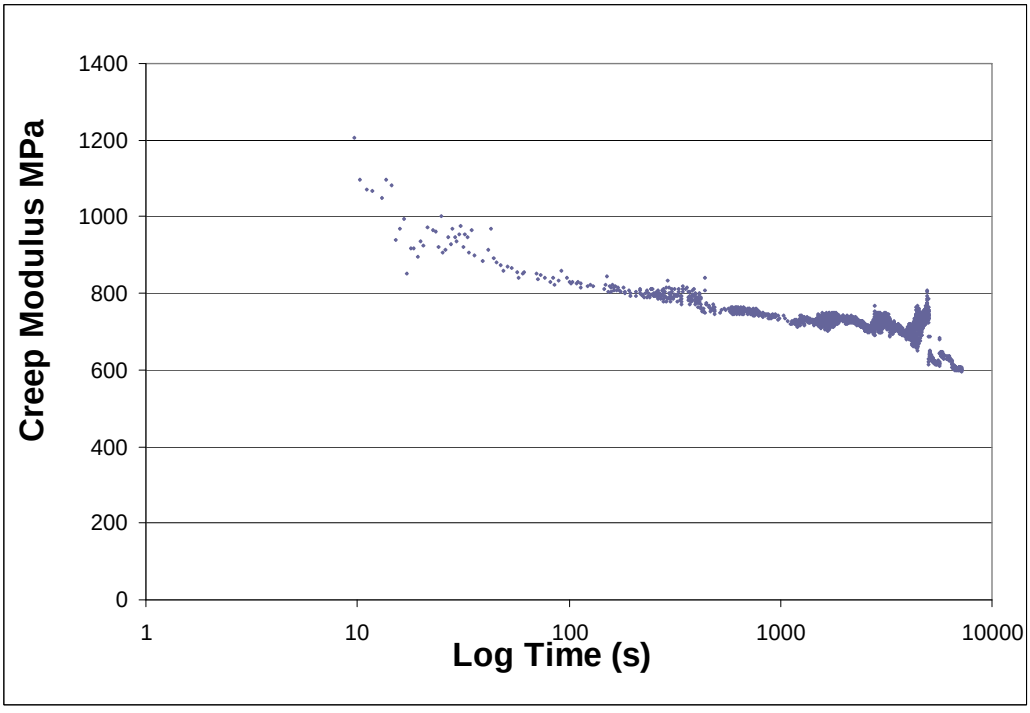
Creep Modulus MPa
1400
1200
1000
800
600
400
200
0
1
10
100
1000
10000
Log Time (s)

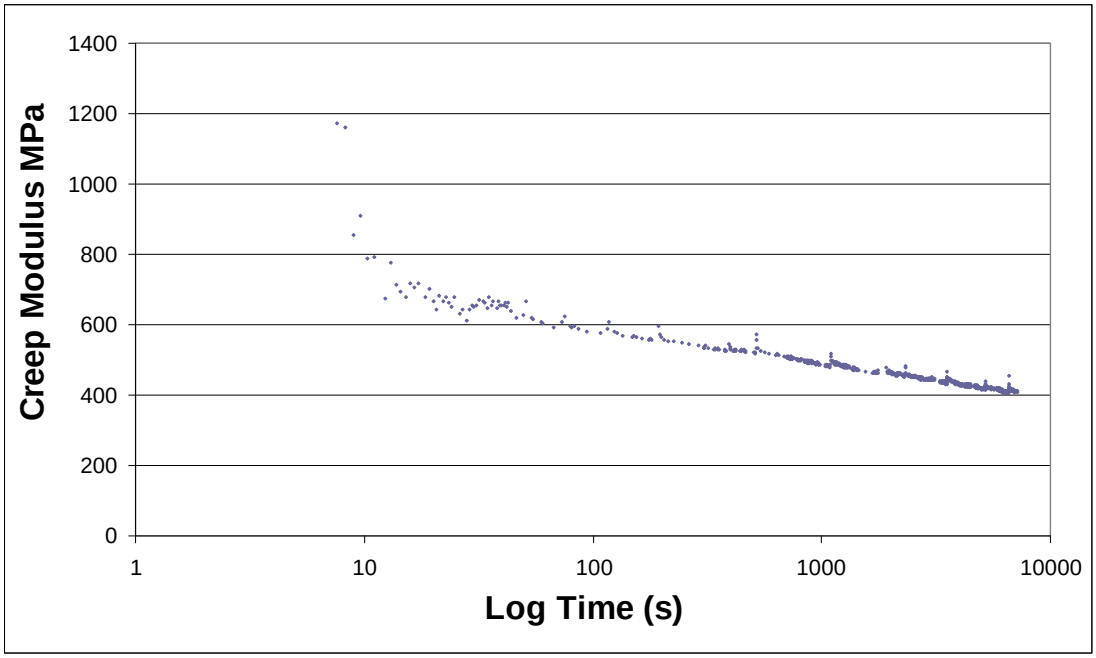
Creep Modulus MPa
1400
1200
1000
800
600
400
200
0
1
10
100
1000
10000
Log Time (s)

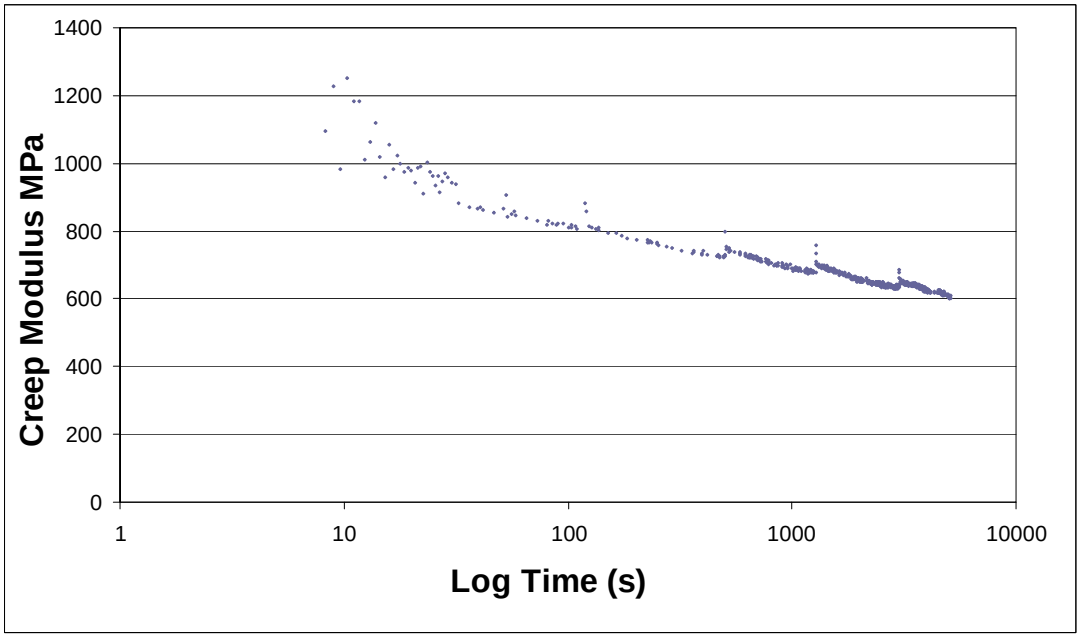
Creep Modulus MPa
1400
1200
1000
800
600
400
200
0
1
10
100
1000
10000
Log Time (s)

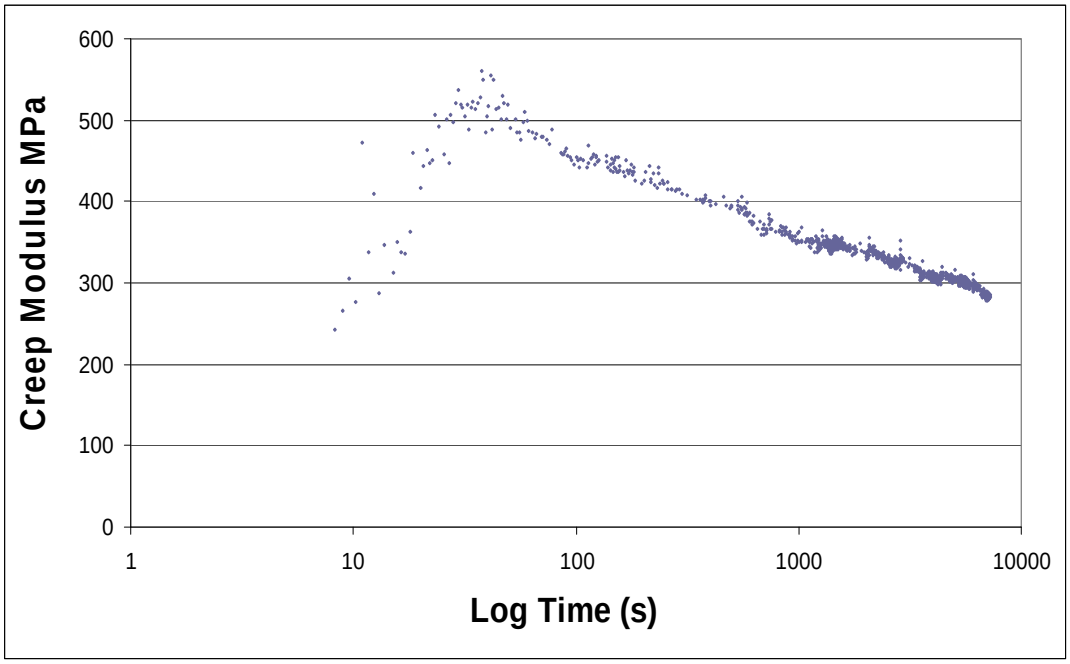
Creep Modulus MPa
600
500
400
300
200
100
0
1
10
100
1000
10000
Log Time (s)

C.2 HOT CREEP TEST RESULTS

C.2.1 Strain vs. Log Time

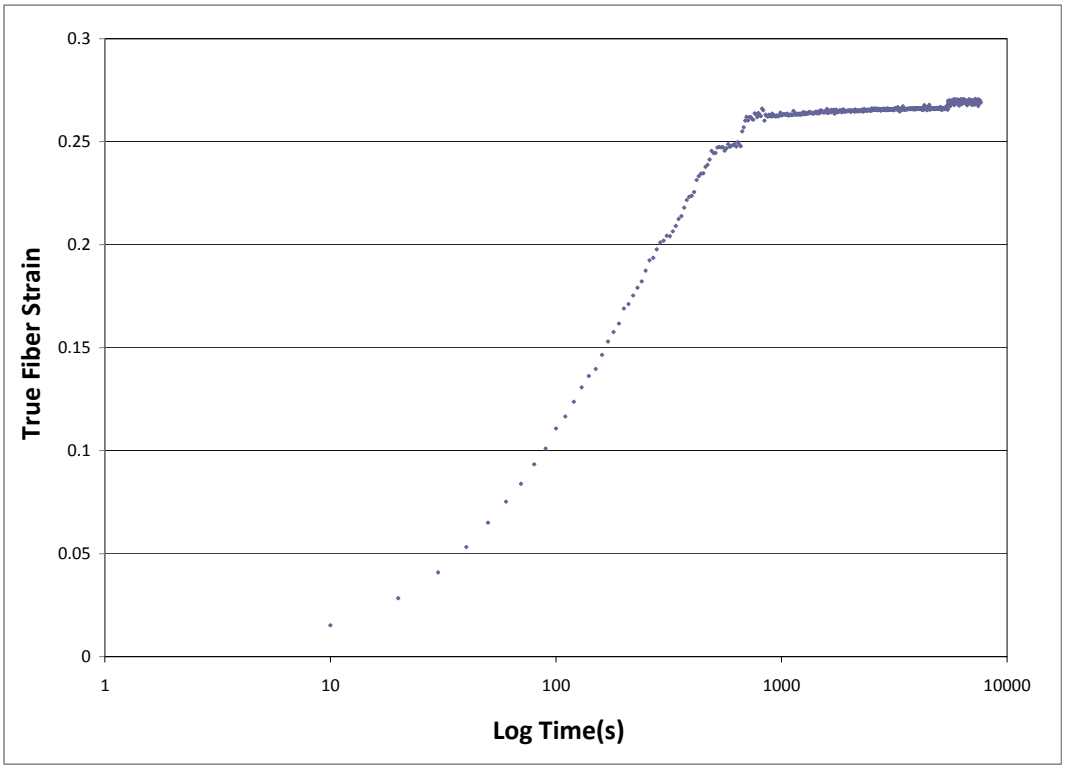

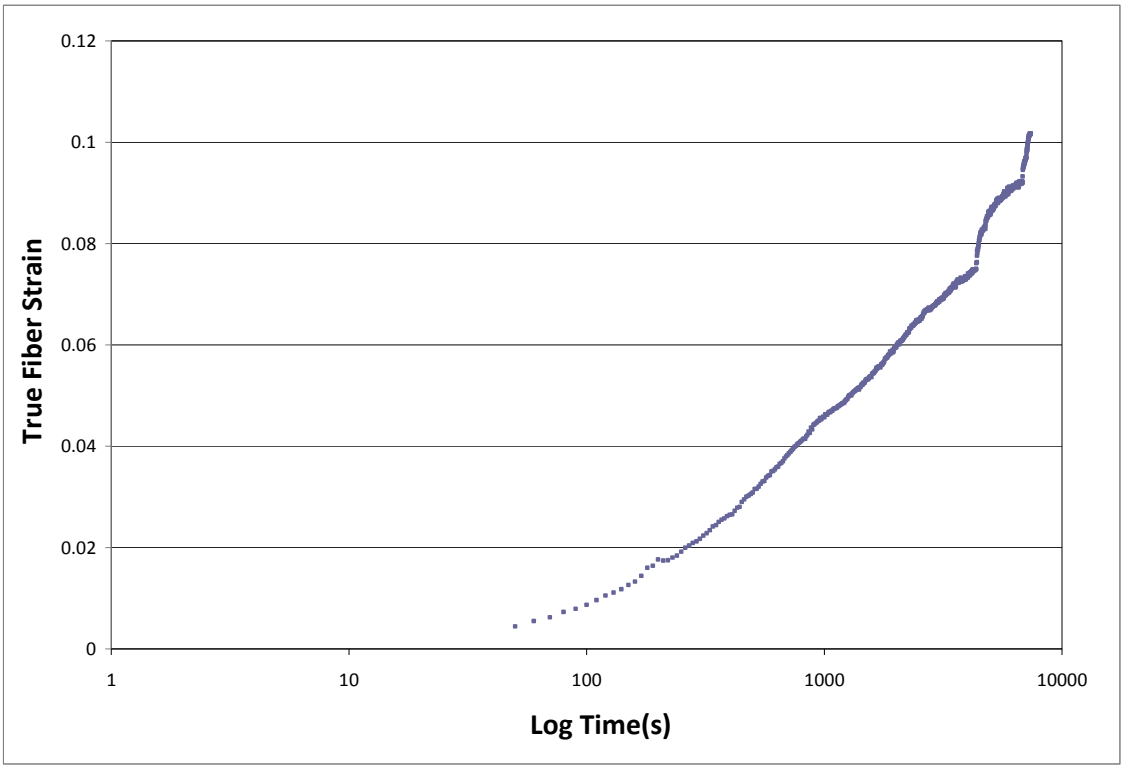
0.12
0.1
0.08
0.06
0.04
0.02
0
True Fiber Strain
1
10
100
1000
10000
Log Time(s)

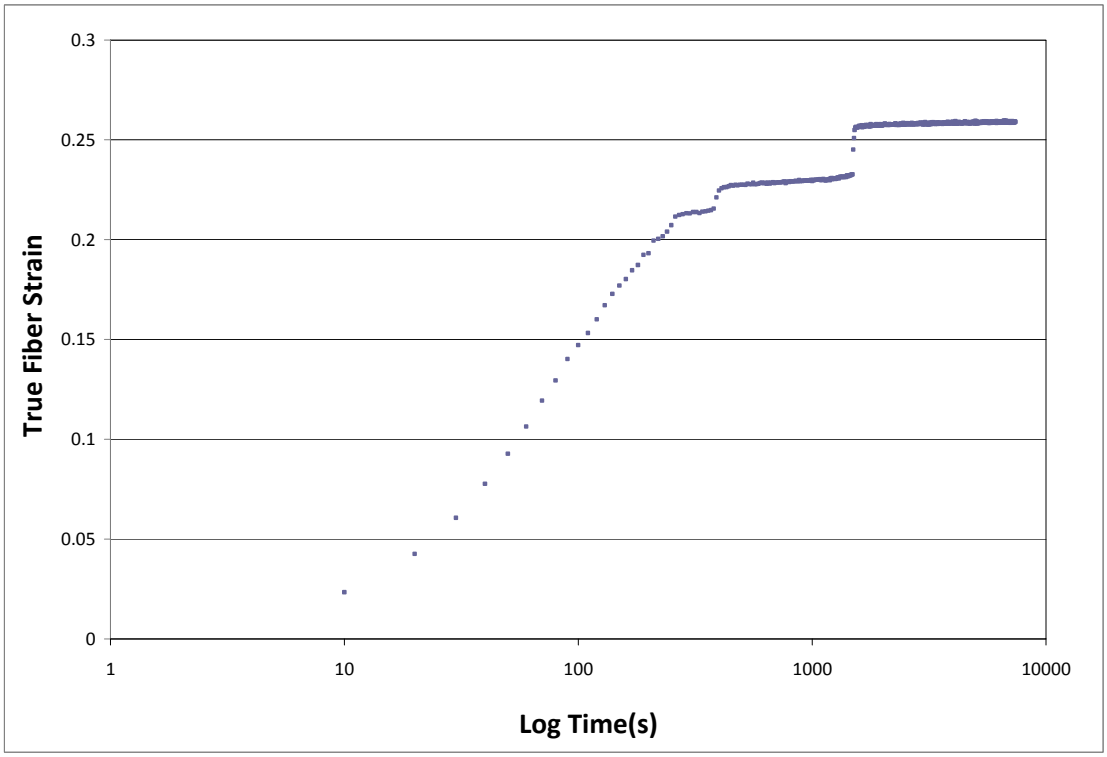
0.3
0.25
0.2
0.15
0.1
0.05
0
True Fiber Strain
1
10
100
1000
10000
Log Time(s)

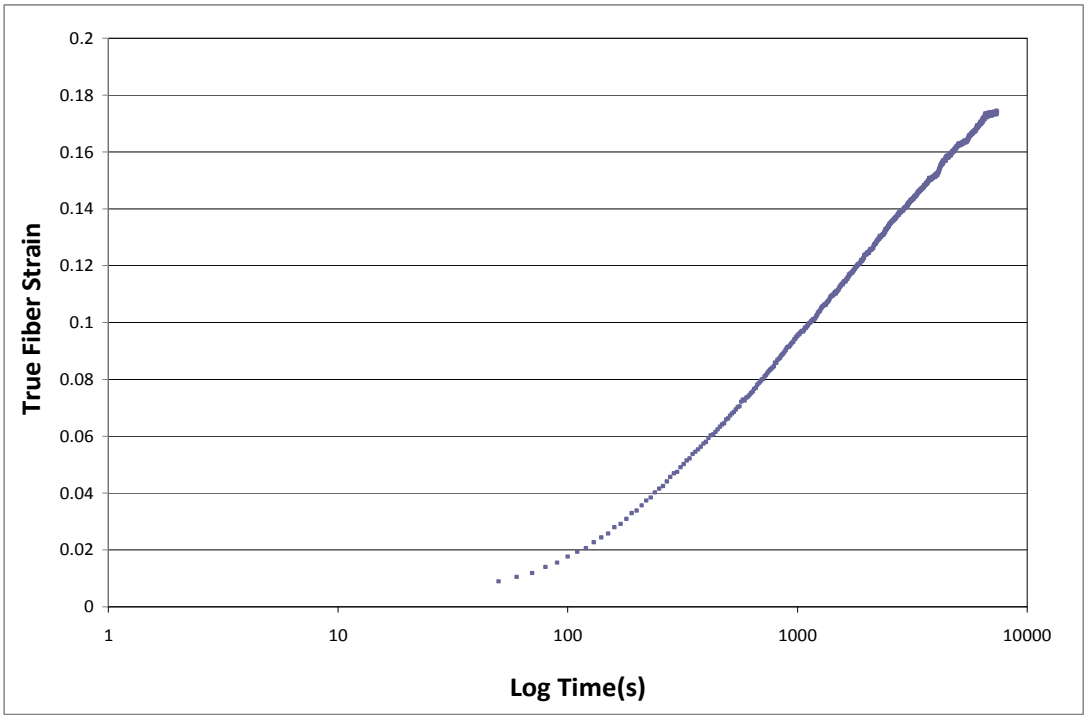
0.2
0.18
0.16
0.14
0.12
0.1
0.08
0.06
0.04
0.02
0
True Fiber Strain
1
10
100
1000
10000
Log Time(s)

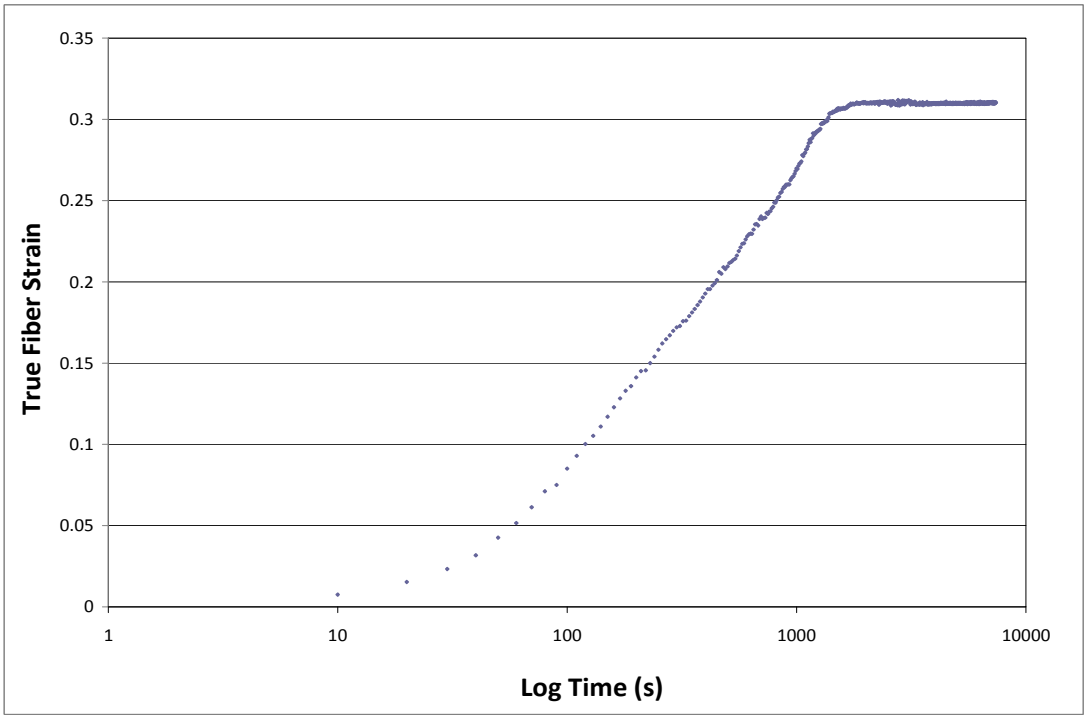
0.35
0.3
0.25
0.2
0.15
0.1
0.05
0
True Fiber Strain
1
10
100
1000
10000
Log Time (s)

C.2.2 Creep Modulus vs. Log Time

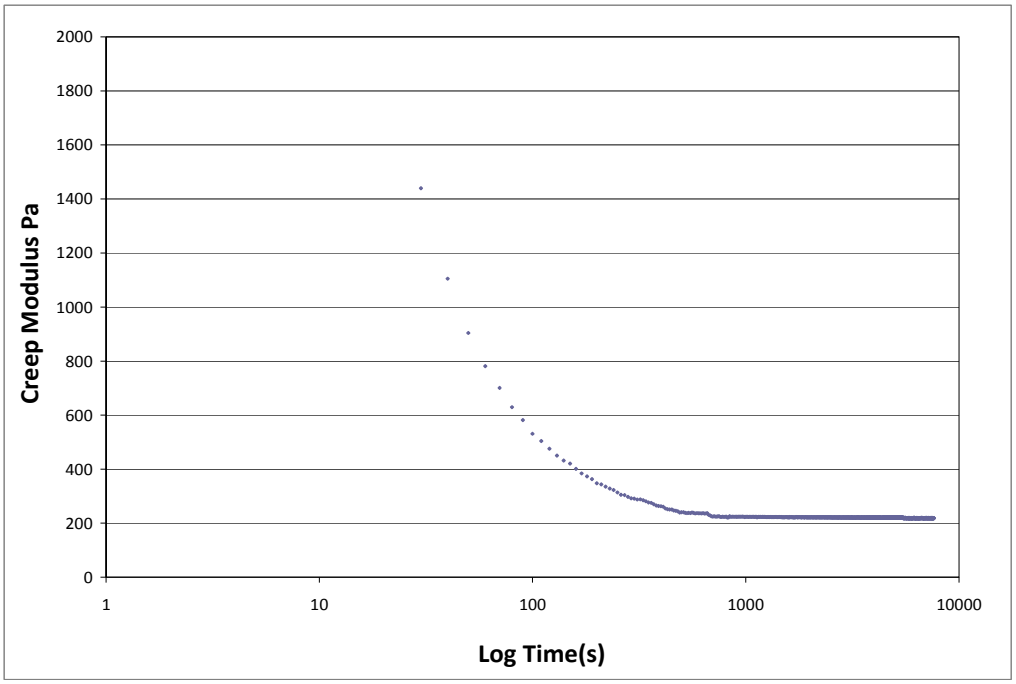

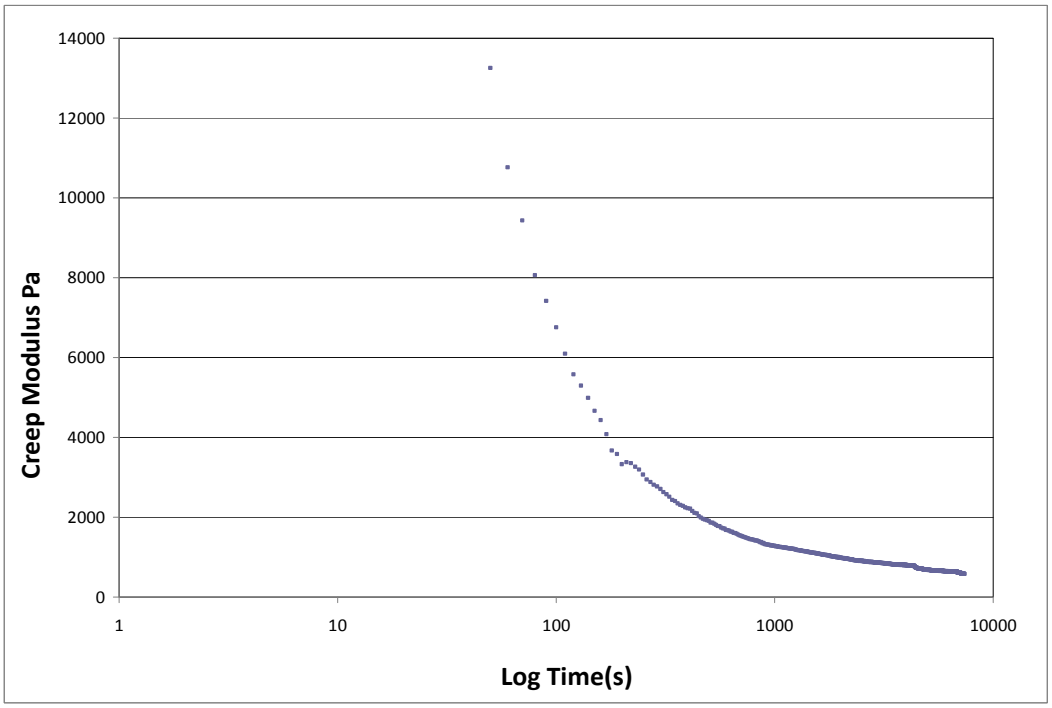

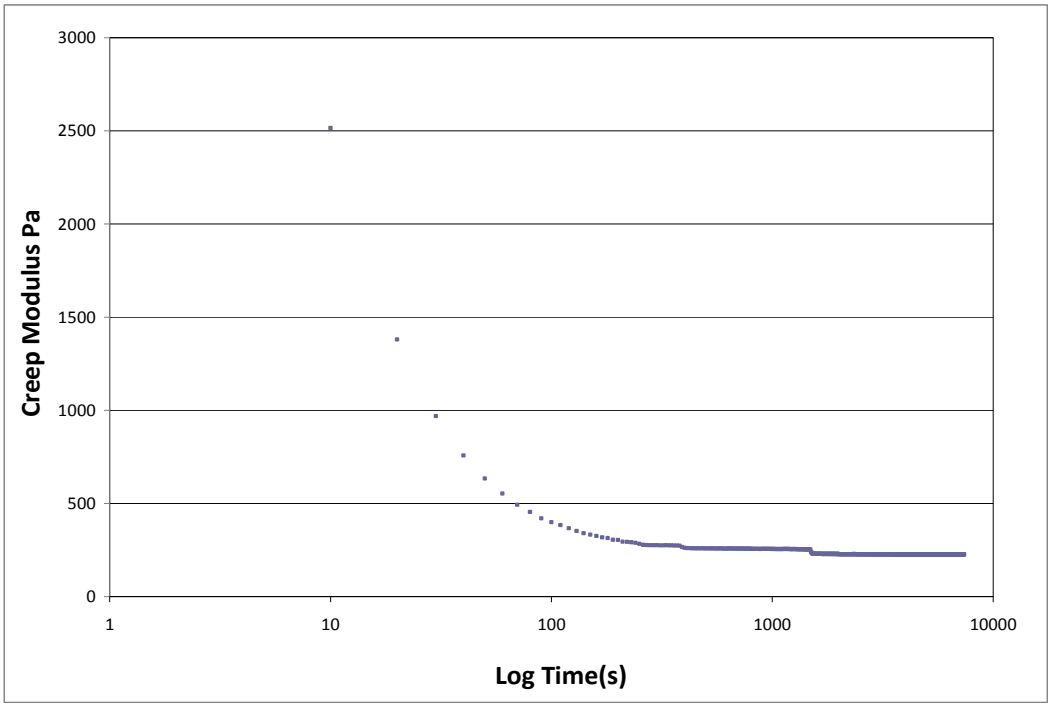
3000
2500
2000
1500
1000
500
0
Creep Modulus Pa
1
10
100
1000
10000
Log Time(s)

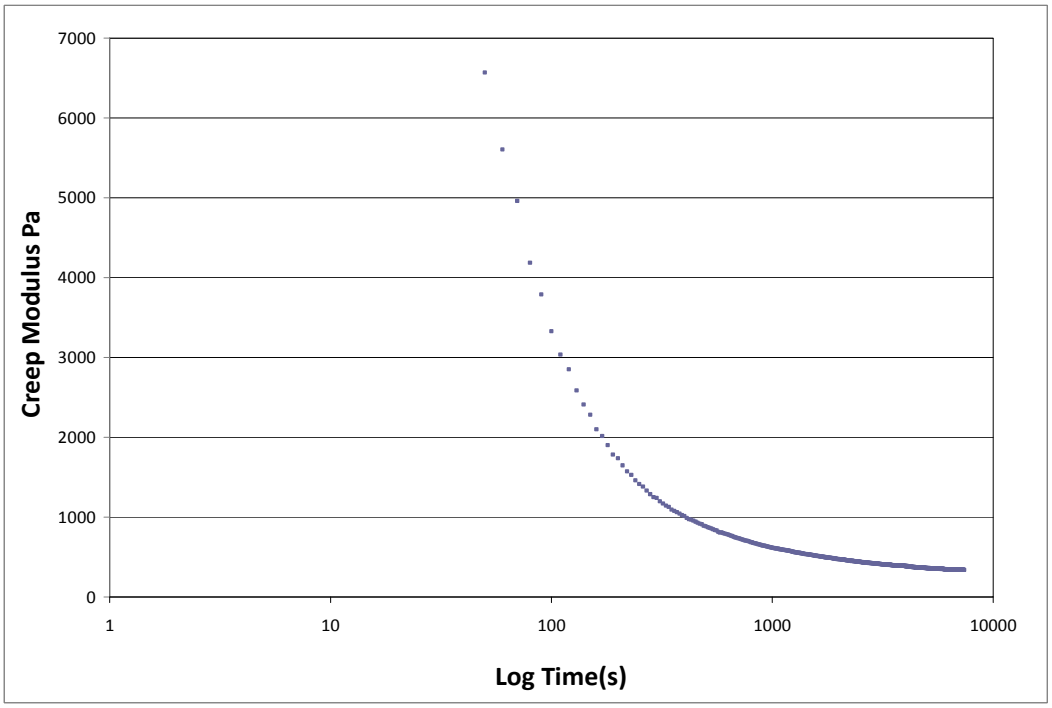
7000
6000
5000
4000
3000
2000
1000
0
Creep Modulus Pa
1
10
100
1000
10000
Log Time(s)

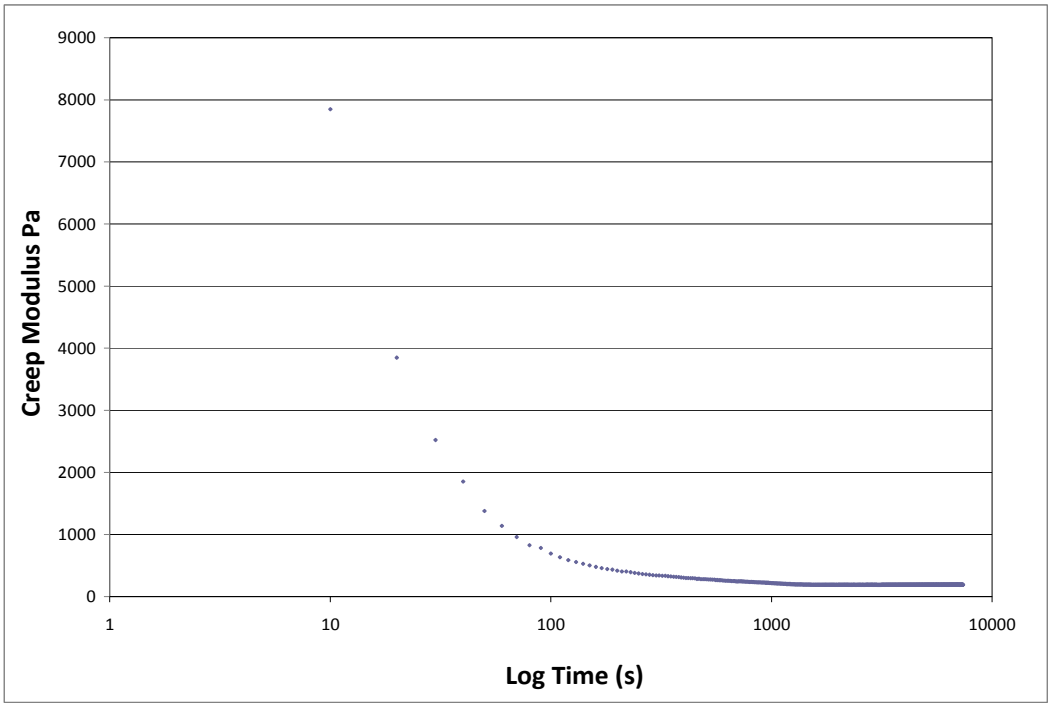
9000
8000
7000
6000
5000
4000
3000
2000
1000
0
Creep Modulus Pa
1
10
100
1000
10000
Log Time (s)

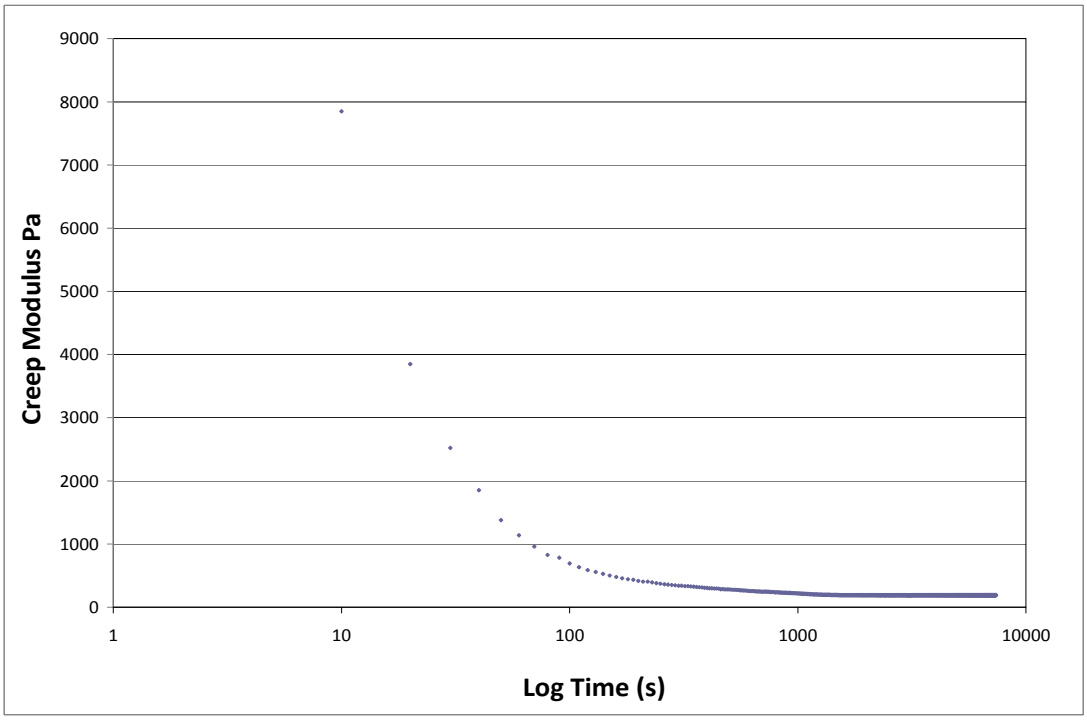
9000
8000
7000
6000
5000
4000
3000
2000
1000
0
Creep Modulus Pa
1
10
100
1000
10000
Log Time (s)

REFERENCES

1. C. Liang, C.A.R., A.E.M. *Investigation of Shape Memory Polymers and Their Hybrid Composites.* Journal of Intelligent Material Systems and Structures, 1997. **8**.

2. Sung Ho Lee. *Shape Memory Polyurethanes Having Crosslinks in Soft and Hard Segments.* Smart Materials and Structures, 2004. **13**.

3. Kelch, A., L.A.S. *Shape-Memory Effect.* Angew. Chem. Int. Ed., 2002. **41**.

4. Ken Gall, C.M.Y., Yiping Liu, Robin Shandas, Nick Willett, Kristi S. Anseth. *Thermomechanics of the Shape Memory Effect in Polymers for Biomedical Applications*. 2004.

5. Z. G. Wei , R.S. *Shape-Memory Materials and Hybrid Composites for Smart Systems.* Journal of Materials Science, 1998. **33**.

6. Rich Beblo, Lisa Weiland. *Polymer Chain Alignment in Shape Memory Polymer*, in *ASME International Mechanical Engineering Congress and Exposition*. 2006.

7. NextGen Aeronautics. *NextGen Aeronautics Successfully Flight-Tests Shape-Changing Morphing Wing*. 2006 [cited; Available from: http://nextgenaero.com/success_mfx2.html.

8. *Morphing Aircraft Structures*. [cited; Available from: http://www.darpa.mil/dso/archives/mas/index.htm.

9. Robert S. Bortolin. *Characterization of Shape Memory Polymers for Use as A Morphing Aircraft Skin Material*. 2005, University of Dayton.

10. NASA. *Active Aeroelastic Wing Rollout Highlights Centennial of Flight*. 2002 [cited; Available from: http://www.nasa.gov/centers/dryden/news/NewsReleases/2002/02-18.html.

11. E.L. Carpenter, H.P.W. *Aerodynamics for Engineering Students*. 5th ed. 2003, Burlington: Butterworth-Heinemann.

12. M.T. Kikuta. *Mechanical Properties of Candidate Materials for Morphing Wings*, in *Mechanical Engineering*. 2003, Virginia Polytechnic Institute and State University.

13. C. Liu, H.Q., P.T.M. *Review of Progress in Shape-Memory Polymers.* Journal of Materials Chemistry, 2007.

14. Yiping Liu, Ken Gall, Martin L. Dunn, Alan R. Greenberg, Julie Diani. *Thermomechanics of Shape Memory Polymers: Uniaxial Experiments and Constitutive Modeling.* International Journal of Plasticity, 2004.

15. T. S. Wilson, W.S.I., W. J. Benett, J. P. Bearinger, D. J. Maitland. *Shape Memory Polymer Therapeutic Devices for Stroke*, in *SPIE Optics East*. 2005: Boston, MA.

16. A. Yousefi-Koma, D.G.Z. *Applications of Smart Structures to Aircraft for Performance Enhancement.* Canadian Aeronautics and Space Journal, 2003. **49**.

17. A. Behl. *Shape Memory Polymers.* Materials Today, 2007. **10**(4).

18. Jae-Sung Bae, Siegler, T., Inman, D. *Aeroelastic Considerations on Shape Control of an Adaptive Wing.* Journal of Intelligent Material Systems and Structures, 2005. **16**.

19. J.N. Kudva. *Overview of the DARPA Smart Wing Project.* Journal of Intelligent Material Systems and Structures, 2004. **15**.

20. J.E. Manzo. *Analysis and Design of Hyper-Elliptical Cambered Span Morphing Aircraft*. 2006, Cornell University.

21. B. Volk. *Characterization of Shape Memory Polymers*.

22. Witold Sokolowski, A.M., Shunichi Hayashi, L'Hocine Yahia, Jean Raymond. *Medical Applications of Shape Memory Polymers.* Biomedical Materials, 2007. **2**.

23. Andreas Lendlein, H.J., Oliver Ju¨ nger and Robert Langer. *Light-Induced Shape-Memory Polymers.* NATURE, 2005. **434**.

24. H Tobushi, D.S., S Hayashi, M Endo. *Shape Fixity and Shape Recovery of Polyurethane Shape-Memory Polymer Foams.* Intstitution of Mechanical Engineers --Part L -- Journal of Materials: Design & Applications, 2003. **21**.

25. Hisaaki Tobushi, K.O., Shunichi Hayashi, Norimitsu Ito. *Thermomechanical Constitutive Model of Shape Memory Polymer.* Mechanics of Materials, 2001. **33**.

26. Takenobu Sakai, T.T., Satoshi Somiya. *Viscoelasticity of Shape Memory Polymer: Polyurethane Series DiARY.* Journal of Solid Mechanics and Materials Engineering, 2007. **1**(4).

27. Ward Small IV, T.S.W., William J. Benett, Jeffrey M. Loge, and Duncan J. Maitland. *Laser-Activated Shape Memory Polymer Intravascular Thrombectomy Device.* Optics Express, 2005. **13**.

28. Yiping Liu, K.G., Martin L. Dunn, Patrick McCluskey. *Thermomechanics of Shape Memory Polymer Nanocomposites.* Mechanics of Materials, 2003. **36**.

29. Patrick R. Buckley, G.H.M., Thomas S. Wilson, Ward Small, IV, William J. Benett, Jane P. Bearinger, Michael W. McElfresh, Duncan J. Maitland. *Inductively Heated Shape Memory Polymer for the Magnetic Actuation of Medical Devices.* IEEE Transactions on Biomedical Engineering, 2006. **53**.

30. H. Tobushi, T.H., S. Hayashi and E. Yamada. *Thermomechanical Constitutive Modeling in Shape Memory Polymer of Polyurethane Series.* Journal of Intelligent Material Systems and Structures, 1997. **8**.

31. John Leinhard IV, J.L.V. *A Heat Transfer Textbook*. 3rd ed. 2008, Cambridge, MA: Phlogiston Press.

32. Rebecca Austman. *Development of an Apparatus and Method for Testing the Viscoelastic Properties of Axolotl Embryos as an Animal Model for Congenital Lordosis.* University of Manitoba. April 21, 2004.